

https://dspace.org/

Rare earth element (REE) ß-diketone complexes as novel corrosion inhibitors for mild steel and stainless steels in a corrosive chloride media

Lawal, Olatunde Johnson

2022

https://hdl.handle.net/10539/34901

Downloaded from a DSpace repository. https://dspace.org/

UNIVERSITY OF THE WITWATERSRAND, JOHANNESBURG

Rare earth element (REE) β-diketone Complexes as Novel Corrosion Inhibitors for Mild Steel and Stainless Steels in Corrosive Chloride Media

OLATUNDE JOHNSON LAWAL

(2213721)

A Dissertation Submitted to the Faculty of Engineering and the Built Environment, University of the Witwatersrand, Johannesburg, in Fulfilment of the Requirements for the Degree of Master of Science in Engineering.

Supervisor: Prof. J. H. Potgieter

Co-supervisors: Prof. C. Billing

Dr. D. J. Whitefield

12th July, 2022

Declaration

I, Olatunde Johnson Lawal (2213721) declare that this dissertation is my unaided work. It is being submitted for the degree of Master of Science in Engineering to the University of the Witwatersrand, Johannesburg, South Africa. It has not been previously submitted for any degree or examination to any other University. I further declare that all the sources that I have used or quoted have been acknowledged by means of complete references.



…… ……..

Signature of Candidate

…12th... day of …July…. year …2022…

Abstract

Currently, chromate compounds are among the most common chemicals used as corrosion inhibitors for different metals and alloys. However, these compounds are highly toxic and carcinogenic, and their application produces serious environmental hazards and toxicity to humans. As a result, novel green rare earth element (REE) β-diketone complexes were proposed as alternatives to chromate inhibitors. Therefore, the research aim was to synthesise, characterise and study the inhibition potential of the synthesised REE β-diketone complexes as a green corrosion inhibitors for mild steel and austenitic stainless steels (304 and 316 SS) in a corrosive chloride media at different temperatures. The synthesised complexes were characterised using melting point analysis, infrared spectroscopy, Raman spectroscopy, mass spectroscopy, and X-ray diffraction.

Four REE β-diketone complexes of cerium and lanthanum acetylacetone and hexafluoroacetylacetone were selected for the investigation as potential corrosion inhibitors for mild steel and austenitic stainless steel using 3.5% NaCl and 0.1 M HCl solutions as corrosive chloride media. Their inhibiting potentials were assessed using weight loss tests and potentiodynamic polarisation scans. Surface analyses using scanning electron microscopy (SEM), fourier transform infrared spectroscopy (FTIR) and Raman spectroscopy (RS) were used to investigate the steel samples after weight loss and electrochemical tests for possible oxide film layer formation on the surface of the steel. SEM and Raman spectroscopy confirmed the formation of protective films of the tested inhibitors on the steel surfaces.

Dedication

In memory of my late mum, Mrs. Dorcas Amujoyeni Julius who passed away on the 18th of February, 2021.

Acknowledgment

First and foremost, I would like to show my heartfelt and deep appreciation to Almighty God for His love, guidance, and protection over my life for the successful completion of my study.

My special appreciation goes to Professor Herman Potgieter for the opportunity he has given to me to work with him. I want to thank him for his financial support, indefatigable supervision constant review, encouragement, patience and guidance. Without him, I would have not been able to complete this program.

My sincere appreciation goes to my Co-supervisors, Professor Caren Billing and Dr. David Whitefield for their unrelenting academic support, guidance, thorough review of my thesis, recommendation, and suggestions. Furthermore, I would also like to thank them for their expertise in the field of corrosion which they always share with me whenever the need arises during the experimental work.

I would like to thank Dr. Thomas Aniokete, Dr. Michael Oluwatosin Bodurin and Mr. Orevaoghene Eterigho-ikelegbe for their constant support, love, advice and encouragement throughout the course of my study.

Lastly, and most importantly, I would like to thank my wife, my siblings, my cousin and his wife, Mr. & Mrs. Felix Oni Omovie and other family members for their constant love, support and encouragement.

Publications emanating from this research study

The following journal articles emerged from this study.

1. The influence of REE β-diketone complexes on the corrosion behaviour of mild steel and 304 SS in 3.5 % NaCl solution. **https://doi.org/10.3390/min12040416**
2. Rare Earth Element (REE) β-diketone Complexes as Novel Corrosion Inhibitors for 304 and 316 Stainless Steel in 0.1 M HCl Solution. (**Accepted for publication**)

Table of Contents

Declaration..... i

Abstract ii

Dedication iii

Acknowledgment..... iv

Publications emanating from this research study..... v

Table of Contents vi

List of Figures xii

List of Tables xvii

List of Abbreviation and symbols ……..……xix

Chapter One: Introduction 1

1.1 Background..... 1

1.2 Problem Statement 2

1.3 Research Questions 3

1.4 Research Aim and Objectives 3

1.5 Hypothesis …….. 3

1.6 Dissertation Outline ……..... 4

1.7 References…… 5

Chapter Two: Literature Review…….. 7

2.1 Introduction……..…..…. 7

2.2 Corrosion Inhibitors…….……... 7

2.3 Mechanisms of actions of inhibitors…….. 8

2.3.1 Anodic Inhibitor…….. 8

2.3.2 Cathodic inhibitors…….. 10

2.3.3 Mixed inhibitors…….. 11

2.4 Inhibitors based on the mode of protection……. 12

2.4.1 Chemical passivators…… 12

2.4.2 Adsorption inhibitors…… 13

2.4.3 Film forming inhibitors…… 13

2.5 β-diketonates and their metal complexes…… 16

2.6 Summary……. 18

2.7 References……... 20

Chapter Three: Synthesis and characterization of a REE β-diketones complexes……. 24

3.1 Synthesis of REE β-diketones complexes……... 24

3.2 Characterization of REE β-diketones complexes…… 24

33 Melting point…….. 25

3.4 Infrared spectroscopy analysis (FTIR)……..... 27

3.5 Raman spectroscopy (RM) results ……. 33

3.6 Mass spectra analysis…….. 40

3.7 X-ray diffraction (XRD) results and analysis……. 43

3.8 Summary and Conclusions …….. 48

3.9 References……... 50

Chapter Four: The influence of REE β-diketone complexes on the corrosion behaviour of mild steel and 304 SS in 3.5 % NaCl solution…….…. 54

Abstract…….…… 55

4.1 Introduction…….…… 56

4.2 Experimental procedures…….…… 58

4.2.1 Test and inhibitor solutions…….……..58

4.3 Material preparation…… 58

4.4 Weight loss tests…….. 59

4.5 Potentiodynamic polarisation experiments……. 60

4.6 Surface analyses of the specimens…….……. 61

4.6.1 Scanning Electron Microscopy (SEM)…….61

4.6.2 Optical microscopy……..61

4.6.3 Raman spectroscopy (RS)…… 62

4.6.4 Fourier-Transform Infrared Spectroscopy (FTIR)……62

4.7 Results and discussion…….…… 62

4.7.1 Weight loss results…… 62

4.7.2 Potentiodynamic polarisation measurements……65

4.8 Surface analysis of the specimens……70

4.8.1 Optical microscopy…….…….. 70

4.13 Scanning electron microscopy and energy-dispersive x-ray spectroscopy analysis (SEM/EDS)……...…74

4.9 surface mapping of the mild steel…… 79

4.9.1 Fourier-Transform Infrared spectroscopy (FTIR) analysis…….. 79

4.9.2.2 Raman spectroscopy……. 80

4.10 Conclusions……..…. 81

4.11 References……..…. 83

Chapter Five: Rare Earth Element (REE) β-diketone Complexes as Novel Corrosion Inhibitors for 304 and 316 Stainless Steel in 0.1 M HCl Solution…….. 89

Abstract……. 90

5.1 Introduction……. 91

5.2 Experimental Section…….. 92

5.2.1 Materials and Preparation…… 92

5.3 Surface Analysis……. 94

5.4 Weight loss Measurements…….. 94

5.5 Potentiodynamic Polarisation Experiments……95

5.6 Results and Discussion……... 95

5.6.1 Weight Loss Measurement……95

5.6.2 Potentiodynamic Polarisation Measurements……96

5.7 Surface Analyses……. 102

5.7.1 Scanning Electron Microscopy (SEM)…… 102

5.8 Raman Spectroscopy…… 106

5.9 Fourier Transform Infrared Spectroscopy (FTIR)…… 108

5.10 Conclusions……110

5.11 References…… 111

Chapter Six: Conclusions and Recommendations……..…… 111

6.1 Conclusions and Recommendations…… 115

6.2 Recommendations……116

APPENDIX

Derivation of formula for the exposed total surface area of coupon…… 119

Calculated yields of the synthesised REE β-diketone complexes…… 121

Reaction equation for the synthesises REE β-diketone complexes…… 122

Calculation for the preparation of 0.1 M hydrochloric acid solution…….. 124

List of Figures

Figure 2.1: Classification of corrosion inhibitors (Modified from Faisal et al., 2018)…… 8

Figure 2.2: Electrochemical behaviour of (a) anodic inhibitor as compared to (b) without inhibitor in a potentiodynamic polarisation curve (Modified from El-Meligi, 2010)…… 9

Figure 2.3: Electrochemical behaviour of (a) cathodic inhibitors as compared to (b) without inhibitor in a potentiodynamic polarisation curve (Modified from El-Meligi, 2010). … …… 11

Figure 2.4: Potentiodynamic polarisation curve describing the behaviour of a solution containing (a) mixed inhibitor as compared to a solution (b) without inhibitor (Modified from El-Meligi, 2010). ……. 12

Figure 2.5: Illustration of inhibitor (represented as blue dots) adsorption on the surface of a metal (Modified from Quraishi et al., 2020)……..13

Figure 3.1: Stacked FT-IR spectra of the synthesised cerium, lanthanum and scandium acetylacetone complexes…… 29

Figure 3.2: Stacked FT-IR spectra of the synthesised cerium, lanthanum and scandium hexafluoroacetylacetone complexes…… 30

Figure 3.3: Stacked FT-IR spectra of the synthesised cerium, lanthanum and scandium trifluoroacetylacetone complexes…… 31

Figure 3.4: Stacked FT-IR spectra of the synthesised cerium, lanthanum and scandium dibenzoylmethane complexes…… 32

Figure 3.5: Stacked FT-IR spectra of the synthesised cerium, lanthanum and scandium thenoyltrifluroacetone complexes…… 33

Figure 3.6: Stacked Raman spectra of the synthesised cerium, lanthanum and scandium acetylacetone complexes……. 36

Figure 3.7: Stacked Raman spectra of the synthesised cerium, lanthanum and scandium hexafluoroacetylacetone complexes…… 37

Figure 3.8: Stacked Raman spectra of the synthesised cerium, lanthanum and scandium trifluoroacetylacetone complexes…….. 38

Figure 3.9: Stacked Raman spectra of the synthesised cerium, lanthanum and scandium dibenzoylmethane complexes…….. 39

Figure 3.10: Stacked Raman spectra of the synthesised cerium, lanthanum and scandium thenoyltrifluroacetone complexes…… 40

Figure 3.11: Mass spectrum of lanthanum dibenzoylmethane, $La(dbm)_3$ complex (Intensity against m/z)…… 42

Figure 3.12: Mass spectrum of Scandium thenoyltrifluoroacetone, $Sc(tta)_3$ complex (Intensity against m/z)…….. 42

Figure 3.13: Mass spectrum of cerium acetylacetone, $Ce(acac)_3$ complex (Intensity against m/z)……... 43

Figure 3.14: Stacked XRD patterns of the synthesised cerium, lanthanum and scandium acetylacetone complexes…….. 44

Figure 3.15: Stacked XRD patterns of the synthesised cerium, lanthanum and scandium hexafluroacetylacetone complexes……... 45

Figure 3.16: Stacked XRD patterns of the synthesised cerium, lanthanum and scandium trifluroacetylacetone complexes…….. 46

Figure 3.17: Stacked XRD patterns of the synthesised cerium, lanthanum and scandium dibenzoylmethane complexes…….. 47

Figure 3.18: Stacked XRD patterns of the synthesised cerium, lanthanum and scandium thenoyltrifluroacetone complexes…… 48

Figure 4.1: Chemical structures of (a) metal acetylacetonate and (b) metal hexafluoroacetylacetone, where M = Ce or La (Okawara et al., 2014).…… 58

Figure 4.2: EDX spectra of (a) and (b) MS coupon exposed to 3.5% NaCl solution containing $La(acac)_3$ and $Ce(acac)_3$, (c) and (d) 304 SS inhibited with $La(hfac)_3$ and $Ce(hfac)_3$……. 64

Figure 4.3: Potentiodynamic polarisation curves of mild steel in 3.5 % NaCl solution with (a) MS without inhibitor (b) $Ce(acac)_3$ (c) $Ce(hfac)_3$ (d) $La(acac)_3$ (e) $La(hfac)_3$ inhibitor…… 67

Figure 4.4: Potentiodynamic polarisation curves of 304 SS in 3.5 % NaCl solution with (f) 304 SS without inhibitor (g) $Ce(acac)_3$ (h) $Ce(hfac)_3$ (i) $La(acac)_3$ (j) $La(hfac)_3$ inhibitor…… 68

Figure 4.5: Optical micrographs of (a) MS and (e) 304 SS electrode samples before exposure to NaCl solution, (b), (c), (d) MS and (f), (g), (h) 304 SS samples obtained at 20^{o}C, 40^{o}C, and 60^{o}C in 3.5 % NaCl solution after performing the electrochemical corrosion tests…… 71

Figure 4.6: Optical micrographs of inhibited mild steel in 3.5 % NaCl solution doped with $Ce(acac)_3$ and $La(acac)_3$ at 20^{o}C, 40^{o}C and 60^{o}C……. 72

Figure 4.7: Optical micrographs of inhibited mild steel in 3.5 % NaCl solution doped with $Ce(hfac)_3$ and $La(hfca)_3$ at 20^{o}C, 40^{o}C and 60^{o}C…… 73

Figure 4.8: SEM micrographs of MS and 304 SS electrode surfaces before exposure in NaCl solution…… 75

Figure 4.9: SEM micrographs of uninhibited MS and 304 SS sample surfaces obtained after exposure to 3.5 % NaCl solution at 20^{o}C, 40^{o}C, and 60^{o}C…… 75

Figure 4.10: SEM micrographs of inhibited mild steel sample surfaces with $Ce(acac)_3$ and $La(acac)_3$ obtained after exposure to 3.5 % NaCl solutions at 20°C, 40°C, and 60°C…… 76

Figure 4.11: SEM micrographs of 304 SS sample surfaces inhibited with $Ce(hfac)_3$ and $La(hfac)_3$ obtained after exposure to 3.5 % NaCl solutions at 20°C, 40°C and 60°C…… 77

Figure 4.12: EDS of (a) and (b) MS in 3.5 % NaCl solution containing 0.5 % wt. (m/v) of $Ce(acac)_3$ and $Ce(hfac)_3$ and (c) and (d) 304 SS with $La(acac)_3$ and $La(hfac)_3$…… 78

Figure 5.1: Chemical structures of (a) metal acetylacetonate and (b) metal hexafluoroacetylacetone, where M = Ce or La (Modified from Andersen et al., 2020)…….....…… 93

Figure 5.2: Potentiodynamic polarisation curves of 304 SS in 0.1 M HCl solution (a) without inhibitor and with (b) $Ce(acac)_3$, (c) $La(acac)_3$, (d) $Ce(hfac)_3$ and (e) $La(hfac)_3$ inhibitors…… 98

Figure 5.3: Potentiodynamic polarisation curves of 316 SS in 0.1 M HCl solution (a) without inhibitors and with (b) $Ce(acac)_3$, (c) $La(acac)_3$, (d) $Ce(hfac)_3$ and (e) $La(hfac)_3$ inhibitors…… 100

Figure 5.4: SEM micrographs of 304 SS sample surfacesin the absence and presence of $Ce(acac)_3$ and $La(acac)_3$ after exposure to 0.1 M HCl solutions at 20, 40 and 60°C…… 103

Figure 5.5: SEM micrographs of 316 SS sample surfaces in the absence and presence of $Ce(acac)_3$, $La(acac)_3$, $Ce(hfac)_3$ and $La(hfac)_3$ after exposure to 0.1 M HCl solutions at 20, 40 and 60°C……....104

Figure 5.6: EDS of 304 SS after exposure to a HCl solution containing (a) $Ce(acac)_3$ at 20°C and (b) $La(acac)_3$ at 60°C with inhibitors at 0.5 % wt. (m/v) concentration…… 105

Figure 5.7: EDS of 316 SS after exposure to a HCl solution containing (c) $Ce(hfac)_3$ 20°C and (d) $La(hfac)_3$ at 60°C with inhibitors at 0.5 % wt. (m/v) concentration…… 106

Figure 5.8: Raman spectra of $Ce(acac)_3$, $La(acac)_3$, $Ce(hfac)_3$and $La(hfac)_3$ inhibitors and the corrosion products formed on 304 and 316 SS……. 107

Figure 5.9: IR spectra of $Ce(acac)_3$, $La(acac)_3$, $Ce(hfac)_3$ and $La(hfac)_3$ inhibitors and the corrosion products formed on 304 and 316 SS……. 109

Figure A1: Suspended coupons in a corrosive media containing REE β-diketone complex shown weight loss test……. 117

Figure A2: Specification for mild steel, 304 and 316 stainless steel coupons used for weight loss test……. 118

Figure A3: A schematic diagram showing the corrosion cell setup including all three electrodes as labelled (working, reference and counter), water pump and water bath…… 120

List of Tables

Table 2.1: Example of some common β-diketones and their structural formula (Huang, 2010)……..…. 17

Table 3.1 Melting points of the synthesised rare earth element complexes and the literature values…… 26

Table 3.2: Significant band of FT-IR spectra of synthesised rare earth element β-diketone complexes…… 28

Table 3.3: Observed Raman band position frequencies of the synthesised rare earth element β-diketone complexes…… 35

Table 3.4: Found and calculated values of the selected synthesised REE β-diketone complexes…… 41

Table 4.1: Nominal compositions of mild steel and 304 stainless steel…… 59

Table 4.2: Comparison of corrosion rate of mild steel and 304 SS and inhibition efficiency in the absence and presence of $Ce(acac)_3$, $Ce(hfac)_3$, $La(acac)_3$ and $La(hfac)_3$ inhibitors in 3.5 % NaCl solution……63

Table 4.3: Electrochemical parameters of MS obtained from the potentiodynamic polarisation curves in 3.5 % NaCl solution and with corrosion inhibitors $Ce(acac)_3$, $Ce(hfac)_3$, $La(acac)_3$ and $La(hfac)_3$ present in the solution…….. 69

Table 4.4: Electrochemical parameters of 304 SS obtained from the potentiodynamic polarisation curves in 3.5 % NaCl solution and with corrosion inhibitors $Ce(acac)_3$, $Ce(hfac)_3$, $La(acac)_3$ and $La(hfac)_3$ present in the solution…….…….... 79

Table 4.5: IR frequency bands of REE $(\beta - diketone)_3$ inhibitors and the corrosion products formed on mild steel and 304 stainless steel…… 81

Table 4.6: Raman frequency shifts of $Ce(acac)_3$, $La(acac)3$, $Ce(hfac)3$ and $La(hfac)3$ inhibitor and the corrosion products on mild steel and 304 stainless steel……. 82

Table 5.1: Comparison of corrosion rates of 304 SS and 316 SS and the inhibition efficiency in the absence and presence of $Ce(acac)_3$, $La(acac)_3$, $Ce(hfac)_3$ and $La(hfac)_3$ in 0.1 M HCl solution…… 97

Table 5.2: Electrochemical parameters of 304 SS obtained from potentiodynamic polarisation curves measured in 0.1 M HCl solution and with corrosion inhibitors $Ce(acac)_3$, $La(acac)_3$, $Ce(hfac)_3$ and $La(hfac)_3$ present in the solution…… 100

Table 5.3: Electrochemical parameters of 316 SS obtained from potentiodynamic polarisation curves measured in 0.1 M HCl solution and with corrosion inhibitors $Ce(acac)_3$, $La(acac)_3$, $Ce(hfac)_3$ and $La(hfac)_3$ present in the solution…… 102

Table 5.4: Raman frequency$Ce(acac)_3$, $La(acac)_3$, $Ce(hfac)_3$and $La(hfac)_3$ inhibitors and the corrosion products formed on 304 and 316 SS…… 109

Table A1: Corrosion rate expression with different units…… 119

Table A2: Calculated area of the exposed to surface area of the mild steel and stainless steels and its density…… 121

Table A3: Actual masses and the yields obtained for the synthesised REE β-diketone complexes…… 123

List of Abbreviation and symbols

Abbreviation and symbols	Full Meaning
acac	Acetylacetone
AFM	Atomic force microscopy
ARL	Aeronautical Research Laboratory
βa	Anodic Tafel slope
βc	Cathodic Tafel slope
bzac	Benzoylacetone
bztfac	Benzoyltrifluoroacetone
Ce	Cerium
$Ce(acac)_3$	Cerium acetylacetone
$CeCl_3$	Cerium chloride
$Ce(hfac)_3$	Cerium hexafluoroacetylacetone
$Ce(dbm)_3$	Cerium dibenzoylmethane
$Ce(tfac)_3$	Cerium trifluoroacetylacetone
$Ce(tta)_3$	Cerium thenoyltrifluoroacetone
CV	Cyclic voltammetry
D	Density
DC	Direct current

CR	Corrosion rate
dbm	Dibenzoylmethane
E_{coor}	Corrosion potential
EIS	Electrochemical impedance spectroscopy
EDS	Energy disperse x-ray spectroscopy
E_{EQ}	Equivalent weight
FTIR	Fourier transform infrared spectroscopy
GNP	Gross national product
hfac	Hexafluoroacetylacetone
HCl	Hydrochloric acid
i_{coor}	Corrosion current
IE	Inhibition efficiency
IR	Infrared spectroscopy
KOH	Potassium hydroxide
La	Lanthanum
$La(acac)_3$	Lanthanum acetylacetone
$LaCl_3$	Lanthanum chloride
$La(dbm)_3$	Lanthanum dibenzoylmethane
$La(hfac)_3$	Lanthanum hexafluoroacetylacetone
$La(tfac)_3$	Lanthanum trifluoroacetylacetone

$La(tta)_3$	Lanthanum thenoyltrifluoroacetone
LPR	Linear polarisation resistance
MP	Melting point
MS	Mild steel
MS	Mass spectroscopy
NaCl	Sodium chloride
NaOH	Sodium hydroxide
OCP	Open circuit potential
OM	Optical microscopy
ppm	Part per million
PDP	Potentiodynamic polarisation
REE	Rare earth element
REM	Rare earth metal
RS	Raman spectroscopy
Sc	Scandium
$Sc(acac)_3$	Scandium acetylacetone
$ScCl_3$	Scandium chloride
$Sc(dbm)_3$	Scandium dibenzoylmethane
$Sc(hfac)_3$	Scandium hexafluoroacetylacetone
$Sc(tfac)_3$	Scandium trifluoroacetylacetone

$Sc(tta)_3$	Scandium thenoyltrifluoroacetone
SEM	Scanning electron microscopy
SS	Stainless steel
tta	Thenoyltrifluoroacetone
tfac	Trifluoroacetylacetone
VPI	Vapour phase inhibitor
VCI	Volatile corrosion inhibitors
XRD	X-ray diffraction

CHAPTER ONE

INTRODUCTION

1.1 BACKGROUND

The word “Corrosion” indicates degradation of a metal or material or surface damage in an aggressive environment. The exposure of metals and alloys to corroding environments results in the degradation of the materials. Corrosion is a chemical or electrochemical oxidation process, in which there is an exchange of electrons between the metal and the environment. The environment, which is also known as an electrolyte, is a solution that is capable of conducting an electrical current or allows the transfer of charge (positively and negatively charged ions called cations and anions, respectively) to take place. This environment can be in the form of a liquid, gas, solid, or a hybrid. For a corrosion process to proceed, it requires at least two half-reactions and this will make the current flow from one reaction to the other reaction. These reactions are termed anodic and cathodic half-reactions (Ahmad, 2006; Perez, 2004; Tanwar et al., 2018).

The driving force that causes metal to corrode is the fact that when metals are exposed to a corrosive environment, they will revert to their original stable states in which they initially occurred (ores) (Schweitzer, 2006; Ahmed et al., 2017). The corrosion of metals has been a fundamental problem for both scientists and engineers, and this has received significant attention in many industries that deal with metals and materials in a corrosive environment. Generally, mild steel and stainless steel are widely used as construction materials in industries due to their low cost and exceptional mechanical properties. Since corrosive media are widely used in industry, the interaction between these media and metals is inevitable. If corrosion problems are not curbed or controlled, it can cause economic losses. (El-Sherik, 2017; Revie, 2008; Sastri, 2015). For the effective protection of metals against corrosion in either acidic, alkaline, or neutral media, the use of inhibitors should be considered as one of the most effective methods. Inhibitors are chemicals or mixtures that when applied in aggressive environments in a minute concentration, isolate the metals from the aggressive environment by forming a passive film or protective layer on the surface of the metals.

It should be noted that the use of anti-corrosion chemicals or inhibitors does not alter the properties of the metallic material. (Forsyth et al., 2014; Forsyth and Hinton, 2014). In contrast

to other processes for corrosion control, corrosion inhibitors are cost-effective, simple to apply, and its broadly used in industrial processes such as oil fields, pickling, acidification of oil and gas wells, cooling water systems, transportation, and storage of metal products. With the improvement in technology and environmental awareness in terms of hazard and toxicity, more attention has been focused on the innovation and application of environmentally benign corrosion inhibitors (Peng et al., 2018; Mohammadi et al., 2020).

The catastrophic effects of corrosion have received attention in several prominent industrial economies, such as the USA, the UK, China, India Japan, Australia, Canada, Germany. This has led to increasing efforts to study the cost and prevention of corrosion. Annually, 3 to 5% of countries' gross national products (GNP), have been expended on corrosion control (Bardal, 2003; Sastri, 2015; El-Sherik, 2017).

1.2 PROBLEM STATEMENT

Corrosion phenomena are well-known in most industries and it is an unavoidable but controllable process. The negative adverse effects of corrosion could cause a disaster in terms of equipment failure and loss of life if adequate care and control are not in place.

Different mechanisms can be employed to mitigate corrosion of metallic structures, but due to the issues of toxicity, environmental degradation caused by some of these inhibitors, such as chromate compounds, heavy metals, amines, and imidazoline based inhibitors that are widely used for corrosion control, there has been a surge in investigation and application of eco-friendly inhibitors, which are also known as green inhibitors that are non-toxic and environmentally benign (Blin et al., 2004; Forsyth et al., 2011).

Rare earth β-diketone complexes of cerium and lanthanum which could be also regarded as green inhibitors will be studied and synthesised as corrosion inhibitors for mild steel and stainless steel in chloride media.

1.3 RESEARCH QUESTIONS

1. Can any of the two rare earth element (REE) complexes of lanthanum (La) and cerium (Ce) β-diketone compounds be considered as suitable corrosion inhibitors when used in HCl and NaCl solutions.
2. Do the inhibitors act as anodic, cathodic, or mixed inhibitors when applied?

1.4 RESEARCH AIM AND OBJECTIVES

The overall aim of the investigation is to synthesize selected REE corrosion inhibitors and test their efficiency in various corrosive media. To achieve this aim, the following objectives need to be met:

1. To synthesise and characterise rare earth element β-diketone inhibitors. The compounds to be used are complexes of lanthanum (La), cerium (Ce) and scandium (Sc) with different β-diketones.
2. To examine the performance of the inhibitors in HCl and acidified NaCl solution to inhibit general corrosion.
3. To establish if the inhibitors act as anodic, cathodic, or mixed inhibitors.

1.5 HYPOTHESIS

This project is not only aimed at synthesising and characterisation of REE β-diketone complexes but also to investigate the inhibition mechanism and mode of action of some synthesised REE complexes. Achieving this will be of great help to determine whether REE β-diketone complexes act as an anodic, cathodic, or mixed type of inhibitor. In recent years, several inorganic compounds of REE origin such as chloride, nitrate, sulfate, and oxide have been investigated as possible replacements for hexavalent toxic and carcinogenic chromate inhibitors. However, an investigation of environmentally benign REE β-diketone inhibitor has not been reported in the literature. Investigations on how the rare-earth β-diketone complexes inhibit the localised corrosion process over the whole alloy surface when applied in a corrosive

environment could reveal knowledge of the inhibitor's mechanism and potential absorbed layer on the metal surface.

1.6 DISSERTATION OUTLINE

This dissertation investigates the corrosion inhibition of a mild steel and austenitic stainless steel (304 and 316 SS) in 3.5% NaCl and 0.1 M HCl solution using novel REE β-diketone complexes. During this investigation the weight-loss method, potentiodynamic polarisation technique and surface analyses will be employed. The dissertation comprises six chapters and a brief outline of each chapter and its layout are provided below.

Chapter one: This chapter provides a brief introduction to corrosion in industries and problems associated with most corrosion inhibitors and the aims and objectives of the study.

Chapter two: This chapter focuses on the literature review; it elucidates the effect of chromate-based inhibitors on humans and their environment. It also explains different types of inhibitors and the mechanism of operation. Finally, it expatiates on the benefit of REE salts as a new form of green inhibitor.

Chapter three: This chapter presents the synthesis and characterisation of various REE β-diketonates complexes that were synthesised.

Chapter four: This chapter studies the influence of REE β-diketone complexes on the corrosion behaviour of mild steel and 304 SS in 3.5 % NaCl solution.

Chapter five: this work examines the efficacy and the mode of action of organo-metallic compounds of β-diketone complexes as a novel form of corrosion inhibitors for 304 and 316 SS in 0.1 M HCl solution.

Chapter six: The chapter summarises overall conclusions drawn from the study and presents some recommendations for future research.

References to all articles and sources used in this study are provided at the end of each chapter of the dissertation. Other relevant information related to this study is presented in the Appendix section.

1.7 REFERENCES

Ahmad, Z. (2006). Principles of Corrosion Engineering and Corrosion Control (1st ed.). Butterworth-Heinemann, Oxford, UK.

Ahmed, M, I., Islam, M. A., & Ali, M. N. (2017). Determination of corrosion rate of mild steel in different medium measuring current density. Proceedings of the International Conference on Mechanical Engineering and Renewable Energy 18–20, Chittagong, Bangladesh.

Bardal, E. (2003). Corrosion and Protection. Springer, London, UK.

Blin, F., Leary, S.G., Wilson, K., Deacon, G.B., Junk, P.C., & Forsyth, M. (2004). Corrosion mitigation of mild steel by new rare earth cinnamate compounds. Applied Electrochemistry, 34(6), pp. 591-599.

El-Sherik, A. M. (2017). Trends in Oil and Gas Corrosion Research and Technologies. Woodhead Publishing. Duxford, UK.

Forsyth, M., Seter, M., Hinton, B., Deacon, G., & Junk, P. (2011). New "Green" corrosion inhibitors based on rare earth compounds. Australian Journal of Chemistry, 64(6), 812–819.

Forsyth, M., Seter, M., Tan, M. Y., & Hinton, B. (2014). Recent developments in corrosion inhibitors based on rare earth metal compounds. Corrosion Engineering Science and Technology, 49(2), 130–135.

Forsyth, M., & Hinton, B. (2014). Rare Earth-based Corrosion Inhibitors. Woodhead Publishing Series, Cambridge, UK.

Mohammadi, I., Shahrabi, T., Mahdavian, M., & Izadi, M. (2020). Cerium/diethyldithiocarbamate complex as a novel corrosion inhibitive pigment for AA2024-T3. Scientific Reports, 1–15.

Peng, Y., Hughes, A. E., Deacon, G. B., Junk, P. C., Hinton, B. R. W., Forsyth, M., Mardel, J. I., & Somers, A. E. (2018). A study of rare-earth 3-(4-methyl benzoyl)-propanoate compounds as corrosion inhibitors for AS1020 mild steel in NaCl solutions. Corrosion

Science, 145, 199–211.

Perez. N. (2004). Electrochemistry and Corrosion Science (1st ed.). Kluwer Academic Publishers, Boston.

Revie. R. W. (2008). Corrosion and corrosion control: An Introduction to Corrosion Science and Engineering (4th ed.). John Wiley & Sons, Inc. New Jersey.

Sastri V. S., (2015). 'Challenges in Corrosion Costs, Causes, Consequences and Control (1st edn.), John Wiley & Sons Inc, Hoboken, New Jersey.

Schweitzer, P. A. (2006). Fundamentals of metallic corrosion. (2nd edn.). CRC Press, Boca Raton, New York.

Tanwar, D., Gohar, S. K., & Sankar, P. R. (2018). Corrosion Inhibition of Mild Steel by Benzotriazole in 1M and 2M Sulfuric Acid Solution. International Journal of Theoretical & Applied Sciences, 10(1) 140-145.

CHAPTER TWO

LITERATURE REVIEW

2.1 INTRODUCTION

Over the years, chromate compounds have been the most extensively used as corrosion inhibitors in aqueous media and protective coatings. However, due to the recent recognition that chromate based compounds are detrimental to human health and the environment, there has been a surge in the search for effective corrosion inhibitors that are environmentally benign (Forsyth et al., 2014; Somers et al., 2018). Inhibitors are used to retard or mitigate the rate of corrosion of metals or alloys and enhance the life span or durability of metallic structures in various corrosive environments (Somers et al., 2018).

REE salts are some of the potential green corrosion inhibitors that have received attention and consideration for corrosion control of a wide range of metals and alloys (Somers et al., 2018). About four decades ago, researchers at the Aeronautical Research Laboratory (ARL), in the USA began to examine the efficacy of REE salts for corrosion mitigation. Similar results from other laboratories (as those by ARL) have proved that REE salts efficiently retard the corrosion of metals and alloys in many scenarios (Hinton, 1992; Raja et al., 2016).

2.2 CORROSION INHIBITORS

Stainless steels are reasonably corrosion resistant and have a wide range of uses as construction materials in many industries, such as power plants, building construction, and transportation, yet they are still susceptible to corrosion in acidic and alkaline media (Baddoo, 2008; Kareem, 2013). Terachi et al. (2012) reported that when stainless steel is been alloyed with noble metals, it helps to increase the corrosion resistance of the steel in an aggressive environment. For any form of stainless steel to be produced, it must have a minimum chromium content of about 12 % wt. (Chiou, 1989; Uwiringiyimana et al., 2016). However, this minimum content of chromium is not enough to retard corrosion in acids like sulphuric acid, or hydrochloric acid.

As a result of the intense acid attack on the metal, the use of inhibitors should be considered as the first line of defence to mitigate or resist any form of a chemical attack on metal.

A corrosion inhibitor can be defined as a chemical additive or substance which decelerates or slows down a reaction in an aggressive environment when applied in a small concentration. The mechanism by which corrosion inhibitors work is by either absorption or by forming a protecting film layer on the metal surface. It can impede the cathodic or anodic reaction or both reactions (Bernal et al., 1995). There are different ways to classify corrosion inhibitors. Some authors may classify them according to their mode of operation or by chemical functionality (Faisal et al., 2018). One of the general methods of classification based on the mode of operation, mechanism, and environment is shown in Figure 2.1.

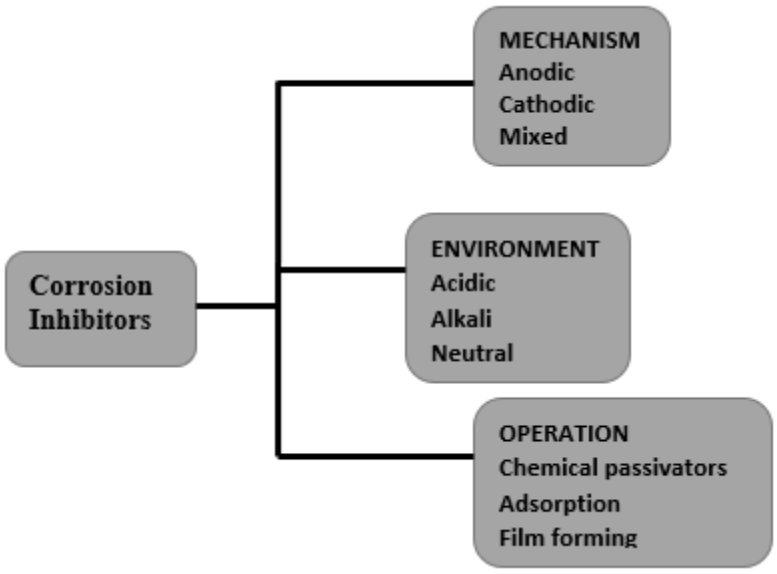


Figure 2.1: Classification of corrosion inhibitors (Modified from Faisal et al., 2018).

2.3 MECHANISMS OF ACTIONS OF INHIBITORS

2.3.1 Anodic Inhibitor

The mechanism of anodic inhibitors, which are also known as passivation inhibitors, is by reducing or blocking the anodic reaction. Anodic inhibitors form an insoluble passivating film

by a reaction to form a corrosion product, which will then be deposited on the metal's surface to protect the metal from corrosion. When the film forms on the metal's surface, there will be an increase in the anodic polarisation and hence an increase in the corrosion potential. (El-Meligi, 2010)

Figure 2.2 shows a potentiodynamic polarisation curve that describes the electrochemical behaviour of anodic inhibitors. The reaction at the anode is affected by the corrosion inhibitors while the corrosion potential is displaced to a more positive value. Likewise, there is a decrease in the value of corrosion current in the polarisation curve upon the addition of an anodic inhibitor.

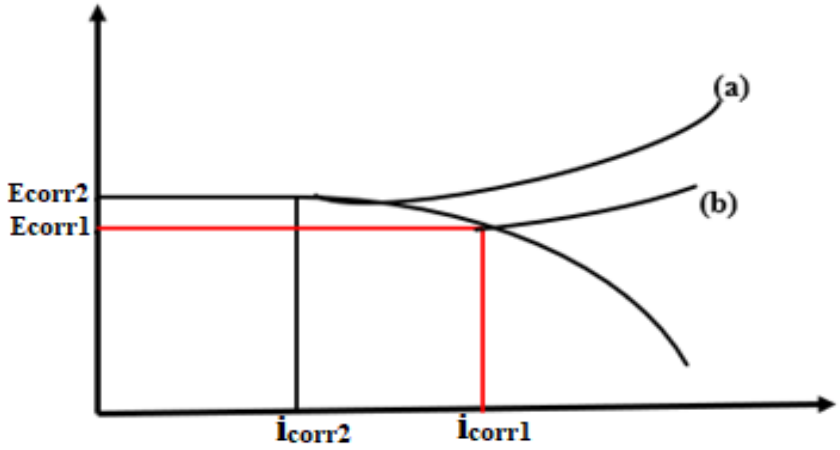


Figure 2.2: Electrochemical behaviour of a metal surface (a) with anodic inhibitor as compared to (b) without inhibitor in a potentiodynamic polarisation curve (Modified from El-Meligi, 2010).

Examples of anodic inhibitors which form a sparingly soluble compounds with high oxygen content that restrain the corrosion reaction taking place at the anode site, are ions of transition metals, phosphates, and chromates (Forsyth et al., 2011). However, if the inhibitors are depleted, present in too low a concentration or dissolution of the passive film left some part of the metal unprotected, it might give rise to a severe local attack. Inorganic inhibitors of molybdates, tungstates, phosphates, silicates compounds and compounds with high oxygen content - ions of transition metals, and chromates are an example of this type of inhibitor (El-Meligi, 2010; Reza et al., 2021).

2.3.2 Cathodic inhibitors

Cathodic inhibitors are a type of inhibitor that slows down corrosion rate at the cathodic site of the electrochemical corrosion reaction. The mechanism of this type of control is by blocking the cathodic area by precipitation (i.e., the cations migrate towards the surface of the cathode and then precipitate at the cathode surface area either chemically or electrochemically and thus block the surface.) Once this has occurred, the cathodic area will be passivated as a result of an increase of impedance of the precipitated metal or metal containing film and reduction in the rate of diffusion of the species involved at the cathodic area (Landolt, 2007). Since hydrogen is formed at the cathodic site in acidic solutions, this decrease will reduce the rate of corrosion at the metal's surface. Cathodic inhibitors are generally safer compared to anodic inhibitors that initiate pitting corrosion when applied at too low a concentration. If an alkaline solution or a closely near-neutral solution are used in the presence of inorganic ions such as sulphite and bisulphite, these ions tend to form a protective film that decelerates the rate of cathodic reaction or limits the oxygen diffusion to the metal's surface (Rashid & Khadom, 2020). Hence, the rate of corrosion can also be reduced effectively if the reaction or environment has been depleted of oxygen. This can be achieved by introducing oxygen scavengers (i.e., sodium sulphite and hydrazine) to the corrosive environment (Reza et al., 2021). The oxygen scavengers react with the oxygen in the solution and remove the oxygen from the solution. Just like in an electrochemical cell where purging takes to remove oxygen content during the electrochemical experiment, boiling to lower the dissolved oxygen concentration or vacuum de-aeration are also effective methods to reduce the oxygen content in a solution. The corrosion potential is shifted to a more negative value upon application of a cathodic inhibitor as shown in Figure 2.3 (Boudellioua et al., 2019; Reza et al., 2021).

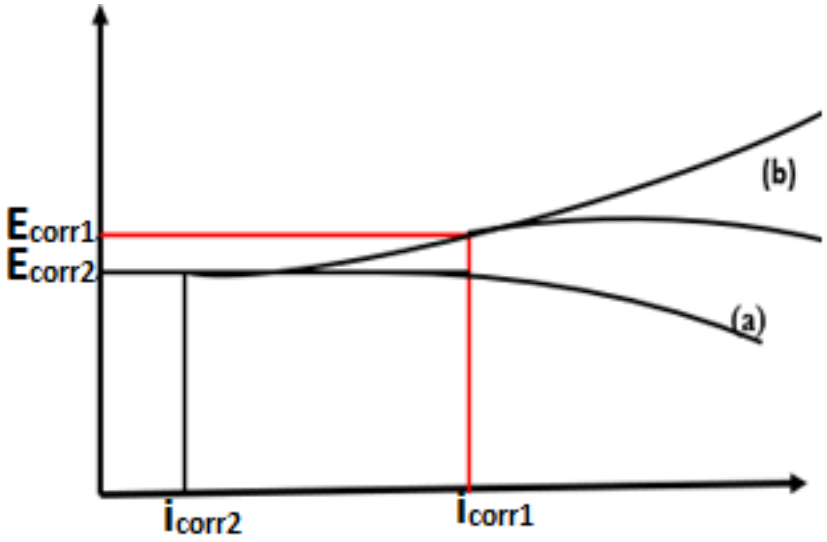


Figure 2.3: Electrochemical behaviour of a metal surface (a) with cathodic inhibitor as compared to (b) without inhibitor in a potentiodynamic polarisation curve (Modified from El-Meligi, 2010).

2.3.3 Mixed inhibitors

These are inhibitors that cannot be designated either as cathodic or anodic. They are called mixed inhibitors since they have the ability to control or inhibit both the anodic and cathodic reactions involved in the corrosion. Inhibitors of this nature block both the anodic and cathodic areas of the metal by precipitating an oxide or hydroxide film-forming compound on the surface of a metal. Mixed inhibitors are safer, unlike anodic inhibitors which tend to initiate pitting corrosion when used in too small an amount of concentration. Typical inhibitors such as silicates and phosphate are good examples of mixed inhibitors, since they control both the anodic and cathodic corrosion reactions (Reza et al., 2021). A mixed type of inhibitor behaviour can be identified in a polarisation curve if there is a decrease in corrosion current upon addition of inhibitor, while the corrosion potential remains the same or only slightly shifts to a higher or lower value as shown in Figure 2.4 (El-Meligi, 2010; Khaled 2013).

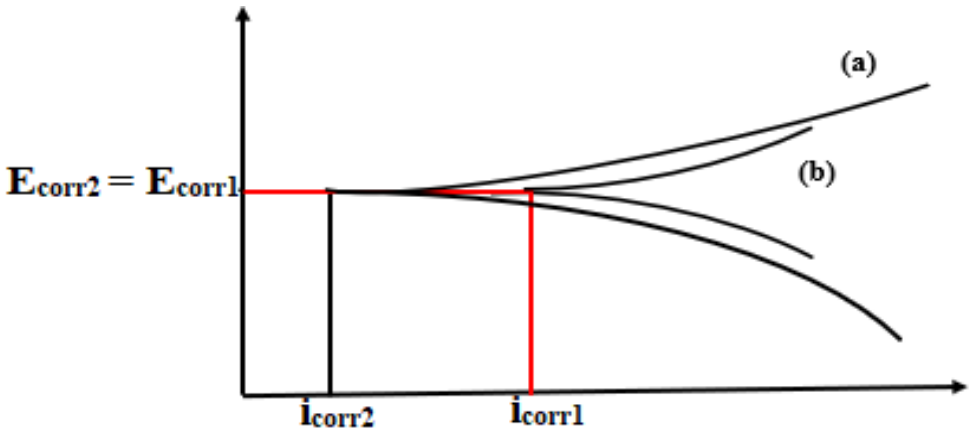


Figure 2.4: Potentiodynamic polarisation curve describing the behaviour of a solution containing (a) mixed inhibitor as compared to a solution (b) without inhibitor (Modified from El-Meligi, 2010).

2.4 INHIBITORS BASED ON MODE OF PROTECTION

2.4.1 Chemical passivators

A chemical passivator is used for the pre-treatment of a metal, which increases the natural passivity of that metal. For instance, the oxidation resistance of stainless steel can be increased by pickling in nitric acid. This is done by immersing the passivated component or metal in a passivating solution at a specific concentration for a certain period and then removing and washing it, followed by drying the component before putting the metal into service. This type of treatment is often employed where the maximum degree of corrosion is required such as the manufacture of pharmaceuticals and semi-conductor materials. In some cases, chemical passivators are anodic inhibitors such as chromate, nitrite, molybdate, and orthophosphate which amplify passivation by raising the electrical potential of the metal. Once the metal attained its passivity, the corrosion rate of such a metal decreases (Kuznetsov, 1996). A chemical passivator like nitrite has been effective, but it does oxidise to nitrate when used in an open system. In the presence of oxygen, orthophosphate and molybdate compounds are excellent passivators. When molybdate is combined with other chemicals, it can be a very effective inhibitor. If orthophosphate is used on its own, it is not considered an oxidizer unless

it has been used in conjunction with oxygen. If iron is immersed in a deoxygenated phosphate solution, the corrosion potential will remain active and the corrosion rate will not reduce (Schweitzer, 2010).

2.4.2 Adsorption inhibitors

Adsorption inhibitors are organic compounds (in most cases) that have the ability to reduce the rate of corrosion by chemisorption, i.e. a process whereby the inhibitor is chemically adsorbed on the surface of the metal and forms a blanketing thin layer on the surface of the metal as shown in Figure 2.5. Examples of adsorption inhibitors are organic amines ($R-NH_2$), thiourea (NH_2CSNH_2), the carboxylic acids ($R-COOH$); and benzoate ($C_6H_5COO^-$) and organic molecules with multiple bonds in their structure (Shahid, 2011).

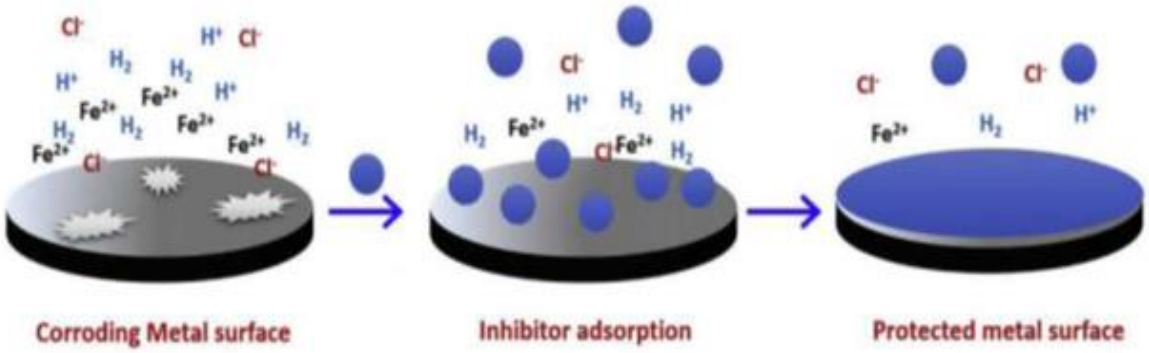


Figure 2.5: Illustration of inhibitor (represented as blue dots) adsorption on the surface of a metal (Modified from Quraishi et al., 2020).

2.4.3 Film forming inhibitors

Unlike the adsorption inhibitors which are chemically adsorbed onto the surface of the metal, film-forming inhibitors inhibit corrosion by forming a barrier film (Barmatov et al., 2015). Such inhibitors are specific to either cathode or anode. Compounds of zinc and calcium are examples of film-forming inhibitors that are widely used (Golfomitsou, 2006).

In most cases, REE compounds of cerium have proven to be effective corrosion inhibitor. According to literature reports, REE compounds behave as cathodic inhibitors (Davo & Damborenea, 2004; Yasakau et al., 2006). They act by blocking the cathodic sites by precipitating a film of REE oxide or hydroxide on the metallic alloys' surfaces (Amadeh et al., 2008). However, this is not always the case.

Somers et al. (2018) proved that REE salts are environmentally benign for corrosion control of metal and alloys. The study conducted to verify the inhibitive efficacy on mild steel using carboxylate compounds [i.e. REE[3-(4-methylbenzoyl)propanoate)] showed that the inhibition was due to the formation of a precipitated film barrier on the metal surface. Further studies of the film using Energy-disperse X-ray spectroscopy (EDS) and Infrared spectroscopy (IR) indicated that the protective film consisted of REE, and other elements such as iron, oxygen, and carbon. The studied compound acted as an anodic inhibitor.

Mohammedi et al. (2015) also proved that hydrated REE salts, namely, yttrium nitrate ($Y(NO_3)_3$) and cerium chloride heptahydrate ($CeCl_3.7H_2O$), when combine with sodium silicate (Na_2SiO_3), are effective corrosion inhibitors when used on carbon steel in an aqueous solution of NaCl. The presence of REE salts in the solution leads to the growth of a complex hydrated oxide film on the carbon steel's surface (Mohammedi et al., 2015). Further studies of the behaviour of these REE salts using potentiodynamic polarisation and impedance spectroscopy indicated that REE salts and sodium silicate salt affected both the anodic and cathodic parts of the reaction. Thus, REE/SiO_3^{2-} acted as a mixed inhibitor, with the cerium salt yielding better protection than the yttrium salt (Mohammedi et al., 2015).

Ghanbari et al., (2009) investigated the inhibitive effect of a β-diketone complex (i.e., acetylacetonate complex) on mild steel at concentrations of 0.01 M at 25°C in 1M phosphoric acid (H_3PO_4), the same H_3PO_4 solution was added separately with another solution of 0.1 M HCl, and also with 0.1 M NaCl. Upon addition of the β-diketone compound to 1 M H_3PO_4, and phosphoric solution containing 0.1 M HCl and 0.1 M NaCl solution, the DC polarisation curves of mild steel without and with the 0.01 M β-diketone compound shifted the corrosion potential toward more negative potentials and there was a reduction in the corrosion rate of mild steel. This was ascribed to adsorption of the β-diketone compound on the mild steel's surface. Adsorption of the β-diketone compound can block the anodic areas of the mild steel surface, thereby leading to a reduction of the electrochemical reaction rate. The reduction of the

cathodic reaction rate can be attributed to the formation of a protective film on a mild steel surface by the inhibitor. The β-diketone compound also increased the cathodic Tafel slope, which suggested that β-diketone acted as a cathodic inhibitor.

In a similar procedure, Amadeh et al. (2008) examined the corrosion behaviour of carbon steel using a mixture of cerium and lanthanum oxide in a ratio of 2:1 in sodium chloride as a corrosive inhibitor. In their studies, it was observed that when 500 ppm of inhibitor was added to a solution of 0.1 M NaCl it changed the cathodic part of the polarisation curve, while there was no significant change in the anodic part of the curve. When the inhibitor concentration was doubled to 1000 ppm, there was a shift in the corrosion potential (E_{corr}) to a more positive potential and the corrosion current density to a lower value (Amadeh et al., 2008). The Tafel polarisation slopes indicated that the inhibitor acted as a cathodic inhibitor at a 500 ppm concentration of inhibitor. However, at 1000 ppm, its behaviour resembled that of a mixed inhibitor.

Fouda et al. (2015) used lanthanum and samarium chloride to mitigate the corrosion of mild steel using a produced water as a corrosive medium. A slight change in the values of corrosion potential (E_{corr}), (in the range of 68 mV) suggested that both compounds behave as mixed types of inhibitors. The results showed that the values of anodic slope βa, (i.e., the Tafel slope at the anode) changed substantially in the presence of both the lanthanum and samarium chloride. Simultaneously with this, a noticeable effect also occurred in βc (i.e., the Tafel slope at the cathode). This suggested that both anodic and cathodic reactions were affected, but the effect on the cathodic reactions were more noticeable. As the concentration of the inhibitors increased from 100 to 400 ppm, the inhibition efficiency also increased proportionally.

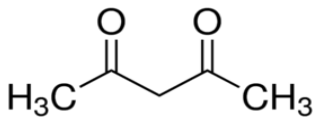
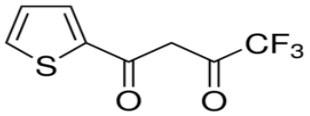
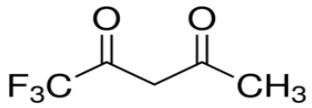
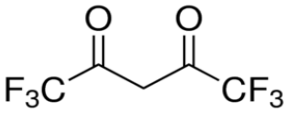
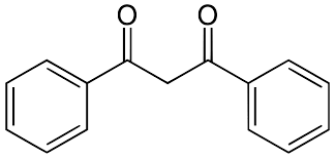
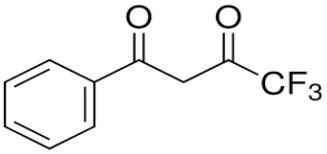
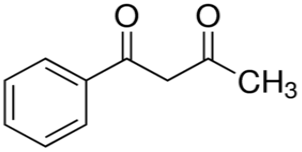
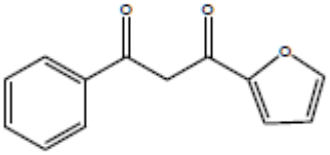
The inhibiting effect of cerium sulphate tetrahydrate on steel in 3.5% NaCl solutions was studied by Khaled (2013). Studies using atomic force microscopy (AFM) measurements revealed that upon the addition of cerium sulphate tetrahydrate to a solution of sodium chloride, the steel specimen surface roughness decreased because of adsorption of cerium oxide or hydroxide on the steel's surface. The corrosion potential in the presence of this inhibitor did not change much.

2.5 β-DIKETONATES AND THEIR METAL COMPLEXES

β-diketones or 1,3-diketones are dicarbonyl compounds that have two carbonyl functional groups which are separated by an α-carbon atom with two hydrogen atoms attached (methylene group, CH_2) (Huang, 2010; Urbaniak et al., 2011). They are of the most widely studied compounds due to their versatile commercial applications in various fields of coordination chemistry (Sumathi et al., 2011; Verma et al., 2011; Kumar & Sharma, 2012; Shokova et al., 2015; Bhise et al., 2019). The simplest β-diketone is acetylacetone (acac) $(CH_3)COCH_2CO(CH_3)$, where the substituents on both carbonyl groups are methyl groups as shown in Table 2.1 (a). The substituent groups that are attached to the carbonyl functional groups can be the same or different groups such as alkyl, aryl, fluorinated or chlorinated alkyl, phenyl, or heteroaromatic groups and the substituent groups are not necessarily equivalent as shown in Table 2.1 (Gschneidner et al., 2005; Huang, 2010; Urbaniak et al., 2011).

All other β-diketones could be considered as derivatives of acetylacetone (Table 2.1 (a)), where an alkyl group attached to a carbon in the carbonyl functional group is replaced by other groups (Table 2.1 (b to h)).

Table 2.1: Examples of some common β-diketones and their structural formula (Huang, 2010).

Name	Structural formula
(a) Acetylacetone (acac)	
(b) Thenoyltrifluoroacetone (tta)	
(c) Trifluoroacetylacetone (tfac)	
(d) Hexafluoroacetylacetone (hfac)	
(e) Dibenzoylmethane (dbm)	
(f) Benzoyltrifluoroacetone (btfac)	
(g) Benzoylacetone (bzac)	
(h) 1-Furan-2-yl-3-phenyl-propane-1,3-dione	

The type of the substituents on the alkyl group influences the chemical properties of the β-diketones and the corresponding REE β-diketone complexes (Gschneidner et al., 2005). For instance, when one or two $-CH_3$ groups in acetylacetonate ligands are replaced by $-CF_3$ group to form trifluoroacetylacetone or hexafluoroacetylacetone, these complexes tend to be more volatile compared to other β-diketones (e.g., dibenzoylmethane and benzoylacetone) due to the influence of volatile fluorine atoms bonded to the carbon atom in the ligand or complex (Gschneidner et al., 2005; Verma et al., 2011). Hence, hexafluoroacetylacetone tends to be more volatile compared to trifluoroacetylacetone and other ligands that do not contain fluorine atoms.

2.6 SUMMARY

There have been substantial advancements in the evolution of corrosion- inhibitors and understanding of the basic processes or mechanisms of how the inhibitors function. This advancement has permitted the current state of materials usage in both common and harsh environments by changing the environment (i.e., the use of inhibitors). Protecting metals or alloys from degradation caused by corrosion will require a strategy of shielding off the metallic structure from an aggressive environment either by coatings or by changing the environment using an inhibitor. In this regard, huge advances in developing eco-friendly inhibitor compounds that exhibit low toxicity and are considered unharmful to health have been made over the last two decades.

However, little is known about the efficacy and inhibitive effect of some novel and newly synthesized rare earth element β-diketone complexes as corrosion inhibitors and their effect when applied in corrosive environments. Several rare-earth element compounds or salts have been used and tested as viable alternatives to chromate inhibitors on various metals and alloys and some of them have shown promising results.

Knowledge of the details of the inhibiting mechanism of rare-earth β-diketones complexes as corrosion inhibitors is still lacking though and requires further attention. Investigations on how the rare-earth β-diketone complexes inhibit the corrosion processes could reveal knowledge of how the mechanism of the inhibitors on the surface of a metal when applied. Surface analyses (using Scanning Electron Microscopy (SEM), Fourier Transform Infrared spectrometer

(FTIR), Raman spectroscopy (RS), and Optical Microscopy (OM)) in conjunction with potentiodynamic tests and gravimetric analysis (weight loss) will be used to study the inhibiting mechanism of some β-diketone complexes in corrosive chloride media. This will be of great help to determine whether it acts as an anodic, cathodic, or mixed type of inhibitor. Also, knowledge and understanding of the potential absorbed layer on the metal surface will be acquired. To achieve this, commercial grade rare earth halide salts and different β-diketones will be used to synthesise the so-called green inhibitors (i.e., REE β-diketones complexes) and then test the efficacy of the synthesised complexes using electrochemical and gravimetric analysis.

2.7 REFERENCES

Amadeh, A., Allahkaram, S. R., Hosseini, S. R., Moradi, H., & Abdolhosseini, A. (2008). The use of rare-earth cations as corrosion inhibitors for carbon steel in aerated NaCl solution. Anti-corrosion Methods and Materials, 55(3), 135-143.

Baddoo, N. R. (2008). Stainless steel in construction : A review of research, applications, challenges and opportunities. Constructional Steel Research, (64), 1199–1206.

Barmatov, E., Hughes, T., & Nagl, M. (2015). Efficiency of film-forming corrosion inhibitors in strong hydrochloric acid under laminar and turbulent flow conditions. Corrosion Science, (92), 85–94.

Bernal, S., Botana, F.J., Calvino, J.J., Marcos, M.J.A., & Perez-Omil, H. V. (1995). Lanthanide salts as alternative corrosion inhibitors. Alloys and Compounds, (225), 638–641.

Bhise, N. A., Al-horaibi, S. A., Gaikwad, S. T., & Rajbhoj, A. S. (2019). Synthesis, Spectral Characterization, and Cyclic Voltammetric Studies of β-Diketone and its Metal Complexes. Rasayan Journal of Chemistry, 12(1), 101–113.

Boudellioua, H., Hamlaoui, Y., Tifouti, L., & Pedraza, F. (2019). Effects of polyethylene glycol (PEG) on the corrosion inhibition of mild steel by cerium nitrate in chloride solution. Applied Surface Science, 473, 449–460

Chiou, S. Y. (1989). A Study of The Effect of Some Inhibitors on The Corrosion Rates of Austenitic Stainless Steels in Sulfuric Acid. (MSc dissertation), New Jersey Institute of Technology, USA.

Davo, B., & e Damborenea, J. J. (2004). Use of rare earth salts as electrochemical corrosion inhibitors for an Al – Li – Cu (8090) alloy in 3 . 56 % NaCl. Electrochimica Acta, (49), 4957–4965.

El-Meligi, A. A. (2010). Corrosion Preventive Strategies as a Crucial Need for Decreasing Environmental Pollution and Saving Economics. Corrosion Science, 2(1), 22–33.

Faisal, M., Saeed, A., Shahzad, D., Abbas, N., Ali Larik, F., Ali Channar, P., Abdul Fattah, T., Muhammad Khan, D., & Aaliya Shehzadi, S. (2018). General properties and comparison

of the corrosion inhibition efficiencies of the triazole derivatives for mild steel. Corrosion Reviews 36(6), 507–545.

Forsyth, M., Seter, M., Tan, M. Y., & Hinton, B. (2014). Recent developments in corrosion inhibitors based on rare earth metal compounds. International Journal of Corrosion Processes and Corrosion Control, 49(2), 130–135.

Forsyth, M., Seter, M., Hinton, B., Deacon, G., & Junk, P. (2011). New "Green" corrosion inhibitors based on rare earth compounds. Australian Journal of Chemistry, 64(6), 812–819.

Fouda, A. S., Abd El-Wahab, S. M., Attia, M. S., Youssef, A. O., & Elmoher, H. O. (2015). Rare earth metals as eco-friendly corrosion inhibitors for mild steel in produced water. Der Pharma Chemica, 7(8), 74–87.

Ghanbari, A., Attar, M., & Mahdavian, M. (2009). Acetylacetonate Complexes as New Corrosion Inhibitors in Phosphoric Acid Media. Progress in Color, Colorants and Coating, 2(2), 115–122.

Golfomitsou, S. (2006). Synergistic effects of additives to benzotriazole solutions applied as corrosion inhibitors to archaeological copper and copper alloy artefacts (PhD dissertation). University of London, United Kingdom.

Gschneidner, K. A, Bünzli, J. & Pecharsky, V. K. (2003). Handbook on the Physics and Chemistry of Rare Earths, (vol 35). 1st ed., Elsevier Science B.V., North Holland.

Hinton, B. R. . (1992). Corrosion Inhibition with Rare Earth Metal Salts. Alloys and Compounds, 180, 15–25.

Huang, C., (2010). 'Rare Earth Coordination' (1st ed.), John Wiley & Sons., Singapore.

Kareem, A. (2013). Effect of Environment on the Mechanical Properties of Mild Steel. ARPN Journal of Science and Technology, 3(9), 915–917.

Khaled, K. F. (2013). Electrochemical evaluation of environmentally friendly cerium salt as corrosion inhibitor for steel in 3.5 % NaCl. International Journal of Electrochemical Science, 8(3), 3974–3987.

Kumar, M., & Sharma, T. R. (2012). Synthesis, characterization and properties of metal complexes of beta-diketonate complexes. Oriental Journal of Chemistry, 28(4), 1827–1831.

Kuznetsov, Y. I. (1996). Organic inhibitors of corrosion of metals. (1 st ed.). Plenum Press, New York.

Landolt, D. (2007). Corrosion and surface chemistry of metals. (1st ed.), CRC Press, Lausanne, Switzerland.

Mohammedi, D., Ismail, F., Rehamnia, R., Bensalem, R., & Savadogo, O. (2015). Corrosion behaviour of steel in the presence of rare earth salts: Synergistic effect. Corrosion Engineering Science and Technology, 50(8), 633–638.

Quraishi, M. A., Chauhan, D. S., & Saji, V. S. (2020). Heterocyclic Organic Corrosion Inhibitors Principles and Applications. (1st ed.), Elsevier Inc, Amsterdam, Netherlands.

Rashid, K. H., & Khadom, A. A. (2020). Sodium sulfite as an oxygen scavenger for the corrosion control of mild steel in petroleum refinery wastewater: optimization, mathematical modeling, surface morphology and reaction kinetics studies. Reaction Kinetics Mechanisms and Catalysis, 129(2), 1027–1046.

Raja, P. B., Ismail, M., Ghoreishiamiri, S., Mirza, J., Ismail, M. C., Kakooei, S., & Rahim, A. A. (2016). Reviews on Corrosion Inhibitors. Chemical Engineering Communications, 203(9), 1145–1156.

Reza, N. A., Akhmal, N. H., Fadil, N. A., & Taib, M. F. M. (2021). A review on plants and biomass wastes as organic green corrosion inhibitors for mild steel in acidic environment. Metals, 11(7), 1–25.

Schweitzer, P. A. (2010). Fundamentals of Corrosion Mechanisms, Causes, and Preventative Methods. CRC Press, New York.

Shahid, M. (2011). Corrosion protection with eco-friendly inhibitors. Advances in Natural Sciences: Nanoscience and Nanotechnology, 2, 1–7.

Shokova, E. A, Kim, J. K., & Kovalev. V. V. (2015). 1,3-Diketones. Synthesis and properties.

Russian Journal of Organic Chemistry, 51(6), 773–847.

Somers, A. E., Hinton, B. R. W., Bruin-Dickason, C. De., Deacon, G. B., Junk, P. C., & Forsyth, M. (2018). New environmentally friendly rare earth carboxylate corrosion inhibitors for mild steel. Corrosion Science, 139(2017), 430–437.

Sumathi, S., Anitha, C., Tharmaraj, P., & Sheela, C. D. (2011). Spectral, NLO, Fluorescence, and biological activity of Knoevenagel condensate of β-diketone ligands and their metal (II) complexes. International Journal of Inorganic Chemistry, 1–8.

Terachi, T., Yamada, T., Miyamoto, T., & Arioka, K. (2012). Corrosion Behavior of Stainless Steels in Simulated PWR Primary Water — Effect of Chromium Content in Alloys and Dissolved Hydrogen. Nuclear Science and Technology, 45(10), 975–984.

Urbaniak, W., Jurek, K., Witt, K., & Gorączko, A. (2011). Properties and application of diketones and their derivatives. Chemik, 65(4), 273-282.

Uwiringiyimana, E., Sylvester, O. D. P., Joseph, I. V, & Adams, F. V. (2016). The effect of corrosion inhibitors on stainless steels and aluminium alloys. African Journal of Pure and Applied Chemistry, 10(2), 23-32.

Verma, P. N., Sheikh, J. I., & Juneja, H. D. (2011). Synthesis of β-diketone and its Metal Complexes. World Applied Sciences, 14(8), 1154–1157.

Yasakau, K. A., Zheludkevich, M. L., Lamaka, S. V., & Ferreira, M. G. S. (2006). Mechanism of corrosion inhibition of AA2024 by rare-earth compounds. Physical Chemistry B, 110(11), 5515–5528.

CHAPTER THREE

3.0 SYNTHESIS AND CHARACTERIZATION OF A REE β-DIKETONES COMPLEXES

3.1 SYNTHESIS OF RARE EARTH β-DIKETONES COMPLEXES

All the β-diketone complexes were synthesized from the two main primary components, a REE halide and the β-diketone ligand. The REE halide, β-diketone, ammonia solution and methanol were bought from Sigma Aldrich and used as received without further purification. The β-diketone complexes were prepared according to the method described in the literature (Reedy, 1974; Sumathi et al., 2011; Kumar & Sharma, 2012; Hanson, 2014). $LaCl_3.7H_2O$ (3.5g, 0.0094 mol) was dissolved in 15 ml of methanol. After complete dissolution, 2.5 ml acetylacetone (β-diketone) (2.4 g, 0.0240 mol) was added to the solution and stirred for about 4 minutes for the mixture to attain homogeneity. Then 25% concentrated ammonia solution (1.5 ml) was added dropwise to the resulting solution. After about 1 hr, a β-diketone crystal complex precipitated which was air-dried in an oven at a temperature of 35 ℃ for 24 hours.

A similar procedure was used for the preparation of all other β-diketone complexes. The yield of each complex was calculated based on the limiting reactant (i.e., β-diketone) and is presented in appendix A (Table A3).

3.2 CHARACTERIZATION OF REE β-DIKETONES COMPLEXES

Characterization of the REE complexes are necessary to be sure that the synthesised complexes were the desired compounds. This was be achieved through various analyses such as melting point, Fourier transform infrared spectroscopy (FT-IR), Raman spectroscopy (RS), X-ray diffraction analysis (XRD) and mass spectrometry (MS) analysis. Comparison of the results with literature values is necessary for final confirmation.

3.3 MELTING POINT

The melting points of the synthesised complexes were carried out using a digital electrothermal melting point apparatus (Stuart melting point apparatus, SMP-10). This was done by heating the synthesised crystal that was stuck in an apparatus in a capillary glass tube and then watching the crystals through a build-in magnifying glass. As the crystal begin to change into a viscous form, the initial melting point was recorded, while the final melting point was taken as the crystal melts completely. The presence of impurities and the heating rate at which the melting point was carried out might be responsible for a difference in the melting point of $La(tfac)_3$ complexes in comparison with the melting point value obtained in the literature, while the melting point for complexes with the other metal ions were not available in the literature, an indication that this was not as expected. The melting points of the synthesised β-diketone complexes are tabulated in Table 3.1.

Table 3.1 Melting points of the synthesised rare earth element complexes and the literature values.

Synthesised REE β-diketone complexes	Melting point range (℃)	Melting point (lit. value) (℃) (Gschneidner et al., 2005)
Cerium acetylacetone ($Ce(acac)_3$)	172-174	Not Available
Lanthanum acetylacetone ($La(acac)_3$)	272-274	274-275
Scandium acetylacetone ($Sc(acac)_3$)	185-187	187-187.5
Cerium hexafluoroacetylacetone ($Ce(hfac)_3$)	Above 300	Not Available
Lanthanum hexafluoroacetylacetone ($La(hfac)_3$)	Above 300	Not Available
Scandium hexafluoroacetylacetone ($Sc(hfac)_3$)	99-101	Not Available
Cerium trifluoroacetylacetone ($Ce(tfac)_3$)	132-138	Not Available
Lanthanum trifluoroacetylacetone ($La(tfac)_3$)	124-126	142-144
Scandium trifluoro acetylacetone ($Sc(tfac)_3$)	149-151	Not Available
Cerium dibenzoylmethane ($Ce(dbm)_3$)	121-125	Not Available
Lanthanum dibenzoylmethane ($La(dbm)_3$)	101-103	99-102
Scandium dibenzoylmethane ($Sc(dbm)_3$)	249-251	Not Available
Cerium thenoyltrifluoroacetone ($Ce(tta)_3$)	123-125	106-108
Lanthanum thenoyltrifluoroacetone ($La(tta)_3$)	133-135	135
Scandium thenoyltrifluoroacetone ($Sc(tta)_3$)	149-151	149

3.4 FOURIER-TRANSFORM INFRARED SPECTROSCOPY ANALYSIS (FTIR)

The infrared spectra (IR) were recorded at room temperature using a Perkin Elmer Fourier Transform–Attenuated Total Reflectance–Infrared spectrometer Spectrum-2 (FT-ATR-IR-2) in the range from 4000-420 cm^{-1}. Table 3.2 and Figures 3.1-3.5 show the absorption band frequencies and the infrared spectra of the synthesised β-diketone complexes. The spectra of the synthesised β-diketone complexes were studied, and the spectra values were compared with literature values. The IR spectra of the various β-diketone complexes are very similar, except where some of the spectra show some slight shift of a vibration band caused by the thiophene ring that is present in thenoyltrifluoroacetone metal complexes. In the infrared spectra, two absorption bands in the range 1693 to 1400 cm^{-1} were observed, which corresponded to the carbonyl groups (C=O) and carbon-carbon double bond (C=C) in the β-diketone complexes (Wu et al., 1993; Al-Wassil et al., 1998; Sumathi et al., 2011; Kumar & Sharma, 2012; Ukken & Ummathur, 2013; Nath et al., 2017; Bhise et al., 2017; Bhise et al., 2019). However, it seems very confusing to distinguish which band to assign to C=O and C=C within the range of 1693-1400 cm^{-1}. According to Haigh, (1970), Kerim et al. (1977) and Uzoukwu, (1990), the C=O stretch in organic molecules is usually more intense than the C=C stretch. Hence, the higher band should be assigned to C=O stretch while the lower band should be assigned to C=C stretch. A weak, broad peak was observed between 3004 and 3578 cm^{-1} which is characteristic of ν(OH) vibrations. This confirmed the presence of hydroxide functional groups in the complexes (Ferenc et al., 2013; Ukken & Ummathur, 2013; Zhang et al., 2013; Kale, 2014), which can be a confirmation of the enol tautomer of the various compounds. The appearance of a band in the region 583 to 518 cm^{-1} indicates bonding of the metal ion with the β-diketone molecules and can be ascribed to the M-O vibration (Wu et al., 1993; Al-Wassil et al., 1998; Sumathi et al., 2011; Kumar & Sharma, 2012; Ferenc et al., 2013; Ukken & Ummathur, 2013; Nath et al., 2017). A band that appears between 1450 and 1350 cm^{-1} could be assigned to the CH_3 bending vibration (Qau et al., 2017). At frequencies between 1142 and 1128 cm^{-1} one observes evidence of the presence of CF_3 for trifluoroacetylacetone and hexafluoroacetylacetone β-diketone complexes (Martín-Ramos et al., 2014; Nath et al., 2017). The stretching of the C-S band in the thiophene ring is identified at 712-720 cm^{-1}, which appears in all the thenoyltrifluoroacetone complexes (Coates, 2004; Magdaline & Chithambarathanu, 2015). The bands in the range 1013-920 cm^{-1} are due to C-H in-plane bending, while the bands at 809-652 cm^{-1} are for C-H out of plane bending vibrations for the heterocyclics and aromatic complexes (i.e. thenoyltrifluoroacetone and dibenzoylmethane

complex) (Jiang et al., 2008; Magdaline & Chithambarathanu, 2015). This band is one of the characteristic features of IR spectra that distinguishes aromatic compounds from non-aromatic ones.

Table 3.2: Significant bands of FT-IR spectra of synthesised rare earth element β-diketone complexes.

Compound	C=O	M-O	O-H	CF_3	CH_3	C=C	C-H	C-S
$Ce(acac)_3$	1584	525	3134	-	1384	1519	921	-
$La(acac)_3$	1595	529	3335	-	1379	1514	808	-
$Sc(acac)_3$	1559	540	3133	-	1355	1519	773	-
$Ce(hfac)_3$	1644	587	3048	1142	-	1404	798	-
$La(hfac)_3$	1648	583	3041	1142	-	1402	800	-
$Sc(hfac)_3$	1651	518	3004	1128	-	1535	724	-
$Ce(tfac)_3$	1622	558	3565	1130	1290	1532	721	-
$La(tfac)_3$	1623	557	3578	1130	1290	1531	703	-
$Sc(tfac)_3$	1615	574	3236	1132	1434	1535	792	-
$Ce(dbm)_3$	1602	524	3351	-	-	1512	652	-
$La(dbm)_3$	1592	531	3356	-	-	1523	679	-
$Sc(dbm)_3$	1590	546	3146	-	-	1521	686	-
$Ce(tta)_3$	1602	578	3308	1134	-	1512	681	713
$La(tta)_3$	1602	577	3326	1131	-	1512	680	712
$Sc(tta)_3$	1576	530	3288	1131	-	1542	688	720

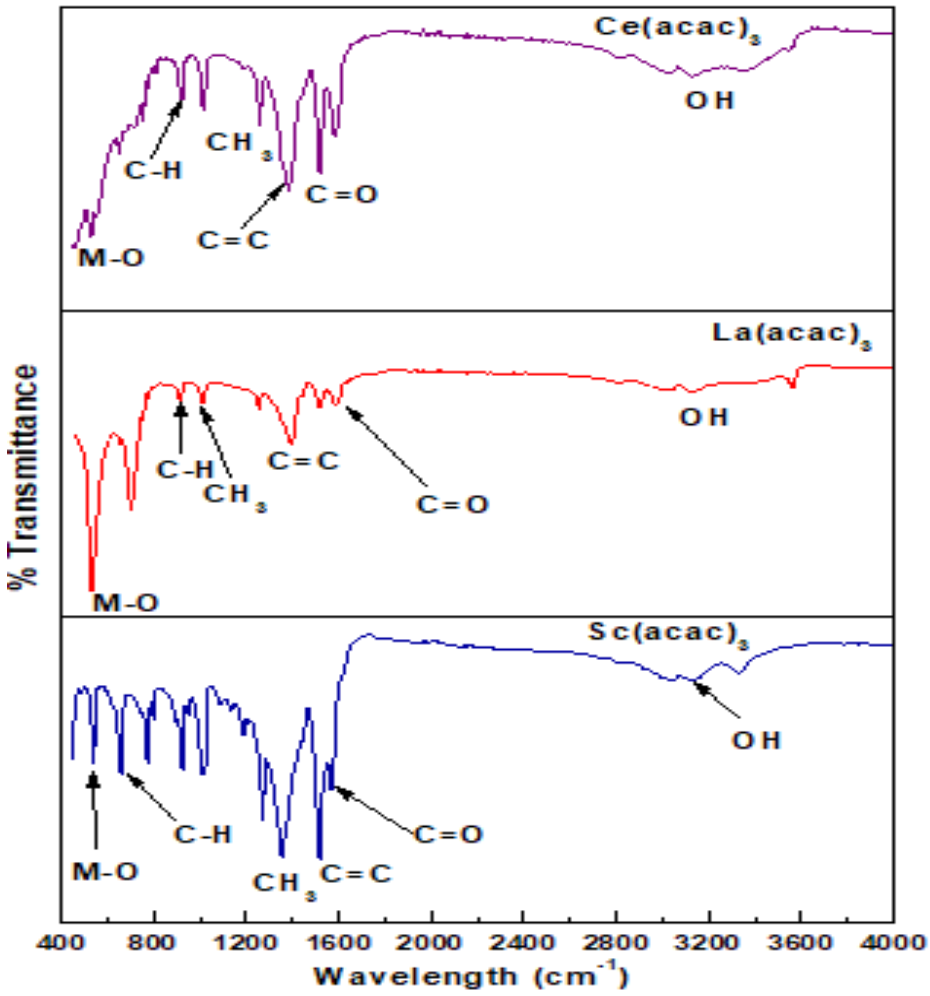


Figure 3.1: Stacked FT-IR spectra of the synthesised cerium, lanthanum and scandium acetylacetone complexes.

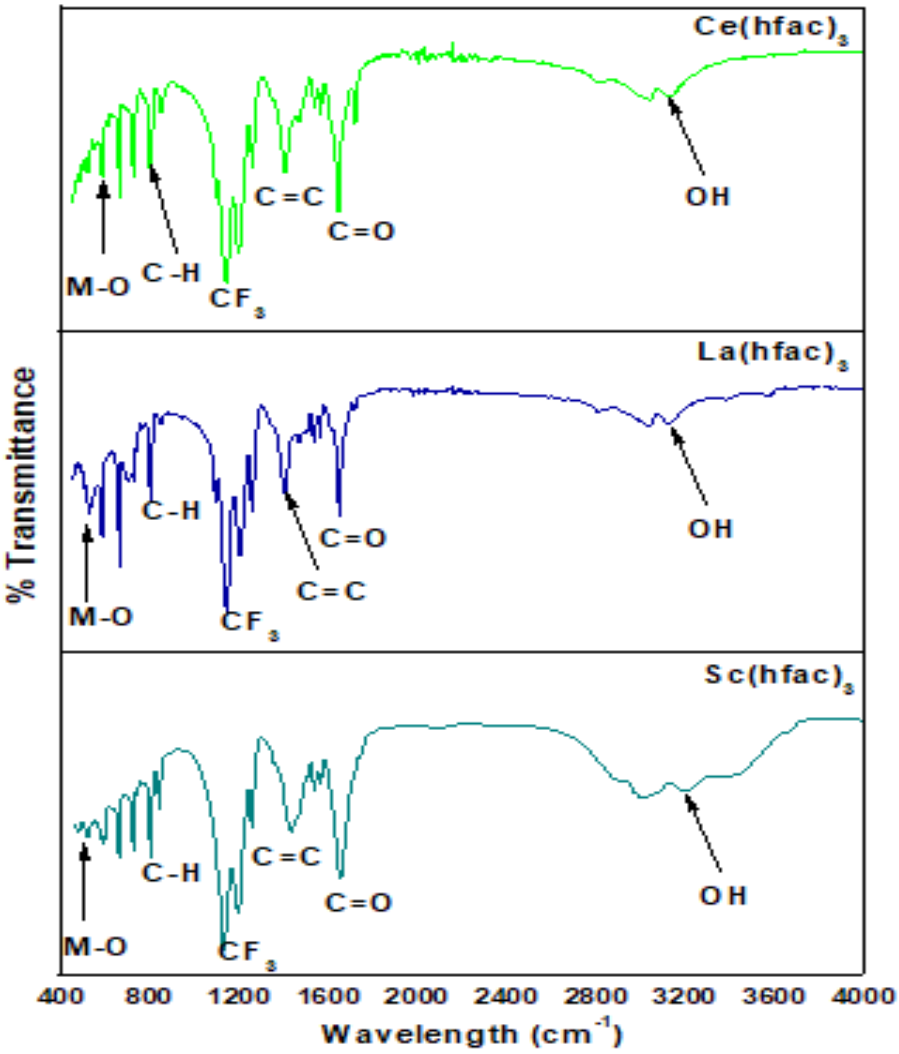


Figure 3.2: Stacked FT-IR spectra of the synthesised cerium, lanthanum and scandium hexafluoroacetylacetone complexes.

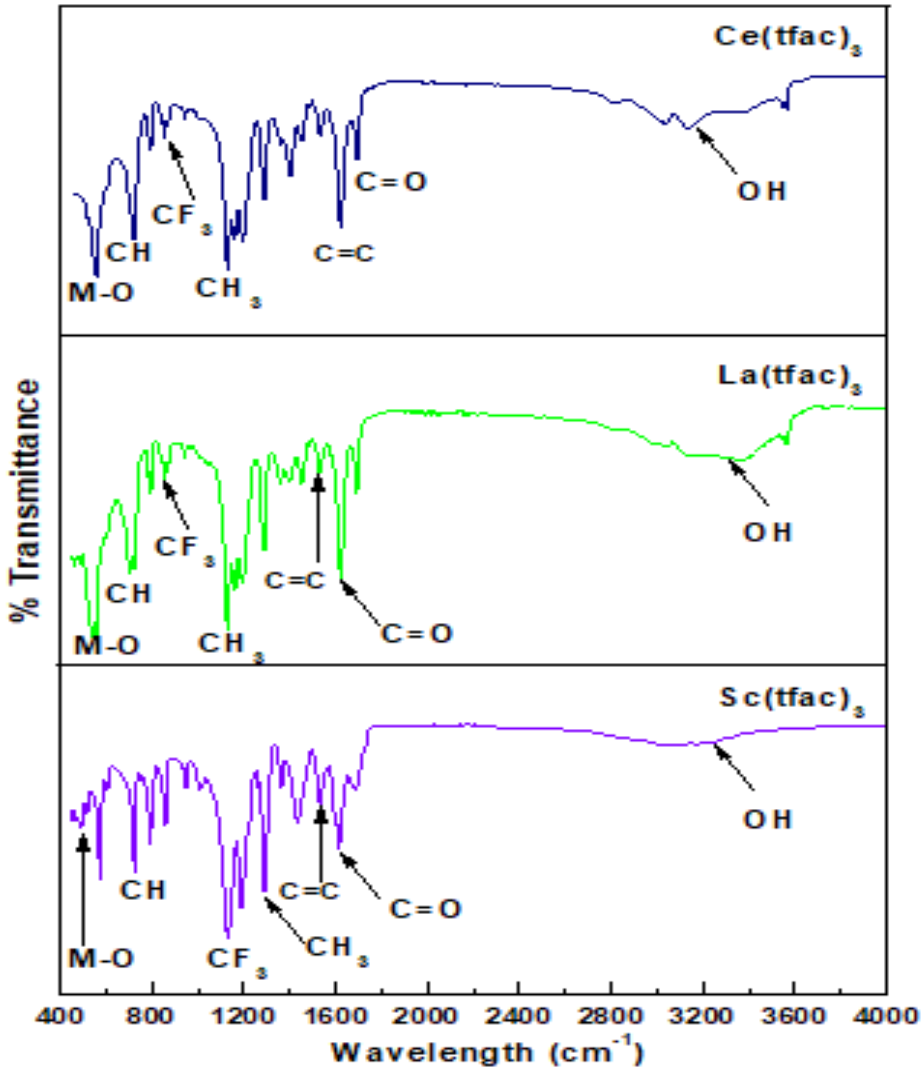


Figure 3.3: Stacked FT-IR spectra of the synthesised cerium, lanthanum and scandium trifluoroacetylacetone complexes.

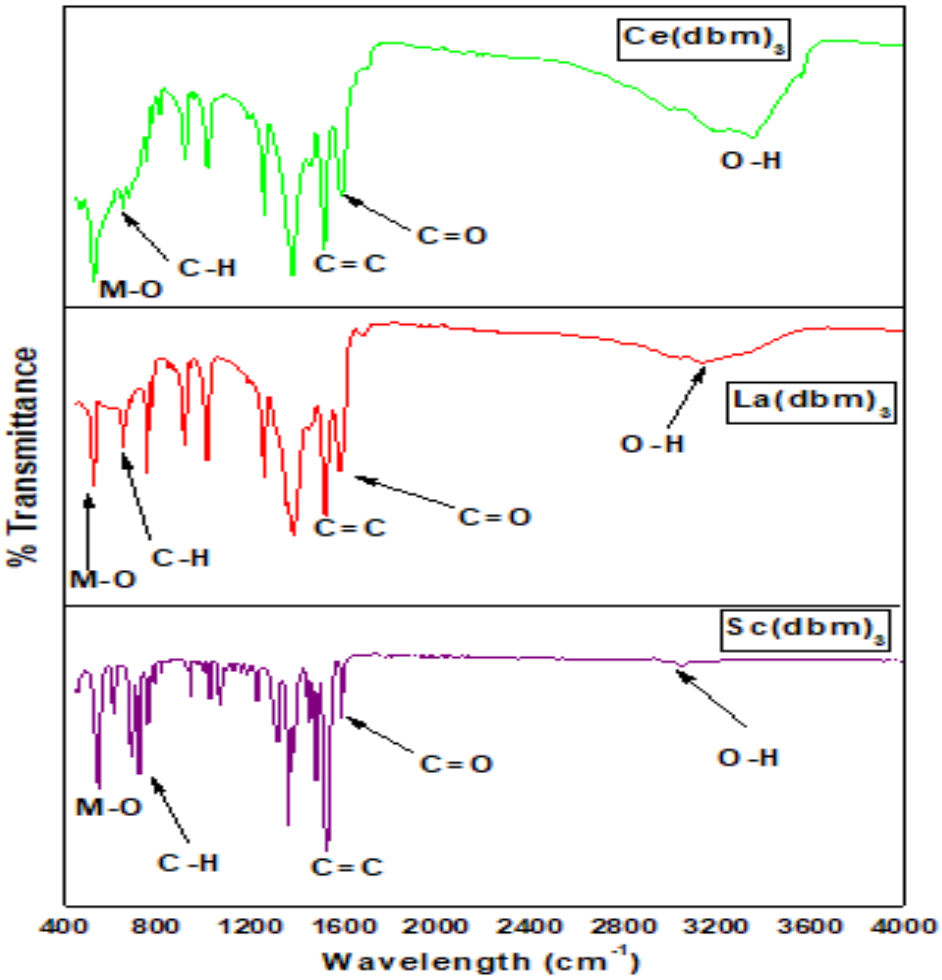


Figure 3.4: Stacked FT-IR spectra of the synthesised cerium, lanthanum and scandium dibenzoylmethane complexes.

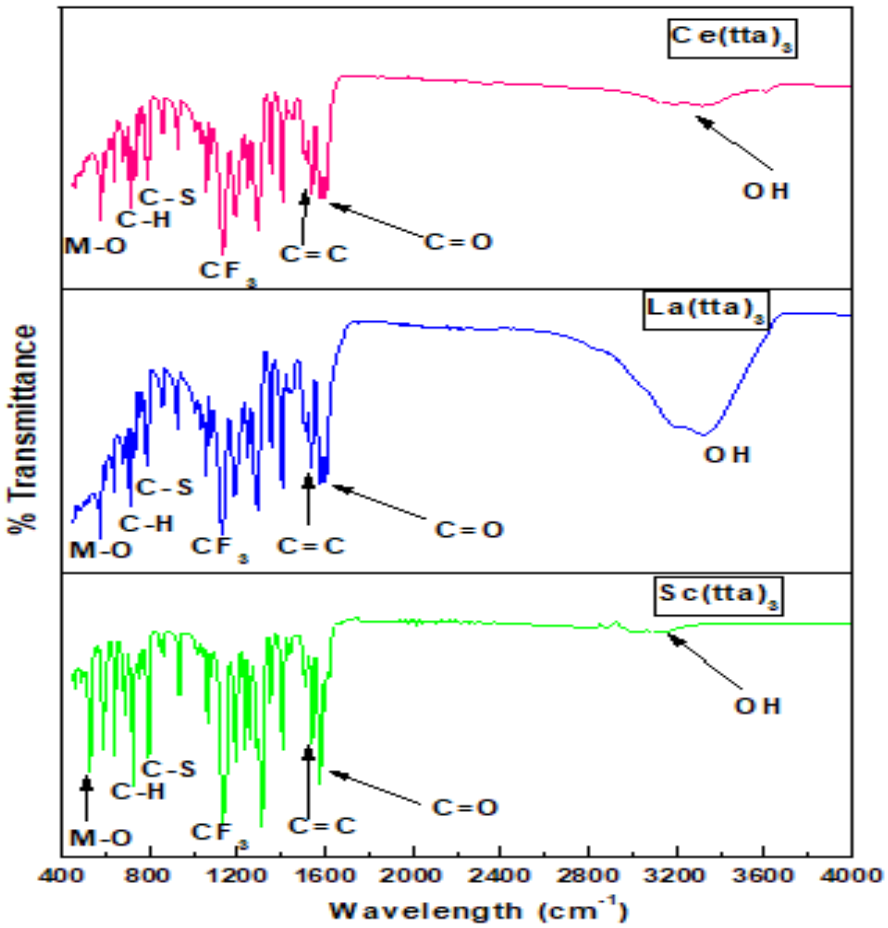


Figure 3.5: Stacked FT-IR spectra of the synthesised cerium, lanthanum and scandium thenoyltrifluroacetone complexes.

3.5 RAMAN SPECTROSCOPY (RS) RESULTS

Raman spectroscopy (RS) is a non-destructive technique that requires a very small amount of sample for the characterisation of organic and inorganic compounds. Raman spectra were acquired using the 514.5 nm line of a Lexel Model 95 SHG argon ion laser as an excitation source and a Horiba LabRAM HR Raman spectrometer equipped with a high-sensitivity Olympus BX41 microscope. The incident beam was focused onto the sample using a 100× objective (N.A. = 0.90) and the backscattered light was dispersed via a 600 lines/mm grating onto a liquid nitrogen cooled CCD detector. The data was acquired using LabSpec v5 software and the spectra were obtained in the range of 3500-50 cm^{-1}. The laser power at the sample was

approximately 0.4 mW to minimise localised heating effects. The results of lanthanum, cerium, and scandium trifluoroacetylacetone complexes (i.e., $La(tfac)_3$, $Ce(tfac)_3$ and $Sc(tfac)_3$) were unsuccessful as the analyses did not show any form of distinctive characteristic peaks that were present in the synthesised complexes, rather it display only a strong fluorescence background.

Similar RS analysis carried out by (Cabo-Fernandez et al., 2019) on a lithium hexafluorophosphate complex ($LiPF_6$), suggested that the fluorescence displayed by the complex could be a result of the impurities embedded within the complexes. Similar cases where impurities were present in a compound that resulted in a display of fluorescence in Raman were also reported (Kagan & Mccreery, 1994; Cebeci et al., 2019).

The range of the fluorescences were measured from around 1900 cm^{-1} up to 3400cm^{-1} without any form of visible peaks, while that of $Sc(tfac)_3$ was measured in full scale which displayed a similar result, as shown in Figure 3.8. No Raman spectra of the synthesised complexes have been reported in the literature so far. Only those for europium, zirconium, hafnium, thorium and other transition metal β-diketone complexes could be found (Liang et al., 1970; Wiedenheft, 1971; Offiong, 1995; Fay, 1996; Tsaryuk et al., 2005; Luber & Reiher 2008; Tsaryuk et al., 2020).

The frequency shift associated with the carbonyl functional group (C=O) is observed in the range between 1681 to 1500 cm^{-1}, while that of carbon-carbon double bond (C=C) was also observed slightly below 1500 cm^{-1}. This is in good agreement with the literature for most β-diketone complexes (Liang et al., 1970; Courrier et al., 1972; Kostova et al., 2007; Nakamoto, 2009; Nakamoto et al., 2009; Martín-Ramos et al., 2014). This spectroscopic shift range that was observed in Raman was also similar to what was observed in FTIR for all the β-diketone complexes. The shift which corresponds to complexation of the metal ion with the β-diketone (M-O) was observed in a position which is in excellent agreement with the literature (Courrier et al., 1972; Offiong, 1995; Kostova et al., 2007; Nakamoto, 2009; Nekoei et al., 2009; Martín-Ramos et al., 2014). Other frequency shifts, which correspond to CF_3, CH_3, C-S for thenoyltrifluoroacetone complexes, and ν(OH) which is the characteristic for ν(OH) vibrations, were reported by other workers for such type of complexes (Liang et al., 1970; Courrier et al., 1972; Offiong, 1995; Kostova et al., 2007; Nekoei et al., 2009; Martín-Ramos et al., 2014; Magdaline & Chithambarathanu, 2015). For example, for cerium thenoyltrifluoroacetone $Ce(tta)_3$, the OH frequency band was observed at 3308 cm^{-1} for FTIR, while the shift appeared

at 3125 cm^{-1} in Raman spectrum. For the M-O bond, the band appeared at 578 cm^{-1} in FTIR, and this shift was observed between 418-519 cm^{-1} with the Raman technique. Details of the individual Raman band and spectrum of each complex are reported in Table 3.3 and Figures 3.6 to 3.10.

Table 3.3: Observed Raman band position frequencies of the synthesised rare earth element β-diketone complexes.

Compound	C=O	M-O	O-H	CF_3	CH_3	C=C	C-H	C-S
$La(acac)_3$	1598	492	3069	-	1290	1444	787	-
$Ce(acac)_3$	1583	455	2931	-	1275	1439	749	-
$Sc(acac)_3$	1447	438	3089	-	1278	1369	668	-
$La(hfac)_3$	1681	455	3152	1165	-	1463	745	-
$Ce(hfac)_3$	1654	445	3157	1162	-	1473	743	-
$Sc(hfac)_3$	1666	466	3078	1157	-	1452	747	-
$La(dbm)_3$	1598	492	3067	-	1289	1493	787	-
$Ce(dbm)_3$	1593	436	3069	-	1318	1486	791	-
$Sc(dbm)_3$	1597	409	3075	-	1295	1446	791	-
$La(tta)_3$	1513	460	3116	1086	1309	1410	752	684
$Ce(tta)_3$	1513	490	3125	1081	1306	1408	749	684
$Sc(tta)_3$	1515	498	3130	1081	1316	1408	752	688

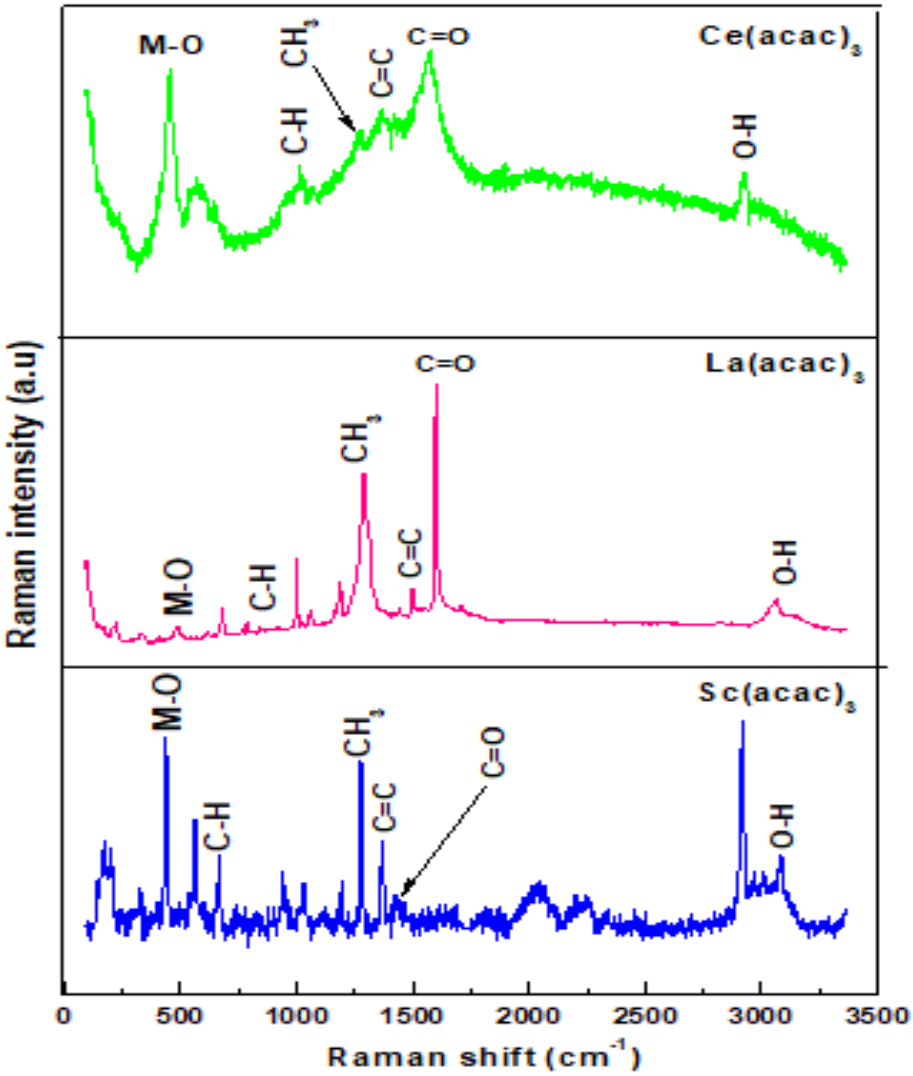


Figure 3.6: Stacked Raman spectra of the synthesised cerium, lanthanum and scandium acetylacetone complexes.

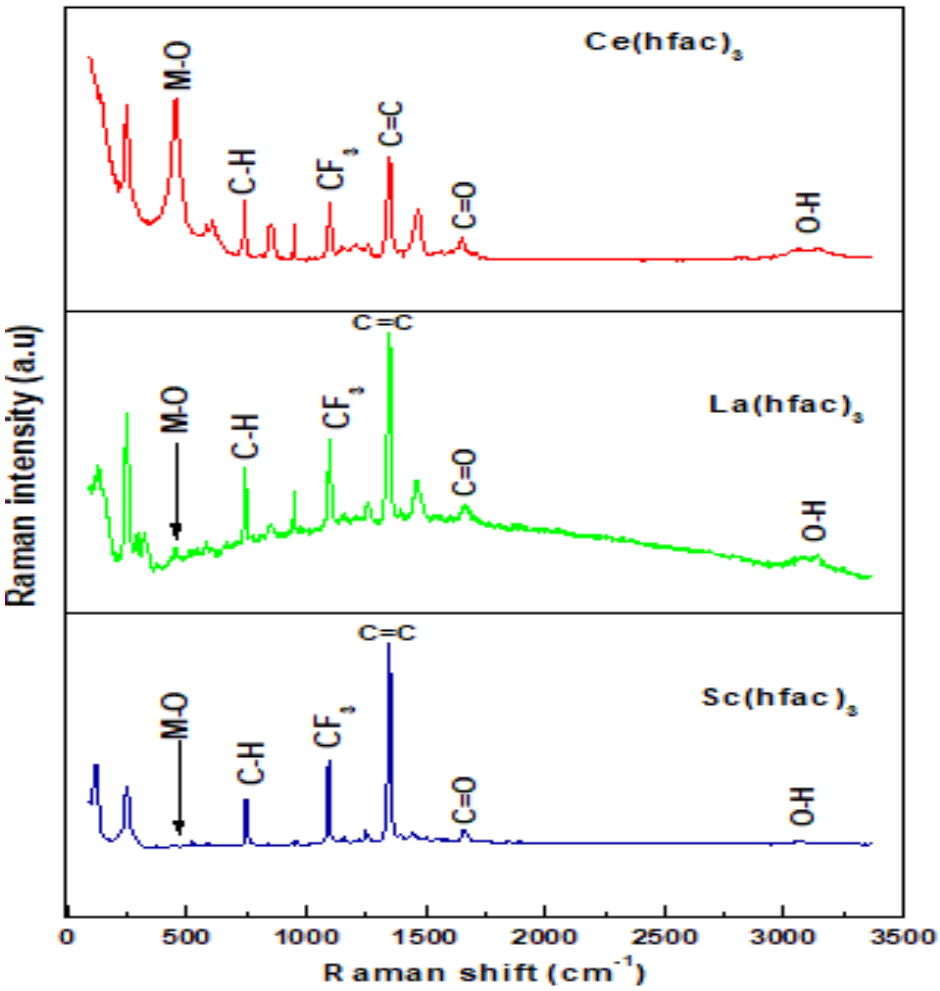


Figure 3.7: Stacked Raman spectra of the synthesised cerium, lanthanum and scandium hexafluoroacetylacetone complexes.

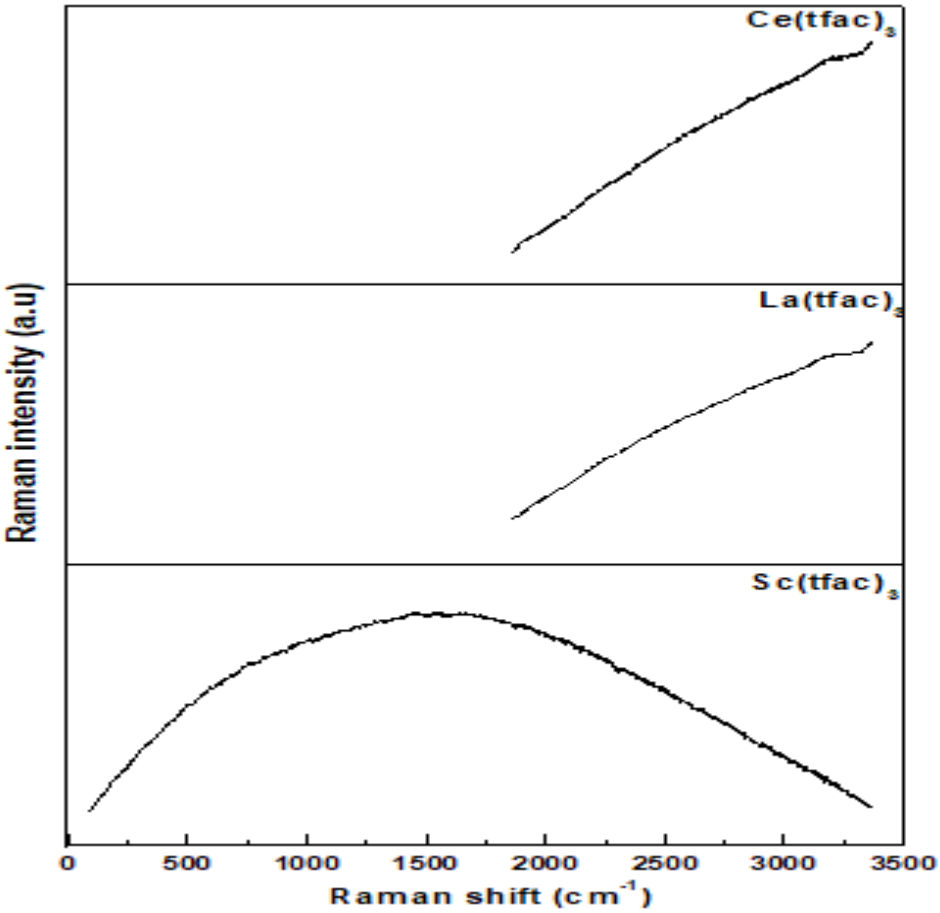


Figure 3.8: Stacked Raman spectra of the synthesised cerium, lanthanum and scandium trifluoroacetylacetone complexes.

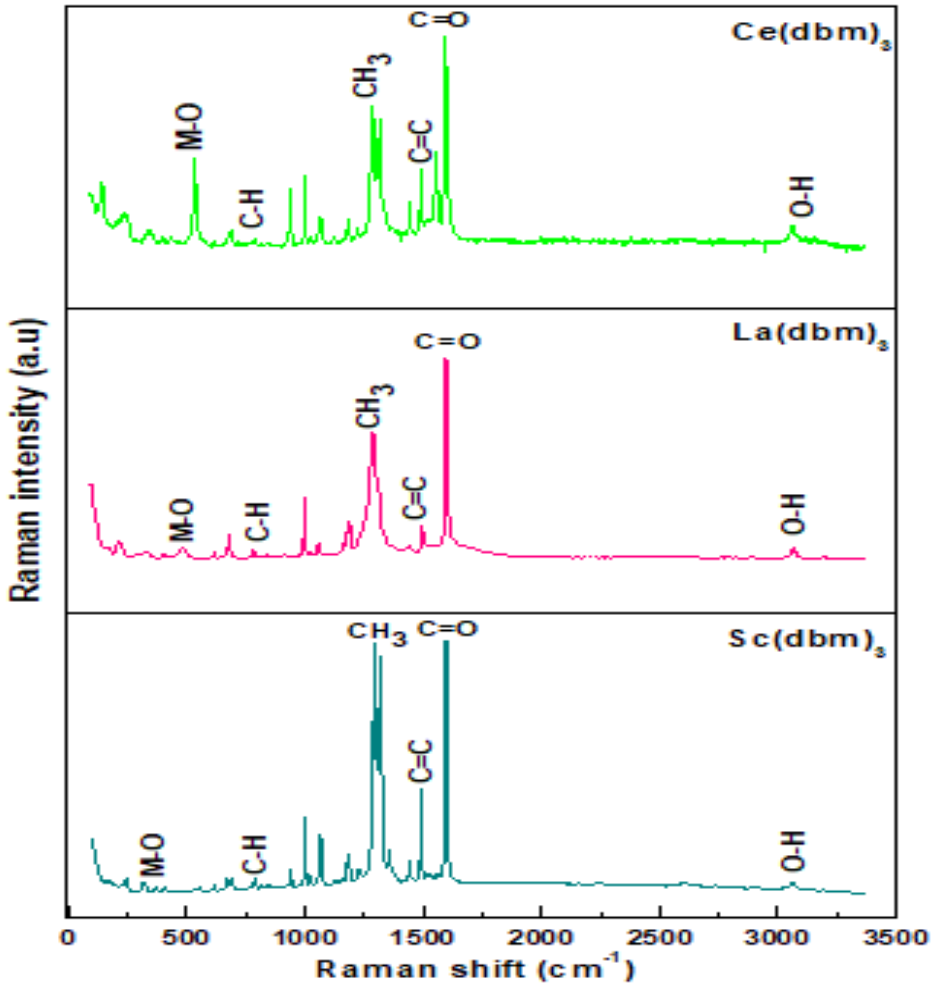


Figure 3.9: Stacked Raman spectra of the synthesised cerium, lanthanum and scandium dibenzoylmethane complexes.

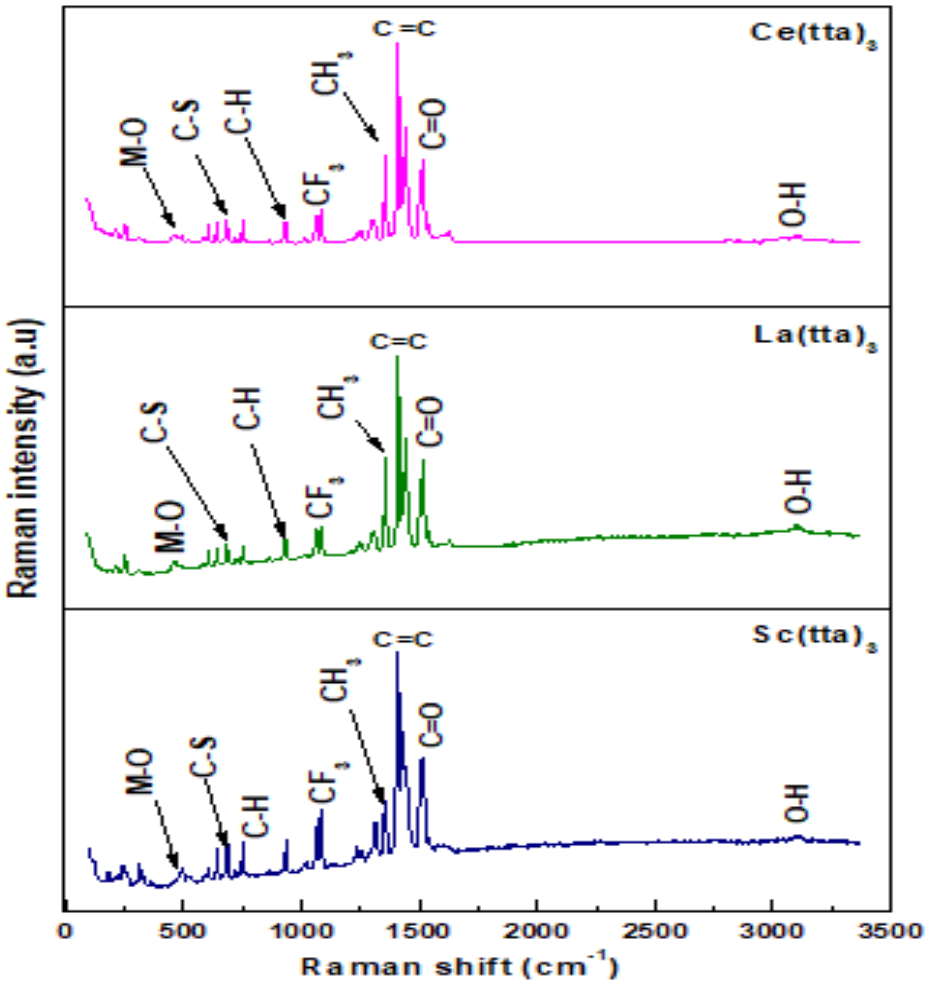


Figure 3.10: Stacked Raman spectra of the synthesised cerium, lanthanum and scandium thenoyltrifluroacetone complexes.

3.6 MASS SPECTRA ANALYSIS

Mass spectrometry (MS) analysis was carried out by injecting 10 µL of the sample into the Dionex Ultimate 3000 Ultra-High Performance Liquid Chromatography High Resolution Mass Spectrometer (UHPLC-HRMS) system (Thermo Scientific, Dionex, Sunnyvale, California, USA) and run through a loop for one minute with 50 % Solvent A consisting of 0.1 % formic acid in H_2O (v/v) and 50 % solvent B consisting of 0.1 % formic acid in acetonitrile (v/v) at a flow rate of 0.3 mL/min. Mass spectra were recorded on a Bruker Compact Q-TOF mass spectrometer (Bruker Daltonics, Bremen, Germany). The UHPLC-HRMS system allowed for

the identification of the mass electron ratio (m/z) of the complexes. Three samples from the cerium, lanthanum, and scandium series of the synthesised rare earth complexes were randomly selected for the analysis. The masses of the selected complexes were confirmed and the mass spectrum analysis was processed using the Bruker Daltonics software. The mass spectra of the selected complexes showed intense molecular ion peaks that correspond to the actual mass of the synthesised complexes, which further confirmed the formulation of the complexes (Krishnankutty et al., 2007; Jiang et al., 2008). The results obtained from the mass spectra of the complexes were in good agreement with the molecular masses calculated from the molecular formulae of the complexes, $Ce(CH_3COCHCOCH_3)_3.yH_2O$, $La(C_6H_5COCHCOC_6H_5)_3.yH_2O$ and $Sc(C_4H_3SCOCHCOCF_3)_3.yH_2O$, where y = 0 for all the complexes. Details of the found and calculated values of the complexes are given in Table 3.4. The confirmation of the masses from MS indicated that the three desired complexes had been synthesised. Since all the complexes were synthesised in a similar process, there is a high probability that the rest of the synthesised complexes will have the desired structures. Details of the mass spectra of the reported complexes can be found in Figures 3.11-3.13.

Table 3.4: Found and calculated values of the selected synthesised REE β-diketone complexes.

Compound	Molecular mass found	Molecular mass calculated
$Ce(CH_3COCHCOCH_3)_3$	438.24	437
$La(C_6H_5COCHCOC_6H_5)_3$	809.10	808
$Sc(C_4H_3SCOCHCOCF_3)_3$	708.91	708

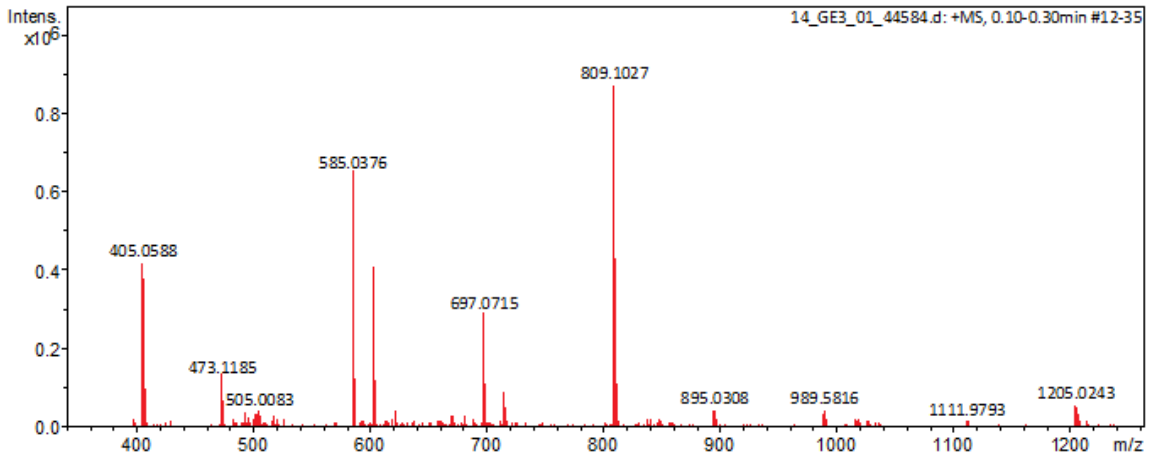


Figure 3.11: Mass spectrum of lanthanum dibenzoylmethane, $La(dbm)_3$ complex (Intensity against m/z).

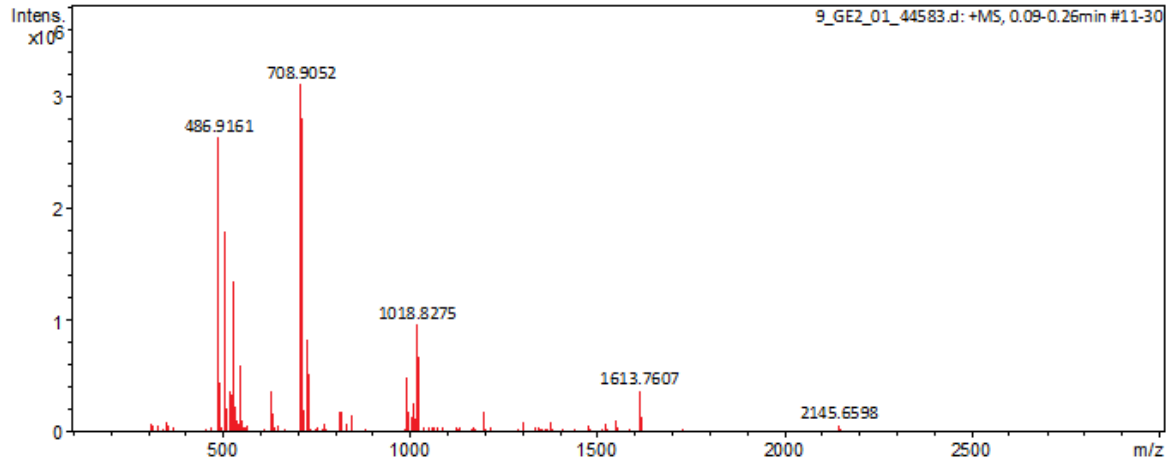


Figure 3.12: Mass spectrum of Scandium thenoyltrifluoroacetone, $Sc(tta)_3$ complex (Intensity against m/z).

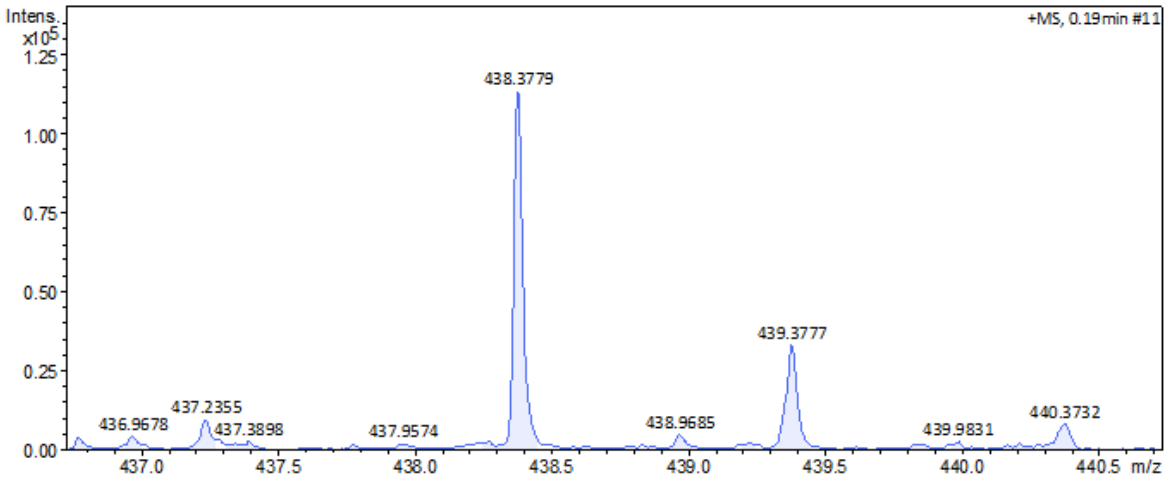


Figure 3.13: Mass spectrum of cerium acetylacetone, $Ce(acac)_3$ complex (Intensity against m/z).

3.7 X-RAY DIFFRACTION (XRD) RESULTS AND ANALYSIS

The X-ray diffraction (XRD) technique is a very useful tool and is one of the most common techniques used to characterise crystals of metal complexes**.** The crystallinity of the metal complexes were checked using an X-ray diffractometer (Bruker D2 phaser diffractometer) equipped with Cu Kα radiation [λ = 1.54184 Å] in the 2-theta range of 5 to 90°, at 0.02° steps with a counting time of 31.4 s per step. XRD analysis of the metal complexes was performed using HighScore Plus software to determine the type of crystal that was formed. A qualitative analysis of XRD patterns showed diffraction peak diagrams of the complexes. The intensity of the diffraction peaks patterns indicates the crystallinity of the obtained complexes. It was observed that all the synthesised complexes showed a high level of crystallinity as indicated in Figures 3.14 to 3.18. It was also observed from the diffraction patterns that some of the crystallised salts that were synthesised with the same base component (β-diketone) have an identical peak pattern. Details of the XRD patterns are shown in Figure 3.14-3.18.

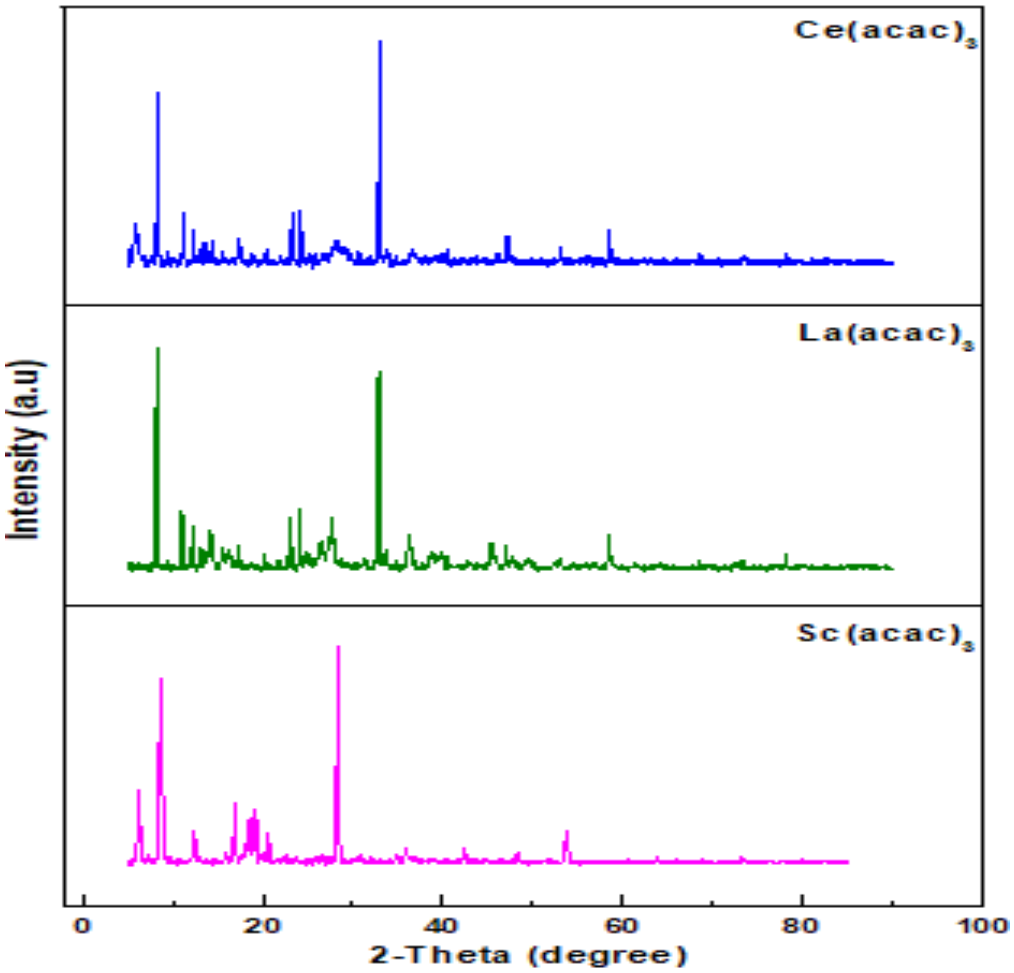


Figure 3.14: Stacked XRD patterns of the synthesised cerium, lanthanum and scandium acetylacetone complexes.

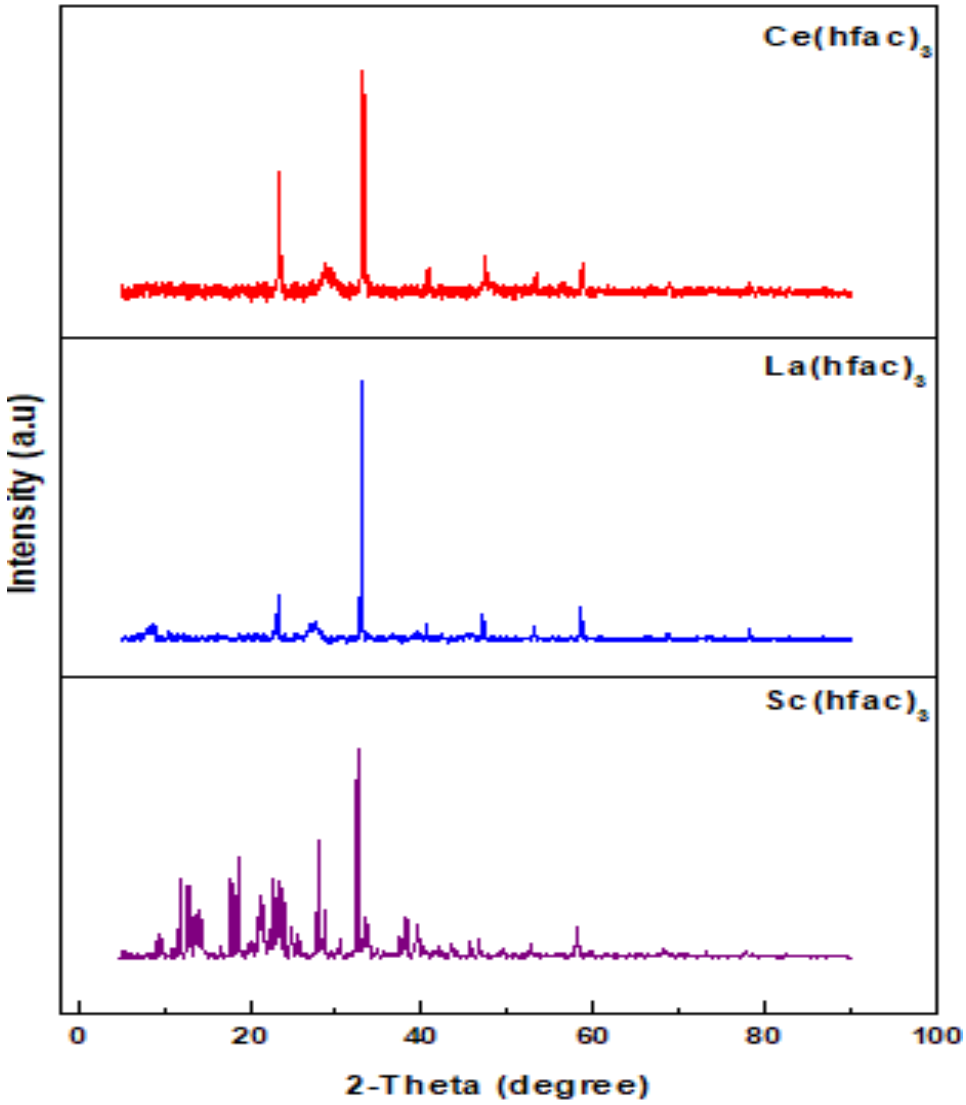


Figure 3.15: Stacked XRD patterns of the synthesised cerium, lanthanum and scandium hexafluroacetylacetone complexes.

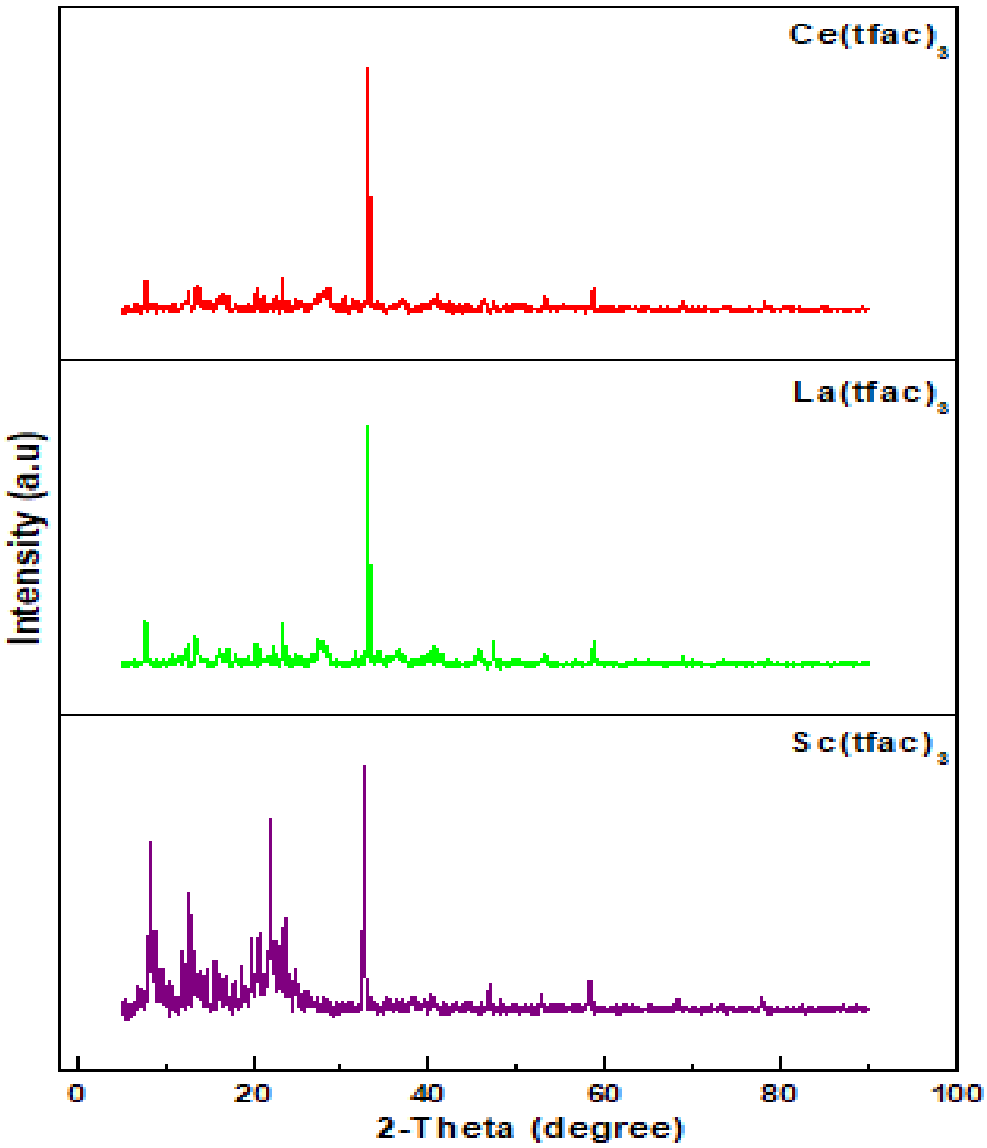


Figure 3.16: Stacked XRD patterns of the synthesised cerium, lanthanum and scandium trifluroacetylacetone complexes.

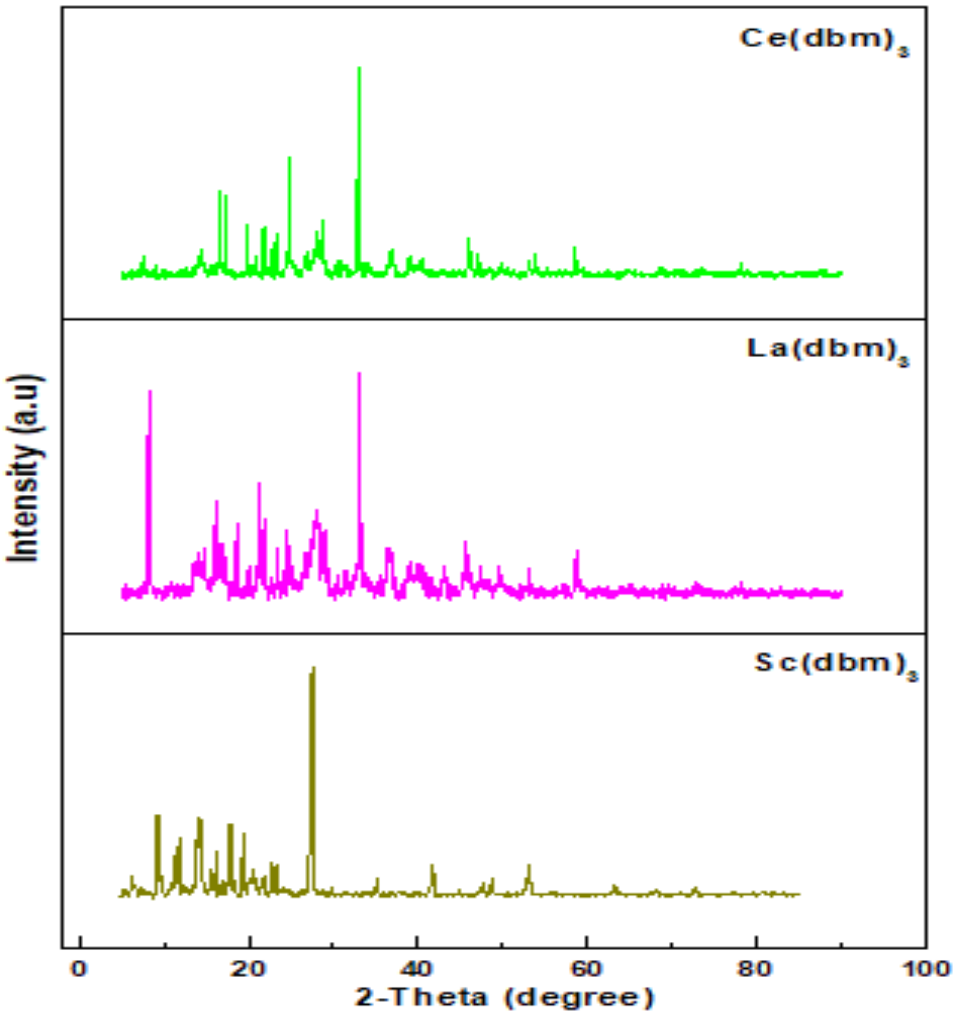


Figure 3.17: Stacked XRD patterns of the synthesised cerium, lanthanum and scandium dibenzoylmethane complexes.

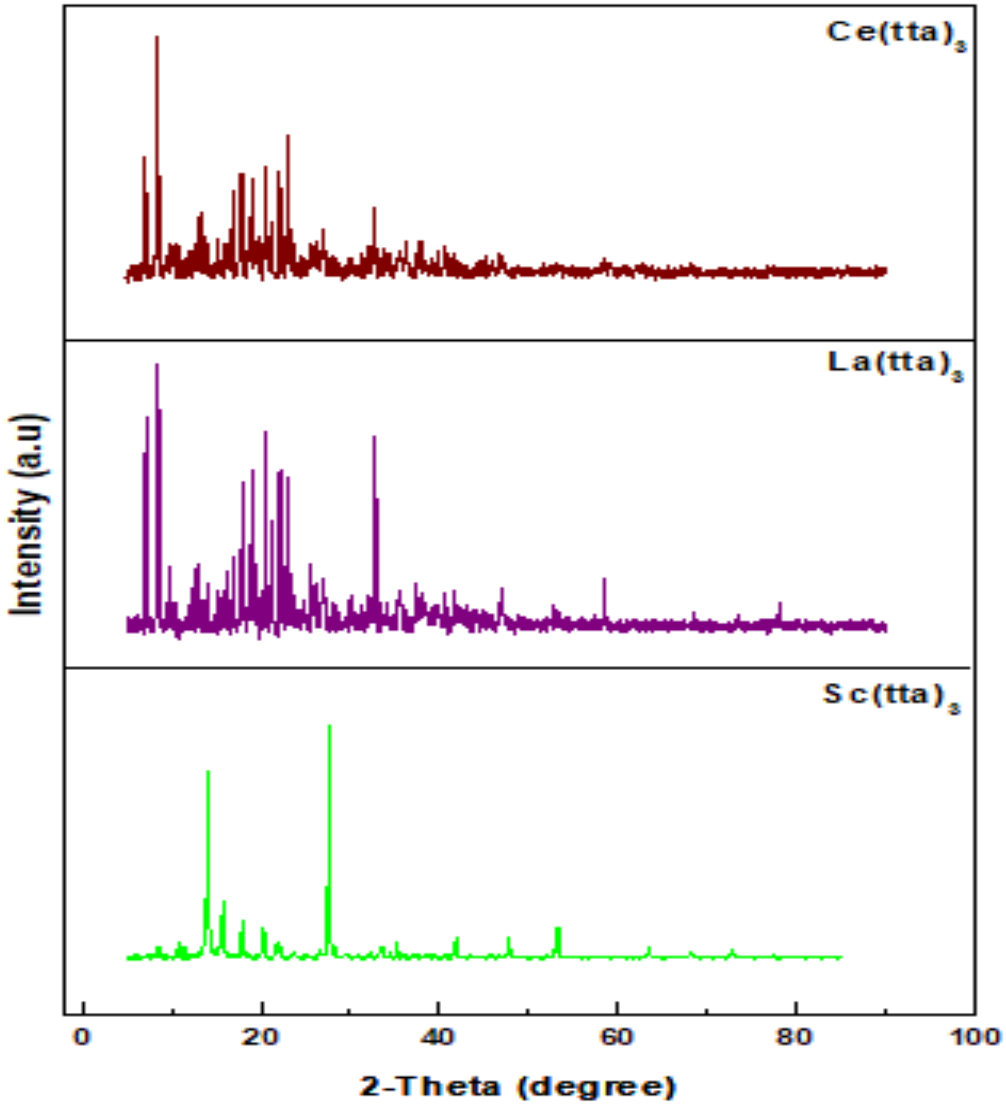


Figure 3.18: Stacked XRD patterns of the synthesised cerium, lanthanum and scandium thenoyltrifluroacetone complexes.

3.8 SUMMARY AND CONCLUSIONS

Synthesis and characterization of various rare earth element β-diketone complexes have been carried out. All the synthesised complexes have a general formula $M(RCOCHCOR')_n$ where M is the rare earth element, R and R′could be a methyl group, fluorinated methyl or alkyl group, thiophene or benzene ring depending on the type of β-diketone ligand that was used as a base component for the synthesis of the REE β-diketone complex. All the complexes were synthesized through the same procedure as described in the literature and they were

characterised using melting point analysis, infrared spectroscopy, Raman spectroscopy, mass spectroscopy and X-ray diffraction. For mass spectroscopy, three samples were selected randomly, one each from cerium, lanthanum and scandium series of the synthesised complexes and their masses were confirmed by mass spectroscopy analysis. The mass values of the analysed complexes were in excellent agreement with the theoretical or calculated value of the actual molecular mass of the complexes indicating that the three desired complexes had been obtained in the synthesis procedure. Since all the complexes were synthesised in a similar manner, there is a high probability that the rest of the synthesised complexes will have the desired structure. The melting point data also confirmed the synthesised complexes as the obtained data corresponded to values published in the literature where available. Furthermore, the IR and Raman bands revealed the characteristic peaks used to identify the formation of the metal complexes. The IR spectra revealed that the prepared compounds possess characteristic peaks in the range of 583 to 518 cm^{-1}, which signify the formation of metal complexes. These peaks were also observed in RS, but slightly below the 500 cm^{-1} range. Hence, it can be concluded that the intended REE β-diketone complexes were successfully synthesized.

3.9 REFERENCES

Al-Wassil, A. I., Al-Farhan, K. A., Mukhalalati, M., & Mahfouz, R. M. (1998). Coordination Chemistry of Thenoyltrifluoroacetone 1- Synthesis and characterization of In^{3+} thenoyltrifluoroacetone Complex. Spectroscopy Letters, 31(2), 299–305.

Bhise, N. A., Agale, A. A., Gaikwad S. T., & Rajbhoj, A. S. (2017). Synthesis and Characterization of Mn(II), Fe(III), Co(II), Ni(II) and Cu(II) Complexes of β-Diketone. Asian Journal of Chemiistry, 29(11), 2372–2378.

Bhise, N. A., Al-horaibi, S. A., Gaikwad, S. T., & Rajbhoj, A. S. (2019). Synthesis, Spectral Characterization, and Cyclic Voltammetric Studies of β-Diketone and its Metal Complexes. Rasayan Journal of Chemistry, 12(1), 101–113.

Cabo-Fernandez, L., Neale, A. R., Braga, F., Sazanovich, I. V., Kostecki, R., & Hardwick, L. J. (2019). Kerr gated Raman spectroscopy of LiPF6 salt and LiPF6-based organic carbonate electrolyte for Li-ion batteries. Physical Chemistry Chemical Physics, 21(43), 23833–23842.

Cebeci, D., Alam, A., Wang, P., Pinal, R., & Ben-amotz, D. (2019). Photobleaching profile of Raman peaks and Fluorescence background. European Pharmaceutical Review, 1–8.

Coates, J. (2004). Interpretation of Infrared Spectra, A Practical Approach. Encyclopedia of Analytical Chemistry, 1–23.

Courrier, W. D., Lock, C. J. L., & Turner, G. (1972). Studies of β-Diketone Complexes of Rhenium. Part 2. Physical Studies of Dihalobis(pentane-2,4-dionato)rhenium(IV) Compounds. Canadian Journal of Chemistry., 50, 1797–1806.

Fay, R. C. (1996). Stereoehemistry and molecular rearrangements of some six, seven and eight coordinate chelates of some transition metals. Coordination Chemistry Reviews, 154, 99–124.

Ferenc, W., Cristóvão, B., & Sarzynski, J. (2013). Magnetic, thermal and spectroscopic properties of lanthanide (III) 2-(4-chlorophenoxy)acetates, $Ln(C_8H_6ClO_3).nH_2O$. Serbian Chemical Society, 78(9), 1335–1349.

Haigh, J. M. (1970). Studies in the field of Metal β-ketoenolate Chemistry (PhD dissertation). The University of Cape Town, South Africa.

Hanson, D. (2014). Synthesis and Thermodynamic Analysis of Volatile Beta-Diketone Complexes of Select Lanthanides via Gas-Phase Separations (PhD dissertation). University of Tennessee, USA.

Jiang, X., Wu, Y., & He, C. (2008). Rare earth dibenzoylmethane complexes for potential application as high-density recordable optical recording materials. Materials Letters, 62(2), 286–288.

Kagan, M. R., & Mccreery, R. L. (1994). Reduction of Fluorescence Interference in Raman Spectroscopy via Analyte Adsorption on Graphitic Carbon. Analytical Chemistry, 66(23), 4159–4165.

Kale, A. A. (2014). Synthesis and Characterization of Metal Complexes derived from Dimedone Derivatives. International Journal of Science and Research (IJSR), 3(10), 1–5.

Kerim, F. M. A., Aly, H. F., & El-agramy, A. (1977). Infrared absorption spectra of some lanthanide acetylacetonate complexes. Proc. Indian Acad. Sci., 85A(6), 559–566.

Kostova, I., Peica, N., & Kiefer, W. (2007). Raman , FT-IR , and DFT studies of 3 , 5-pyrazoledicarboxylic acid and its Ce (III) and Nd (III) complexes. Raman Spectroscopy, 1–10.

Krishnankutty, K., Ummathur, M. B., & Ukken M. P. (2007). Some unsaturated β-diketones and their metal chelates. Analytical Chemistry, 6(2), 4–8.

Kumar, M., & Sharma, T. R. (2012). Synthesis, characterization and properties of metal complexes of beta-diketonate complexes. Oriental Journal of Chemistry, 28(4), 1827–1831.

Liang, C. F., Schmitschek, E. J., & Trias, J. A. (1970). I.R. and Raman spectra of europium(III) β-diketonates. Inorganic and Nuclear Chemistry, 32(3), 811–831.

Luber, S., & Reiher, M. (2008). Raman optical activity spectra of chiral transition metal

complexes. Chemical Physics, 346(1), 212–223.

Magdaline, J. D., & Chithambarathanu, T. (2015). Vibrational Spectra (FT-IR, FT-Raman), NBO and HOMO, LUMO Studies of 2-Thiophene Carboxylic Acid Based On Density Functional Method. IOSR Journal of Applied Chemistry, version 1, 8(5), 6–14.

Martín-Ramos, P., Coya, C., Lavín, V., Martín, I. R., Silva, M. R., Silva, P. S. P., García-Vélez, M., Álvarez, A. L., & Martín-Gil, J. (2014). Active layer solution-processed NIR-OLEDs based on ternary erbium(iii) complexes with 1,1,1-trifluoro-2,4-pentanedione and different N,N-donors. Dalton Transactions, 43(48), 18087–18096.

Nakamoto, K. (2009). Infrared and Raman Spectra of Inorganic and Coordination Compounds (6th ed.), John Wiley & Sons, New Jersey, USA.

Nath, P., Bharty, M. K., Dani, R. K., Tomar, M. S., & Acharya, A. (2017). Mn(II), Co(III), Ni(II), Cd(II) and Cu(II) Complexes of 2-Thenoyltrifluoroacetone: Syntheses, Structures, Photoluminescence, Thermal, Electrochemical and Antitumor Studies on Dalton's Lymphoma Cells. Chemistry Select, 2(32), 10449–10458.

Nekoei, A. R., Tayyari, S. F., Vakili, M., Holakoei, S., Hamidian, A. H., & Sammelson, R. E. (2009). Conformation and vibrational spectra and assignment of 2-thenoyltrifluoroacetone. Molecular Structure, 932(1–3), 112–122.

Qau, M. S., Islamabad, I., Ziab, P., Qau, K., Saleem, R., Fsd, U., & Pakistan, F. (2017). Synthesis and Chemical Characterization of Metals (Al, Cr, Co, Mn and VO) Complexes with Acetylacetone (β-diketone). Natural Sciences Research, 7(19), 49–55.

Reedy, J. D. (1974). Preparation of metal complexes of 1,3-diketones. Williamstown, West Virginia. USP1976033946057.

Sumathi, S., Anitha, C., Tharmaraj, P., & Sheela, C. D. (2011). Spectral, NLO, Fluorescence, and Biological Activity of Knoevenagel Condensate of β-Diketone Ligands and Their Metal(II) Complexes. International Journal of Inorganic Chemistry, 2011, 1–8.

Tsaryuk, Zolin, V., Legendziewicz, J., Szostak, R., & Sokolnicki, J. (2005). Effect of ligand radicals on vibrational IR, Raman and vibronic spectra of Europium β-diketonates.

Spectrochimica Acta - Part A, 61, 185–191.

Tsaryuk, V. I., Zhuravlev, K. P., Szostak, R., & Vologzhanina, A. V. (2020). Structure, Luminescence, and Raman Spectroscopy of europium and terbium dipivaloylmethanates and other β-diketonates with 2,2′-bipyridine. Structural Chemistry, 61(7), 1026–1037.

Ukken, M. P., & Ummathur, M. B. (2013). Synthesis and characterization of two conjugated β-diketones and their metal complexes. Archives of Applied Science Research, 5(1), 247–250.

Uzoukwu, B. A. (1990). Some metal complexes of 1,3-diketone: syntheses, UV-Vis, IR, 1H, 13C and 19F NMR spectral studies of the complexes of U(VI), Fe(III), V(V) and Ca(II) with 2-thenoyltrifluoroacetone (HTTA). Inorganica Chimica Acta, 176(1), 143–148.

Wiedenheft, C. J. (1971). Raman Spectra of some β-diketone Metal Complexes. Inorganic Nuclear Chemistry Letters, 7, 439–442.

Wu, J. G., Deng, R. W., & Chen, Z. N. (1993). Transition metal complexes of 2-thenoyltrifluoroacetone isonicotinoyl hydrazone. Transition Metal Chemistry, 18(1), 23–26.

Zhang, J., Zhang, L., Chen, Y., Huang, X., Wang, L., & Zhang, Q. (2013). Influence of different carboxylic acid ligands on luminescent properties of Eu(Lc)3phen (Lc = MAA, AA, BA, SA) complexes. Nanomaterials, 2013, 1–7.

CHAPTER FOUR

The influence of REE β-diketone complexes on the corrosion behaviour of mild steel and 304 SS in 3.5 % NaCl solution.

O.J. Lawal[1], J.H. Potgieter[1,2*], C. Billing[3]., and D.J. Whitefield[1].

[1]School of Chemical and Metallurgical Engineering, University of the Witwatersrand, Private Bag X3, Wits, 2050, South Africa

[2]Department of Natural Science, Faculty of Science and Engineering, Manchester Metropolitan University, Manchester, M1 5GD, UK

[3]Molecular Sciences Institute, School of Chemistry, University of the Witwatersrand, Private Bag X3, Wits, 2050, South Africa

*Corresponding author: herman.potgieter@wits.ac.za

ABSTRACT

In the present investigation, four REE β-diketone complexes, namely cerium acetylacetone, cerium hexafluoroacetylacetone, lanthanum acetylacetone and lanthanum hexafluoroacetylacetone were investigated as potential corrosion inhibitors for mild steel and 304 stainless steel in 3.5 % NaCl solution. The corrosion inhibition effect of the REE β-diketone complexes were investigated using weight loss measurements and potentiodynamic polarisation scans. Surface analyses using optical microscopy and scanning electron microscopy (SEM) were used to investigate the morphology of the mild steel and 304 stainless steel after the weight loss and potentiodynamic tests in 3.5 % NaCl solution containing 0.5 % wt. (m/v) concentration of the tested inhibitor. Fourier transform infrared spectroscopy and Raman spectroscopy were further used to probe the type of inhibitor film that forms on the surface of the tested samples. The obtained results revealed that the four REE β-diketone complexes are very effective inhibitors against corrosion of mild steel and 304 stainless steel in a 3.5 % NaCl in a temperature range of 20–60°C.

Keywords: REE β-diketone complexes, corrosion inhibitors, potentiodynamic polarisation, Raman spectroscopy.

4.1 INTRODUCTION

Mild steel (MS) and austenitic stainless steel (304 SS) are two of the most reliable and durable metals that are widely used in various industrial applications due to their corrosion resistance, good mechanical properties as well as reasonable cost (Fouda et al., 2015; Al-Amiery et al., 2016). However, when these steels are exposed to a corrosive environment that contains chloride ions, it degrades and undergoes pitting corrosion (Esmailzadeh et al., 2018). Pitting corrosion is considered to be one of the most dangerous forms of corrosion because it is difficult to predict and detect, as the pits formed on the alloys are usually small and narrow with relatively minimal overall metal loss. This can lead to catastrophic failure of infrastructure without prior notice. Inhibitors are often employed to address this challenge. However, most of these inhibitors are highly toxic, carcinogenic, and thus hazardous to humans and the environment (Volarič & Milošev, 2017; Gharbi et al., 2018). For this reason, there is a restriction of the use of such inhibitors, and a concerted drive is underway to replace these corrosion inhibitors with ones having a less negative ecological impact on the environment (Blin et al., 2004; Gharbi et al., 2018).

Over the years, researchers have found that various rare earth element (REE) compounds have shown good inhibiting properties when investigated in both acidic and alkaline environments that compare favourably to those of chromate compounds and could thus be a possible replacement for chromates (Gharbi et al., 2018).

Somers et al. (2018) investigated rare-earth (La, Ce, Nd, and Y) 3-(4-methyl benzoyl) propanoate compounds, $REE(mbp)_3$, as corrosion inhibitors for mild steel in a 0.01 M NaCl solution. Detailed surface analysis using an optical microscope and a scanning electron microscope after immersion and electrochemical tests revealed that the inhibitors greatly improve the corrosion resistance of mild steel in the NaCl solution. Analysis from FTIR and EDS showed the presence of a thin film containing inhibitor components on the surface of the tested steel specimens.

Fragoza-Mar et al. (2012) studied the efficacy of 1,3-diketone malonates as corrosion inhibitors for mild steel in an aqueous 1.0 M hydrochloric acid solution. Their study revealed that the efficiency of the inhibitors was 75–96% for an inhibitor concentration of 100 mg/L. Their efficiency improved when the temperature was increased from 25 to 55 ^{o}C. it was also shown that the inhibition is mainly related to the tautomerism of the compound at equilibrium.

Nam et al. (2019) conducted an investigation using cerium hydroxycinnamate as a corrosion inhibitor for mild steel in 0.6 M NaCl solution, polarisation results indicated that it can effectively inhibit mild steel corrosion in NaCl solution. The results also indicated that the cerium hydroxycinnamate behaves as a mixed inhibitor. Analysis carried out using electrochemical impedance spectroscopy (EIS) revealed that cerium hydroxycinnamate produced a protective deposit on the steel surface when the inhibitor concentration was increased from 0.22 mM to 0.63 mM. Several other researchers have investigated different REE compounds, such as cerium nitrate, cerium sulphate, lanthanum nitrate, cerium diethyldithiocarbamate, cerium chloride, lanthanum chloride, using different metal alloys varying from aluminium to mild steel. Their reports have shown that the REE compounds are highly effective corrosion inhibitors that can replace and match the inhibiting potency of chromic compounds (Ruiz et al., 1995; Blin et al., 2006; Markley et al., 2007; Nam et al., 2016; Peng et al., 2018; Boudellioua et al., 2019; Nam et al., 2019; Cotting & Aoki, 2020; Mohammadi et al., 2020).

Available research has also proved that REE chloride and β-diketones, which are the two major components used in the formulation of REE β-diketone complexes, are environmentally friendly with no reported cases of toxicity in humans or other adverse ecological effects (Fragoza-Mar et al., 2012; Volarič & Milošev, 2017). Other researchers have also used different di-carbonyl compounds (β-diketones) on their own, without incorporation of metals ions in the structure, as corrosion inhibitors for metals in corrosive acidic and alkaline environments (Horiguchi et al., 1968; Desa & Desai, 1984; Gao et al., 2009; Avdeev et al., 2013).

The inhibition mechanism and effect of REE β-diketones complexes have received little attention to date. The only metal acetylacetone compounds investigated so far, were those of the transition metals zinc (II), manganese (II), cobalt (II), and copper (II) in phosphoric acid. The results obtained from these electrochemical tests showed promising results in the application of corrosion reduction of mild steel using 0.01M of each transition metal complex at 25°C (Ghanbari et al., 2009). Therefore, in this present study cerium and complexes with acetylacetone ($CH_3COCHCOCH_3$) and hexafluoroacetylacetone ($CF_3COCHCOCF_3$) are investigated as potential green corrosion inhibitors for mild steel and 304 stainless steel in a 3.5 % chloride medium. The investigation is not only aimed at finding more environmentally

friendly and acceptable corrosion inhibitors which can reduce the degradation of steels in a chloride containing solution, but also to identify what type of inhibitor they are.

4.2 EXPERIMENTAL PROCEDURES

4.2.1 TEST AND INHIBITOR SOLUTIONS

The test solutions were prepared by dissolving analytical grade NaCl in distilled water to produce a 3.5 % NaCl solution. Thereafter, 0.5 % wt. (m/v) inhibitor was dissolved in separate NaCl solutions. Cerium acetylacetone ($Ce(acac)_3$), cerium hexafluoroacetylacetone ($Ce(hfac)_3$), lanthanum acetylacetone ($La(acac)_3$), and lanthanum hexafluoroacetylacetone ($La(hfac)_3$) complexes were the inhibitors used. The structural formulae of the four REE β-diketone complexes are shown in Figure. 4.1.

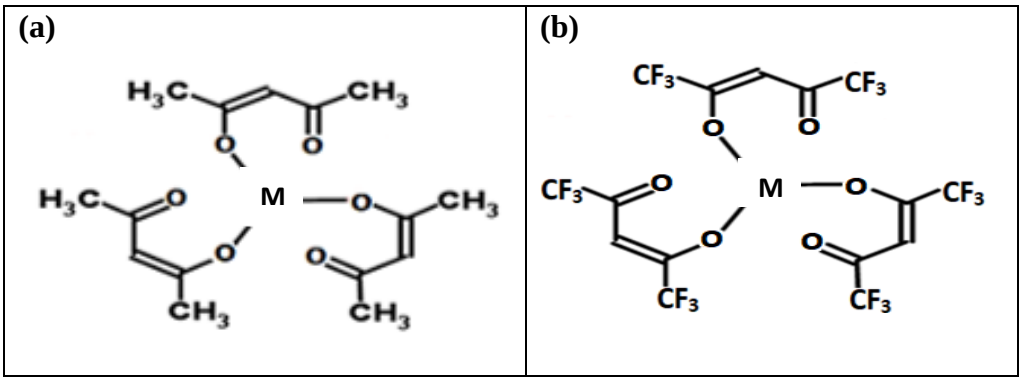


Figure 4.1: Chemical structures of (a) metal acetylacetonate and (b) metal hexafluoroacetylacetone, where M = Ce or La (Okawara et al., 2014).

4.3 MATERIAL PREPARATION

Mild steel and 304 SS specimens with a nominal composition (in wt %) as shown in Table 4.1, were machined to a size of 2 cm x 3 cm x 0.95 cm and 2 cm x 3 cm x 0.12 cm, respectively, and ground with successively finer carbide papers ranging from 600 to 1500 grit size until a mirror-like surface was achieved. Thereafter, all surfaces were rinsed with distilled water and

then with acetone to remove any possible oil and impurities from the surface and dried at room temperature. For the electrochemical corrosion tests, a mild steel sample and 304 SS sample with a cross-sectional area of 0.7 cm^2 were prepared by mounting the sample in a resin to ensure that only the tested cross-sectional area of the samples were exposed to the NaCl solution. Thereafter, the samples were prepared in the same manner and procedure as those for the weight loss experiments by grinding it to a mirror-like surface using silicon carbide paper down to 2800 grit size and then using an alumina paste (6 microns) on a polishing cloth. The samples were then cleaned using distilled water, followed by drying with acetone before performing the electrochemical corrosion test.

Table 4.1: Nominal compositions of mild steel and 304 stainless steel.

Nominal composition (wt. %)	C	S	Si	Mn	Cr	Ni	Mo	Fe
Mild steel	0.12	0.040	0.015	0.8	-	-	-	Balance
Stainless steel (type 304)	0.05	0.019	0.320	1.5	18.5	9.0	0.46	Balance

4.4 WEIGHT LOSS TESTS

Weight loss tests were carried out after morphological analysis of the specimens. A hole of 3 mm diameter was drilled at one end of each sample, through which a chemically resistant polyethylene string was threaded to suspend the coupons in the corrosive media to avoid any galvanic corrosion. The polished samples were weighed (W_O), suspended in separate beakers containing the 3.5% NaCl solution doped with 0.5 % wt. (m/v) REE β-diketone complex at room temperature. Control samples were also tested in 3.5% NaCl solutions without inhibitor. After 45 days of immersion, the coupons were cleaned with a nylon brush, rinsed with de-ionized water, and finally with acetone, and then air-dried and reweighed (W_1). Each set of the experiment were performed in triplicate and the standard deviation for each was calculated (ASTM G31-72, 1999). The average corrosion rate, (CR_{AV}) in micrometers per year (μmpy) and the inhibition efficiency (IE), were calculated using Equations 1 and 2, respectively.

$$\text{Corrosion rate (CR)} = 3.65\ x\ 10^6\ \frac{W_O - W_1}{DAT} \ldots\ldots\ldots\ldots\ldots\ldots\ldots\ldots \quad (1)$$

where W_O and W_1 are the mass of the coupon before and after immersion (in grams),

D is the density of the coupon (in g/cm^3), T is the time of exposure (in days) and

A is the exposed area of the coupon in the test solution (in cm^2).

$$\text{The inhibitor efficiency IE, (\%)} = \frac{100(CR_{AV} - CR_{iAV})}{CR_{AV}} \ldots\ldots\ldots\ldots\ldots\ldots\ldots\ldots \quad (2)$$

Where CR_{AV} AND CR_{iAV} are the average corrosion rates of the uninhibited and inhibited steel samples, respectively.

4.5 POTENTIODYNAMIC POLARISATION EXPERIMENTS

The electrochemical polarisation experiments were performed using a Metrohm Autolab-1 Potentiostat/Galvanostat equipped with Nova 2.1 software. The experiments were conducted at 20, 40, and 60℃ in a double jacketed corrosion cell containing 200 ml of NaCl solution. A three-electrode system with a platinum counter electrode and an Ag/AgCl (3M KCl) reference electrode was used and all potentials are quoted relative to this reference. Before commencing each experiment, the open circuit potential (OCP) was allowed to stabilize for 30 minutes. Thereafter, cathodic potentiodynamic polarisation scans employing a slow scan rate of 5 mV/s were initiated from 200 mV more negative than the OCP, followed by anodic polarisation scans up to 800 mV more positive than the OCP (ASTM G5-94, 2004). Standard software was employed to obtained the corrosion parameters, such as corrosion potential (E_{corr}), Tafel slopes (βa and βc) and corrosion current density (i_{corr}) from the current density-potential graphs. The corrosion rate (CR), as well as inhibition efficiency (IE), were calculated using Equations 3 to 5.

$$CR = K\left(\frac{i_{corr} E_{EQ}}{D}\right) \ldots\ldots\ldots\ldots\ldots\ldots\ldots\ldots\ldots\ldots\ldots\ldots\ldots\ldots\ldots\ldots \quad (3)$$

CR is the rate of corrosion.

K = is a constant whose value varies depending on the adopted units. For the density of a working electrode in g/cm^3 and a current density in µA/cm^2, the value of K will be taken as 3.27 micrometer/year (µm/y) (Sastri et al., 2007).

i_{corr} is the corrosion current density (in µA/cm^2).

$$E_{EQ} = \left(\sum \left(\frac{f_i z_i}{M_i}\right)\right)^{-1} \quad \text{(4)}$$

E_{EQ} = equivalent weight of mild steel and 304 stainless steel which were calculated to be 28.25 and 25.15 respectively.

$$IE = \frac{i_{corr} - i_{corr(inh)}}{i_{corr}} \times 100 \quad \text{(5)}$$

Where i_{corr} and $i_{corr(inh)}$ are the corrosion current densities of the uninhibited and inhibited steel samples, respectively.

4.6 SURFACE ANALYSES OF THE SPECIMENS

4.6.1 SCANNING ELECTRON MICROSCOPY (SEM)

A JEOL (JSM 6390) Scanning Electron Microscope (SEM) equipped with energy disperse X-ray spectroscopy (EDX) was utilised. This instrument was used to check the surface morphology of the mild steel and 304 SS. EDX was used to qualitatively analyse the chemical composition of the film layer formed after exposure of the mild steel and stainless steel electrodes exposed to a solution with and without inhibitors. This was done after both the weight loss tests and electrochemical tests in 3.5 % NaCl solution.

4.6.2 OPTICAL MICROSCOPY

An Olympus GX 41F optical microscope, with a magnification up to 500X was used to examine the surface microstructure of the specimens before and after immersion in the solutions with or without inhibitor for 45 days.

4.6.3 RAMAN SPECTROSCOPY (RS)

Raman spectra were acquired using the 514.5 nm line of a Lexel Model 95 SHG argon-ion laser as an excitation source and a Horiba LabRAM HR Raman spectrometer equipped with a high-sensitivity Olympus BX41 microscope. Raman spectroscopy (RS) was used to map the surface of the steel specimens to analyse the nature of the adsorbed film formed on the surface during the corrosion experiments.

4.6.4 FOURIER-TRANSFORM INFRARED SPECTROSCOPY (FTIR)

The infrared (IR) spectra were recorded at room temperature using a Perkin Elmer Fourier transform-attenuated total reflectance – infrared spectrometer spectrum two (FT-ATR-IR-2) in the range from 4000-420 cm^{-1}.

4.7 RESULTS AND DISCUSSION

4.7.1 WEIGHT LOSS RESULTS

The inhibition of the corrosion of the mild steel and 304 SS after exposure to a solutions without and with 0.5 % wt. (m/v) concentration of $Ce(acac)_3$, $Ce(hfac)_3$, $La(acac)_3$ and $La(hfac)_3$ inhibitors were examined at room temperature (approximately 25°C) using weight loss measurements. After 45 days of immersion in each inhibited solution, the average corrosion rate was calculated and is presented in Table 4.2. Whereas all four corrosion inhibitors are only effective to a degree to reduce the corrosion rate of mild steel in the 3.5% NaCl solution, they are 100% effective to stop any corrosion of the stainless steel. There is not much difference in the degree of protection of the mild steel with a change in the metal ion in the complex of the inhibitor, or the β-diketone of the complex.

A visual inspection of the coupons that were immersed in a solution containing $Ce(acac)_3$, $Ce(hfac)_3$, $La(acac)_3$ and $La(hfac)_3$ showed a brownish deposit, presumably a rare-earth oxide or hydroxide covering the surface of the coupon. The colour of the coupons remain intact after being washed with de-ionised water and rinsed with acetone. EDX analysis revealed that

the colour of the coupon could been due to a corrosion product film, which predominantly contains the rare-earth element compounds used as inhibitors. EDX spectra are shown in Figure 4.2. This observation had been reported by several authors using REE compounds, who all concluded that the observed colour on the surface of the investigated specimens in the presence of REE compounds was a result of the formation of a rare earth oxide on the surface of the coupons (Hinton, 1992; Lin & Li, 2006; Forsyth et al., 2011; Carneiro et al., 2012; Matter et al., 2012; Gobara et al., 2020).

Table 4.2: Comparison of corrosion rate of mild steel and 304 SS and inhibition efficiency in the absence and presence of $Ce(acac)_3$, $Ce(hfac)_3$, $La(acac)_3$ and $La(hfac)_3$ inhibitors in 3.5 % NaCl solution.

	REE inhibitor	CR with inhibitor (μm/y)	CR without inhibitor (μm/y)	IE (%)
Mild steel	$Ce(acac)_3$	42	156	74
	$Ce(hfac)_3$	41	166	75
	$La(acac)_3$	43	180	76
	$La(hfac)_3$	45	159	72
304 SS	$Ce(acac)_3$	0.0	0.7498	100
	$Ce(hfac)_3$	0.0	0.6722	100
	$La(acac)_3$	0.0	0.5430	100
	$La(hfac)_3$	0.0	0.6378	100

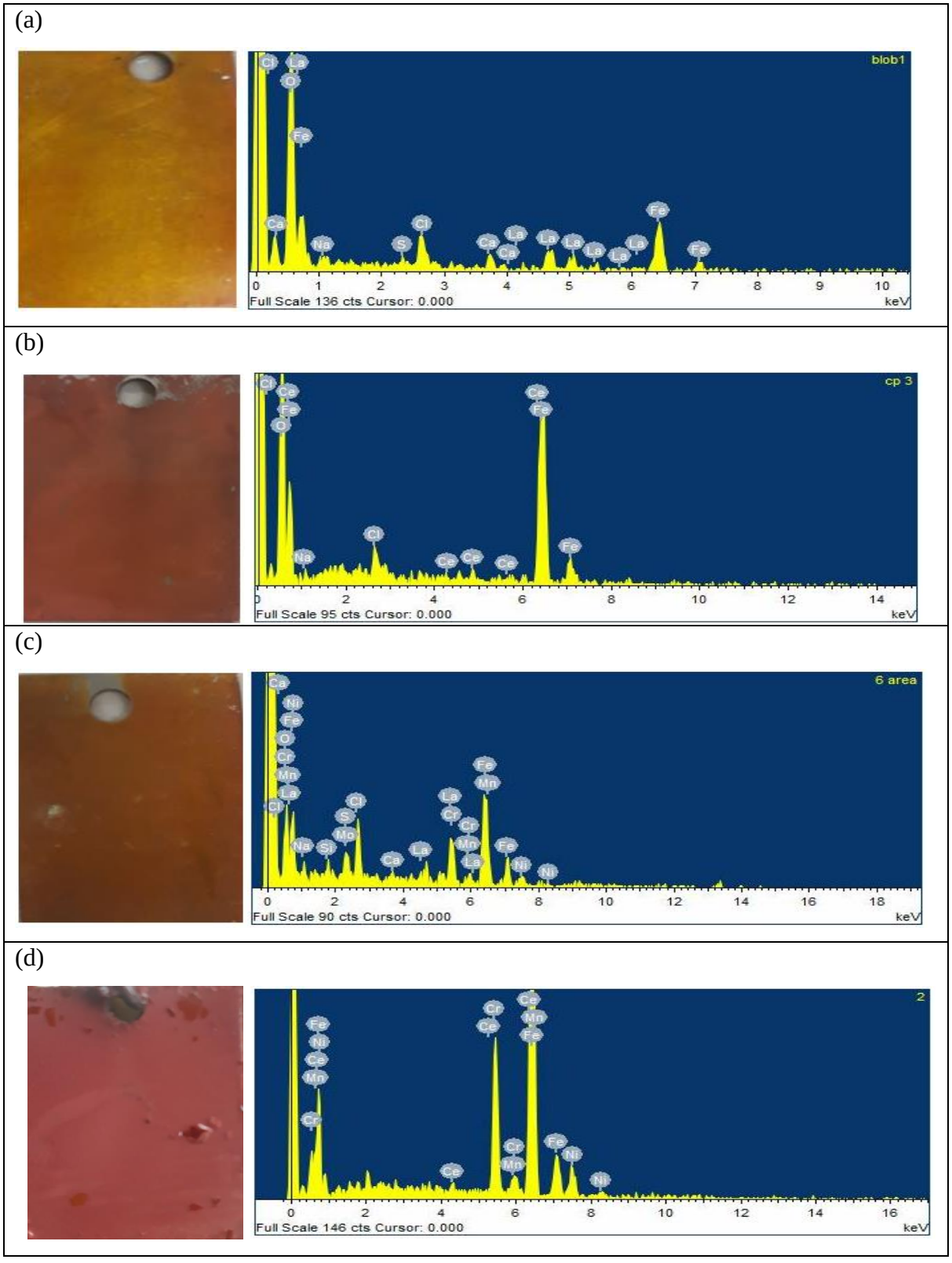


Figure 4.2: EDX spectra of (a) and (b) MS coupon exposed to 3.5% NaCl solution containing $La(acac)_3$ and $Ce(acac)_3$, (c) and (d) 304 SS inhibited with $La(hfac)_3$ and $Ce(hfac)_3$.

4.7.2 POTENTIODYNAMIC POLARISATION MEASUREMENTS

The electrochemical parameters obtained from the potentiodynamic polarisation (PDP) curves for MS and 304 SS in 3.5% NaCl solution with and without inhibitors at 20, 40 and 60°C have been tabulated in Tables 4.3 and 4.4. The data obtained from the PDP curves showed that the corrosion rate values decreased slightly in the presence of REE β-diketone inhibitor compared to a 3.5% NaCl solution without inhibitor. This phenomenon can be attributed to the adsorption of REE β-diketone inhibitor onto the metal surface as suggested by other authors (Forsyth et al., 2002; Go et al., 2020). There is remarkably little change in and the difference between the corrosion potential and corrosion current density of the mild steel in the 3.5% NaCl solution with anyone of the four corrosion inhibitors investigated, compared to the mild steel under the same conditions when no inhibitor was used at all. This is in agreement with the low corrosion inhibitor efficiency calculated for all four corrosion inhibitors evaluated. It is clear that a concentration of 0.5% is insufficient to provide corrosion protection for mild steel in 3.5% NaCl at all the tested temperatures. The general trend is for the cathodic Tafel constants to be decrease compared to the cases where no inhibitor was present. Furthermore, when the $La(hfac)_3$ inhibitor was used, the corrosion potential was distinctly more negative compared to the samples exposed in the sodium chloride solution without any inhibitor. Both these indications point to the REE β-diketone inhibitors, or at the very least the $La(hfac)_3$ inhibitor acting as a cathodic corrosion inhibitor.

Table 4.3: Electrochemical parameters of MS obtained from the potentiodynamic polarisation curves in 3.5 % NaCl solution and with corrosion inhibitors $Ce(acac)_3$, $Ce(hfac)_3$, $La(acac)_3$ and $La(hfac)_3$ present in the solution.

3.5 % NaCl solution without inhibitor						
Temp. (°C)	E_{corr} (V)	i_{corr} (A/cm^2)	βa (mV/dec)	βc (mV/dec)	CR (µm/y)	IE (%)
20	-0.552	1.62 x 10^{-5}	54	360	191	
40	-0.626	2.41 x 10^{-5}	42	314	284	
60	-0.591	2.89 x 10^{-5}	64	284	340	
$Ce(acac)_3$						
Temp. (°C)	E_{corr} (V)	i_{corr} (A/cm^2)	βa (mV/dec)	βc (mV/dec)	CR (µm/y)	IE (%)
20	-0.434	1.01 x 10^{-5}	109	186	118	38.0
40	-0.604	1.54 x 10^{-5}	69	207	181	36.0
60	-0.630	1.60 x 10^{-5}	47	215	188	33.5
$Ce(hfac)_3$						
Temp. (°C)	E_{corr} (V)	i_{corr} (A/cm^2)	βa (mV/dec)	βc (mV/dec)	CR (µm/y)	IE (%)
20	-0.554	1.00 x 10^{-5}	135	81	104	46.0
40	-0.643	1.57 x 10^{-5}	54	120	163	43.0
60	-0.597	1.94 x 10^{-5}	46	301	200	41.0
$La(acac)_3$						
Temp. (°C)	E_{corr} (V)	i_{corr} (A/cm^2)	βa (mV/dec)	βc (mV/dec)	CR (µm/y)	IE (%)
20	-0.575	1.04 x 10^{-5}	126	211	109	36.0
40	-0.592	1.61 x 10^{-5}	125	182	169	33.0
60	-0.584	2.09 x 10^{-5}	66	151	219	28.0
$La(hfac)_3$						
Temp. (°C)	E_{corr} (V)	i_{corr} (A/cm^2)	βa (mV/dec)	βc (mV/dec)	CR (µm/y)	IE (%)
20	-0.650	1.01x 10^{-5}	212	116	119	38.0
40	-0.637	1.58 x 10^{-5}	69	164	186	34.0
60	-0.691	2.04 x 10^{-5}	92	127	240	29.0

The potentiodynamic curves of the mild steel for all the tested temperatures and corrosion inhibitors in the 3.5% NaCl solutions are shown in Figure 4.3, while the corresponding test results with 304 SS under similar conditions are displayed in Figure 4.4.

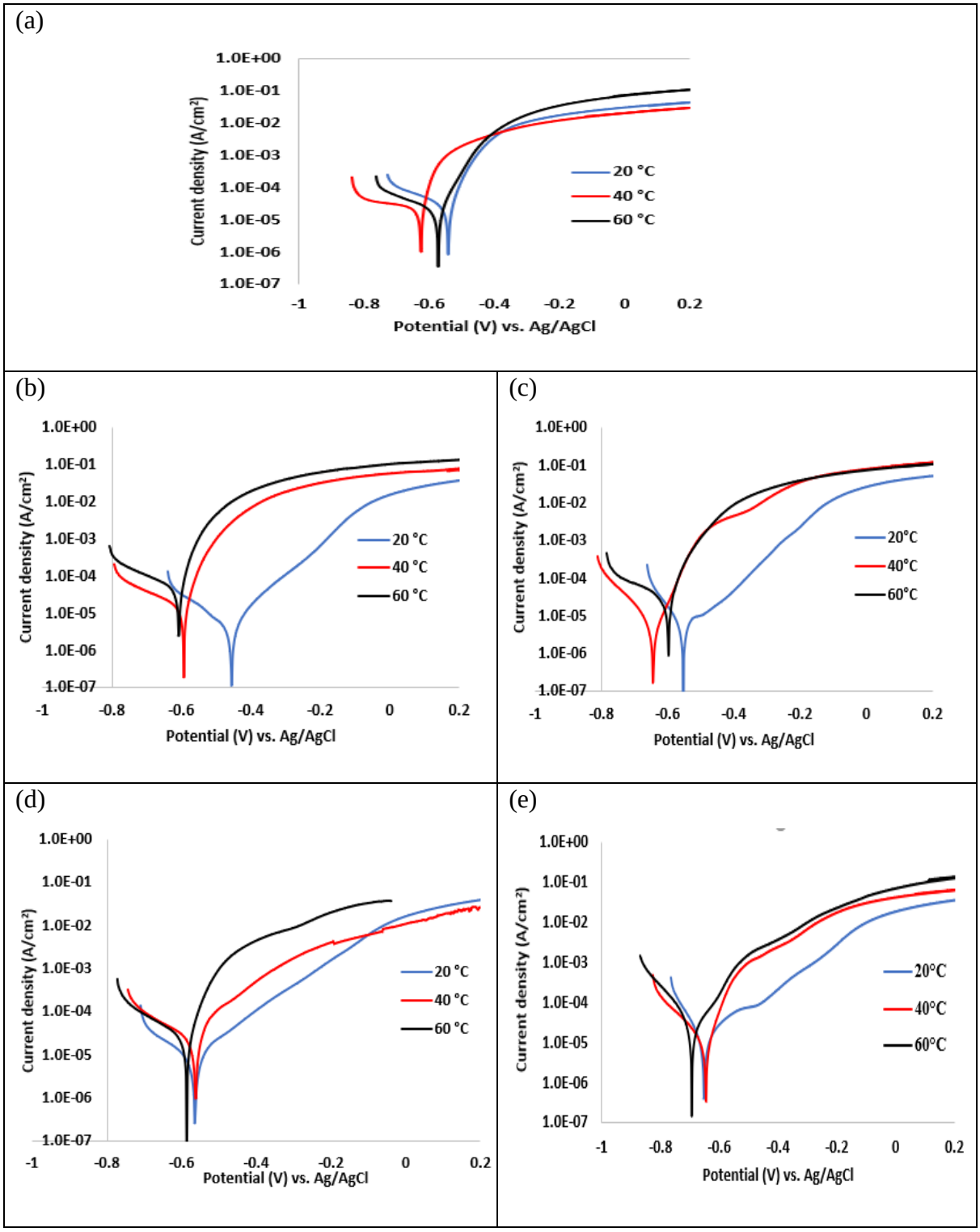


Figure 4.3: Potentiodynamic polarisation curves of mild steel in 3.5 % NaCl solution with (a) MS without inhibitor (b) $Ce(acac)_3$ (c) $Ce(hfac)_3$ (d) $La(acac)_3$ (e) $La(hfac)_3$ inhibitor.

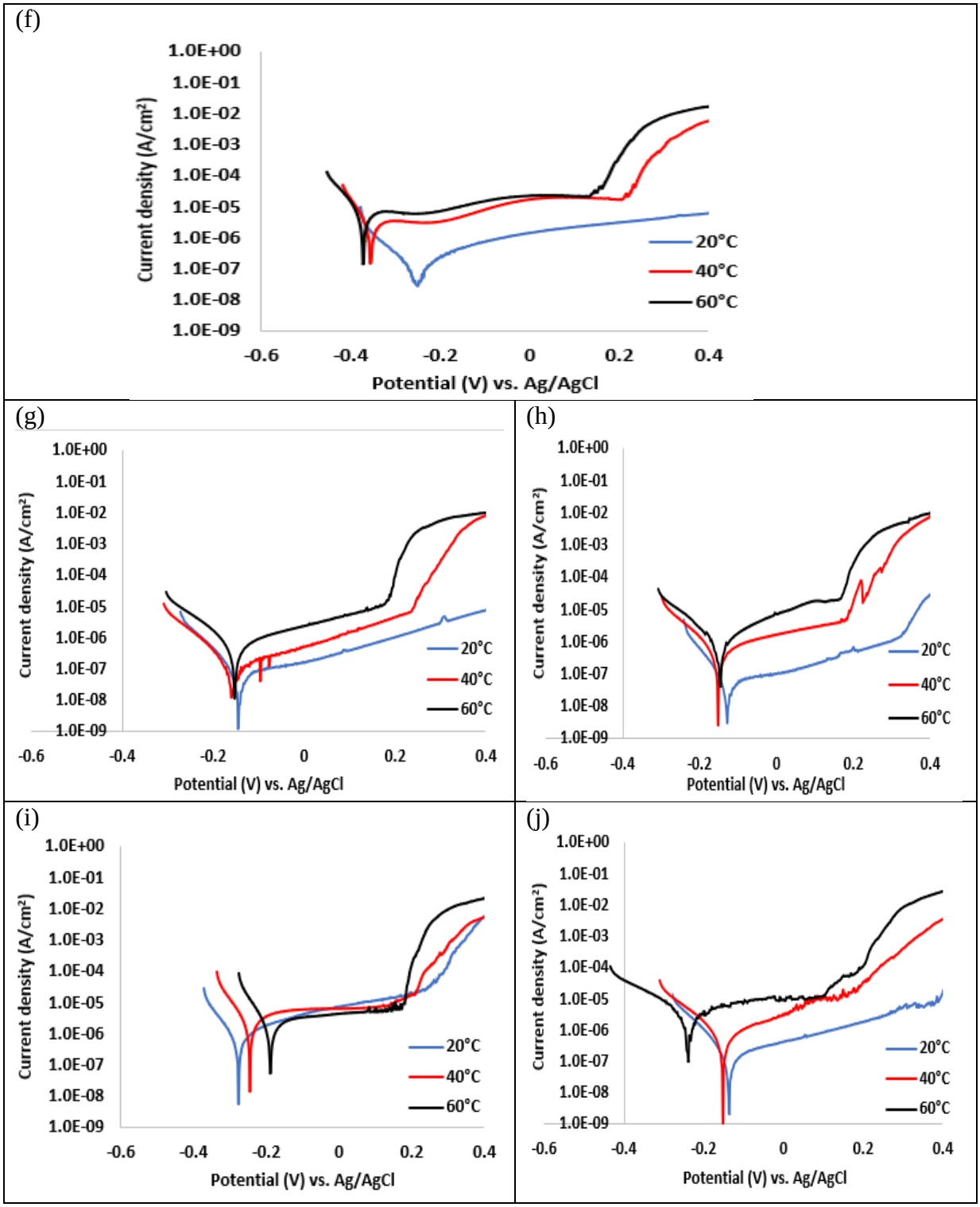


Figure 4.4: Potentiodynamic polarisation curves of 304 SS in 3.5 % NaCl solution with (f) 304 SS without inhibitor (g) $Ce(acac)_3$ (h) $Ce(hfac)_3$ (i) $La(acac)_3$ (j) $La(hfac)_3$ inhibitor.

Table 4.4: Electrochemical parameters of 304 SS obtained from the potentiodynamic polarisation curves in 3.5 % NaCl solution and with corrosion inhibitors $Ce(acac)_3$, $Ce(hfac)_3$, $La(acac)_3$ and $La(hfac)_3$ present in the solution.

3.5 % NaCl solution without inhibitor						
Temp. (°C)	E_{corr} (V)	i_{corr} (A/cm^2)	βa (mV/dec)	βc (mV/dec)	CR (µm/y)	IE (%)
20	-0.287	3.66 x 10^{-7}	351	67	3.79	
40	-0.359	1.40 x 10^{-6}	76	49	14.50	
60	-0.370	4.47x 10^{-6}	123	57	56.66	
			$Ce(acac)_3$			
Temp. (°C)	E_{corr} (V)	i_{corr} (A/cm^2)	βa (mV/dec)	βc (mV/dec)	CR (µm/y)	IE (%)
20	-0.434	1.01 x 10^{-5}	109	186	118	38.0
40	-0.604	1.54 x 10^{-5}	69	207	181	36.0
60	-0.630	1.60 x 10^{-5}	47	215	188	33.5
			$Ce(hfac)_3$			
Temp. (°C)	E_{corr} (V)	i_{corr} (A/cm^2)	βa (mV/dec)	βc (mV/dec)	CR (µm/y)	IE (%)
20	-0.554	1.00 x 10^{-5}	135	81	104	46
40	-0.643	1.57 x 10^{-5}	54	120	163	43
60	-0.597	1.94 x 10^{-5}	46	301	200	41
			$La(acac)_3$			
Temp. (°C)	E_{corr} (V)	i_{corr} (A/cm^2)	βa (mV/dec)	βc (mV/dec)	CR (µm/y)	IE (%)
20	-0.575	1.04 x 10^{-5}	126	211	109	36
40	-0.592	1.61 x 10^{-5}	125	182	169	33
60	-0.592	2.09 x 10^{-5}	66	151	219	28
			$La(hfac)_3$			
Temp. (°C)	E_{corr} (V)	i_{corr} (A/cm^2)	βa (mV/dec)	βc (mV/dec)	CR (µm/y)	IE (%)
20	-0.650	1.01x 10^{-5}	212	116	119	38
40	-0.592	1.58x 10^{-5}	69	164	186	34
60	-0.691	2.04x 10^{-5}	92	127	240	29

The table above (Table 4.4) summarises the relevant electrochemical parameters derived from the potentiodynamic curves in Figure 4.4 for the evaluations done with 304 SS in the various solutions.

Two substantial deductions immediately become apparent when evaluating the results in Table 4.4. Firstly, there is generally a significant decrease in the corrosion rate of the material when the different corrosion inhibitors are present in the solution as compared to that in the solution without any inhibitor. With the stainless steel samples exposed to 3.5% NaCl, there is a definitive shift in the corrosion potential to more noble values in the presence of all four corrosion inhibitors, hinting that they act as anodic type inhibitors. The efficiency of the different inhibitors to reduce the corrosion rates in the NaCl solution with the stainless steel samples is also substantially higher than in the case of the mild steel, especially at the lower temperatures. As was the case with the mild steel in the NaCl solution, these tests showed that the inhibitors were not 100% effective in their corrosion inhibition efficiency. Secondly, there is a definite decrease in corrosion inhibitor efficiency with an increase in the temperature of the corrosive solution, a trend that was not so clear or pronounced in the case of the mild steel samples when the solution temperature increased to 60^{o}C.

4.8 SURFACE ANALYSIS OF THE SPECIMENS

4.8.1 OPTICAL MICROSCOPY

The images of the MS and 304 SS specimens were taken using an optical microscope before exposure and after the electrochemical tests in a NaCl solution and with $Ce(acac)_3$, $Ce(hfac)_3$, $La(acac)_3$ and $La(hfac)_3$ inhibitors are shown in Figures 4.5, 4.6 and 4.7. The images revealed the formation of pitting corrosion uniformly distributed on the surface of the MS electrodes that were retrieved from NaCl solutions at 40 and 60^{o}C. However, at a concentration of 0.5 wt. % (m/v) in $Ce(acac)_3$ and $La(acac)_3$ inhibitors, there was a reduction in pitting corrosion of the mild steel, while no pitting was observed for 304 SS with $Ce(hfac)_3$ and $La(hfac)_3$ inhibitors. The micrographs after the potentiodynamic tests showed that both MS and 304 SS were well protected against localised corrosion. The observed results agree with the investigation of Forsyth et al. (2008) and Somers et al. (2018) where they used different REE compounds on mild steel and an aluminium alloy to prevent pitting corrosion. Boudellioua et

al. (2020) also confirmed this observation in their investigation when using cerium nitrate at an optimal concentration of 600 mg/L on mild steel in 0.1 M NaCl solution in a temperature range of 25 – 75^{o}C to reduce pitting corrosion.

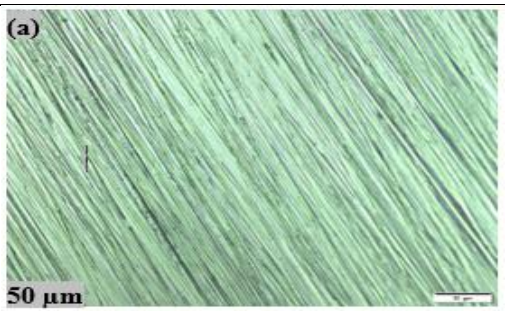
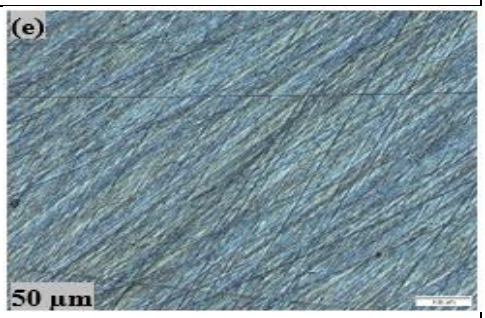
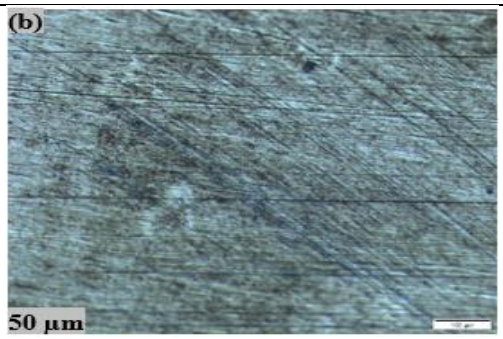
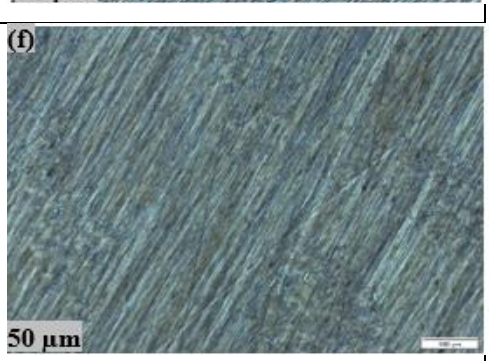
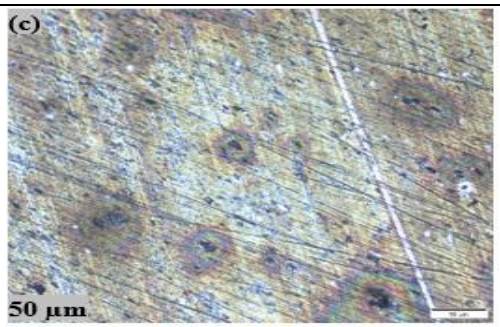
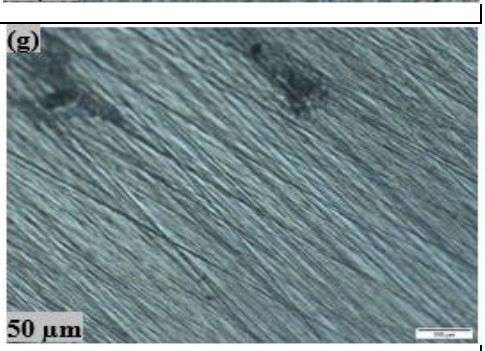
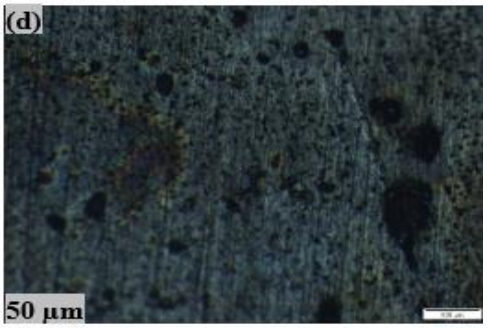
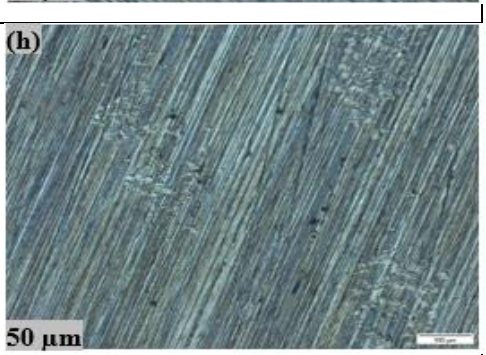
	MS	304 SS
		
20^{o}C		
40^{o}C		
60^{o}C		

Figure 4.5: Optical micrographs of (a) MS and (e) 304 SS electrode samples before exposure to NaCl solution, (b), (c), (d) MS and (f), (g), (h) 304 SS samples obtained at 20^{o}C, 40^{o}C, and 60^{o}C in 3.5 % NaCl solution after performing the electrochemical corrosion tests.

The micrographs in Figure 4.5 confirm what one would expect on a theoretical basis, i.e. that the degree of pitting increases with an increase in temperature and that the pits on the stainless steel surface are far fewer and much smaller than those on the mild steel under similar conditions. The manner in which the appearance of the mild steel and stainless steel in the presence of the various corrosion inhibitors changes, is illustrated in Figures 4.6 and 4.7.

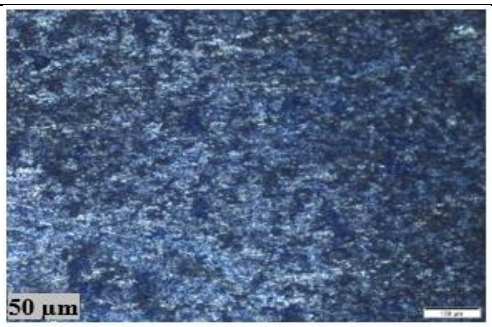
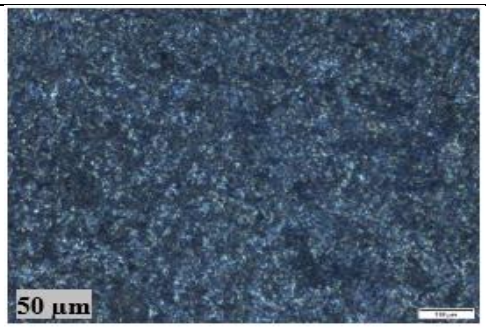
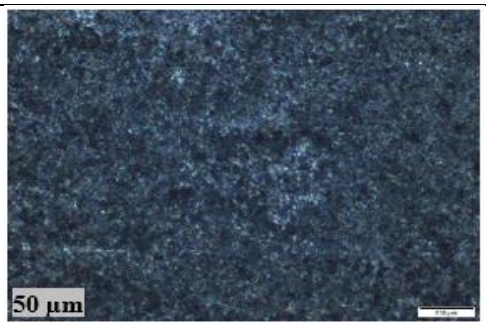
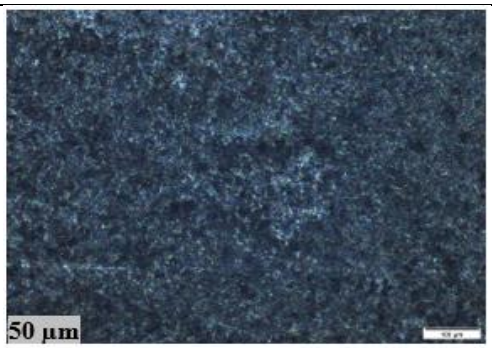
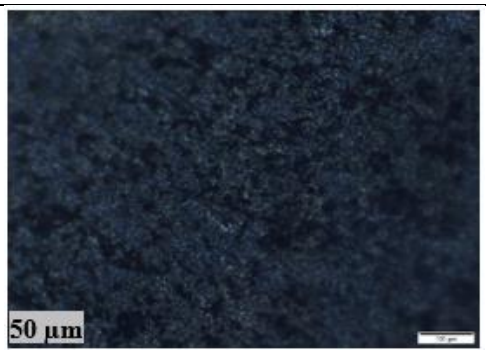
	Inhibited MS with $Ce(acac)_3$	Inhibited MS with $La(acac)_3$
20^{o}C		
40^{o}C		
60^{o}C		

Figure 4.6: Optical micrographs of inhibited mild steel in 3.5 % NaCl solution doped with $Ce(acac)_3$ and $La(acac)_3$ at 20^{o}C, 40^{o}C and 60^{o}C.

From the micrographs displayed in Figure 4.6, it appears that there are fewer and smaller pits on the surfaces of the mild steel samples exposed to the sodium chloride solution when the inhibitors are present than without them. One cannot distinguish a difference between the pitting corrosion occurring in the presence of the two different inhibitors. It is therefore questionable if the type of REE in the inhibitor plays a significant role in the efficiency of the inhibitor. This corresponds to the values summarised in Tables 4.3 and 4.4 in terms of the percentage efficiency of the different corrosion inhibitors. Further work with similar β-diketone inhibitors in other REE complexes can confirm whether this is indeed the case and should be pursued in the future. Apart from the fact that there is clearly much less pitting on the surfaces of the stainless steel samples compared to the mild steel samples, similar observation can be made about the presence of the different corrosion inhibitors.

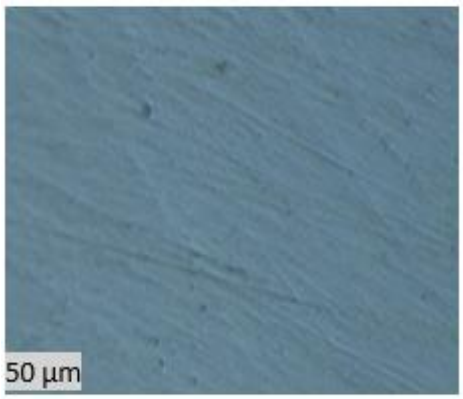
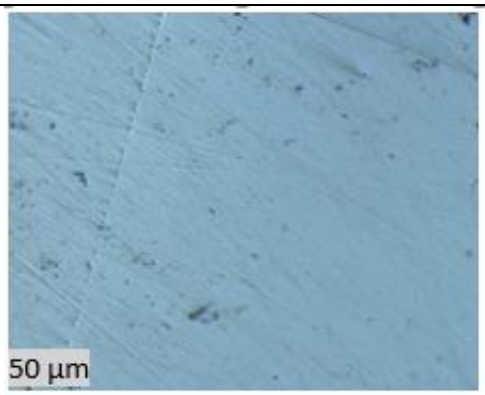
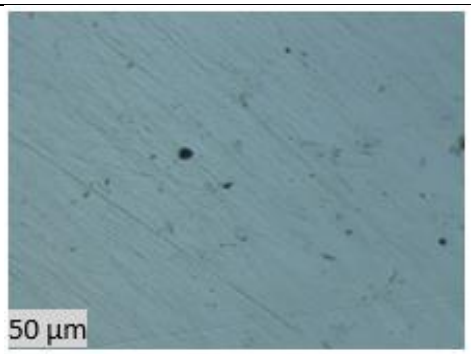
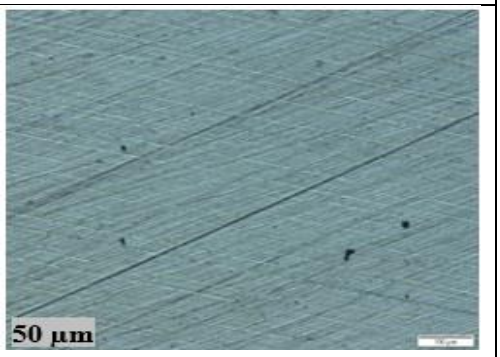
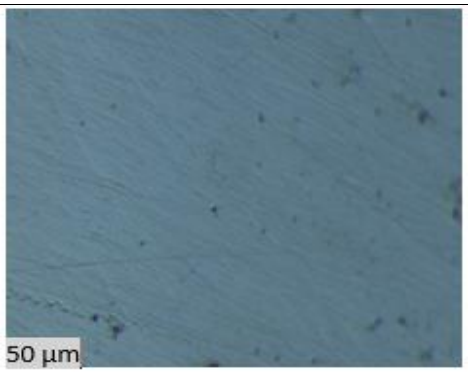
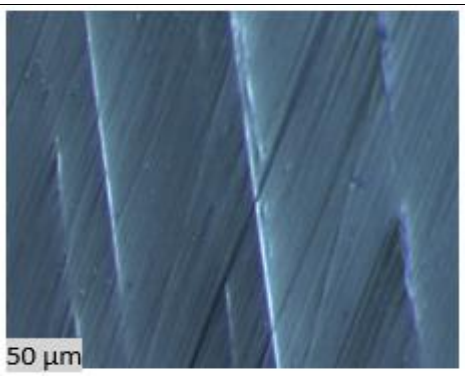
	304 SS with $Ce(hfac)_3$	304 SS with $La(hfac)_3$
20°C		
40°C		
60°C		

Figure 4.7: Optical micrographs of inhibited mild steel in 3.5 % NaCl solution doped with $Ce(hfac)_3$ and $La(hfca)_3$ at 20°C, 40°C and 60°C.

4.8.2 SCANNING ELECTRON MICROSCOPY AND ENERGY-DISPERSIVE X-RAY SPECTROSCOPY ANALYSIS (SEM/EDS)

Figures 4.8, 4.9, and 4.10 show the SEM images of MS and 304 SS working electrodes before and after exposure with and without the REE β-diketone inhibitor complexes at 20°C, 40°C, and 60°C. As the temperature of the solution containing $Ce(acac)_3$, $Ce(hfac)_3$, $La(acac)_3$ and

$La(hfac)_3$ inhibitors increases to 60°C, the surface morphologies of both MS and 304 SS change compared to the ones retrieved at lower temperatures under the same conditions and similar environments. Analysis with EDS (Figure 13) on the MS and 304 SS electrode surfaces that were exposed to solutions that contained $Ce(acac)_{3,}$ $Ce(hfac)_3$, $La(acac)_3$ and $La(hfac)_3$ revealed the formation of RE oxide and iron oxide containing films. These indicate that the main elements present in the corrosion product films are Ce or La, and Fe and O on the surfaces of MS and 304 SS electrodes. The observed results are in agreement with other authors' observations that have used REE compounds as a corrosion inhibitor for different alloys (Blin et al., 2006; Yasakau et al., 2006; Forsyth et al., 2008; Somers et al., 2018).

Amadeh et al., (2008) used a mixture of RE oxide (Ce and La) as a corrosion inhibitor for carbon steel in 0.6 M NaCl solutions. SEM and EDS analysis of the nature of the deposit formed on the surface of the tested sample reveals that the sample was covered with a layer of corrosion products consisting of particles with irregular shapes containing cerium (Ce) and iron (Fe) deposit.

A similar investigation was carried out by Somers et al. (2018) using SEM/EDS analysis on the film deposits formed on mild steel when rare-earth (La, Ce. Nd, and Y) methyl benzoyl propanoate compounds, $REE(mbp)_3$, were used as corrosion inhibitors in 0.01 M NaCl solution. EDS analysis showed that the corrosion product deposits predominantly consisted of compounds containing La and Y together with a large amount of Fe and O. For Ce and Nd methyl benzoyl propanoate complexes, only Fe and O were detected with no indication of Ce and Nd elements as part of the corrosion product which had been formed on the surface on the mild steel.

Mohammadi et al. (2020) studied corrosion inhibitive pigment for aluminium AA2024-T3 by using cerium diethyldithiocarbamate complex (Ce-DEDTC). SEM/EDS results of the tested alloy indicated that the surface of the specimen from the solution containing Ce-DEDTC, contained C, N, S, and Ce elements in the inhibitor film on the aluminium surface.

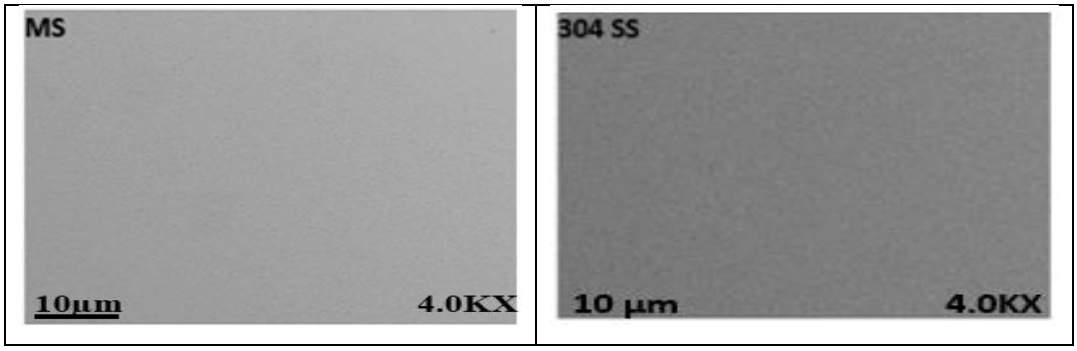


Figure 4.8: SEM micrographs of MS and 304 SS electrode surfaces before exposure in NaCl solution.

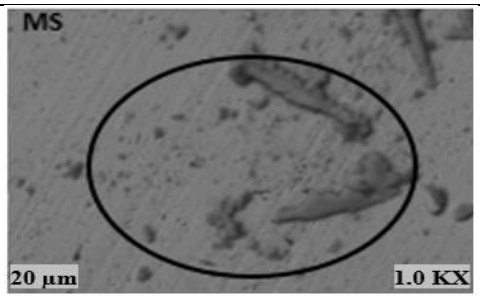
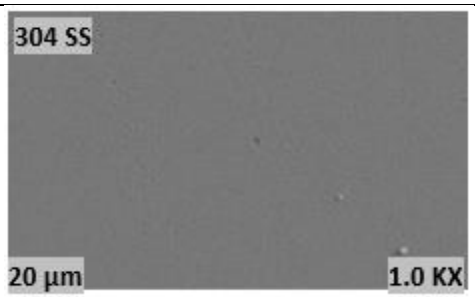
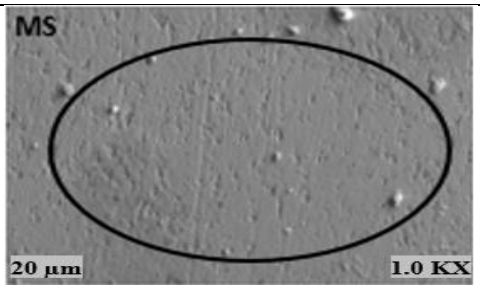
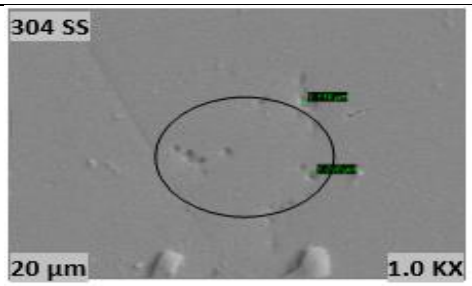
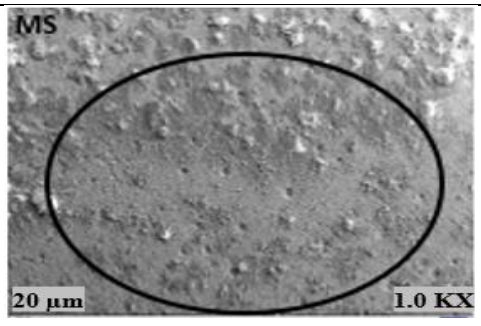
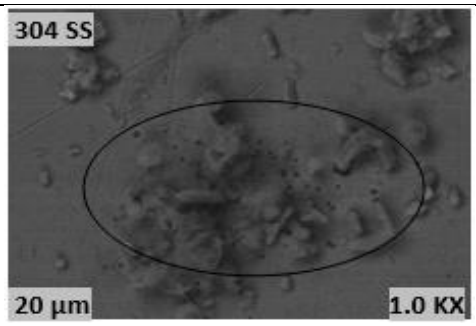
	Uninhibited MS	Uninhibited 304 SS
20°C		
40°C		
60°C		

Figure 4.9: SEM micrographs of uninhibited MS and 304 SS sample surfaces obtained after exposure to 3.5 % NaCl solution at 20°C, 40°C, and 60°C.

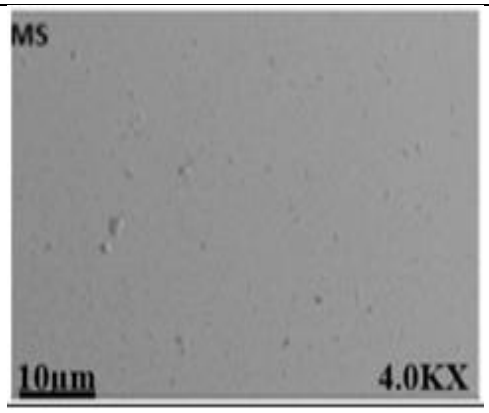
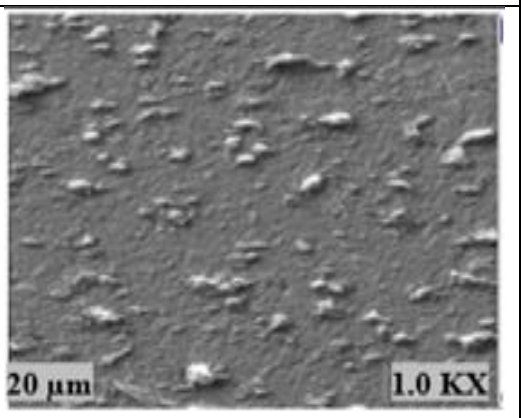
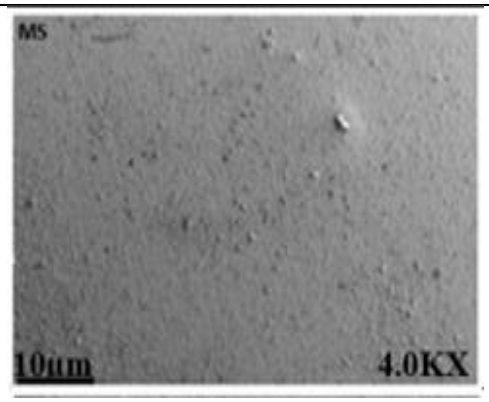
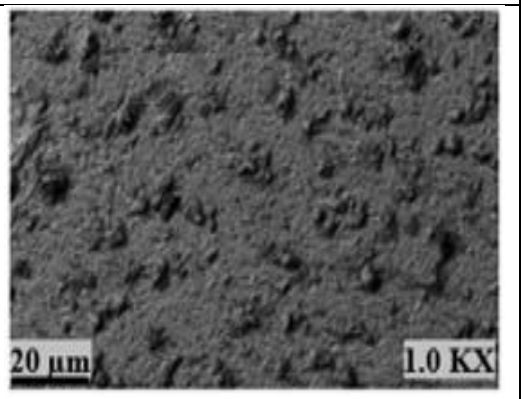
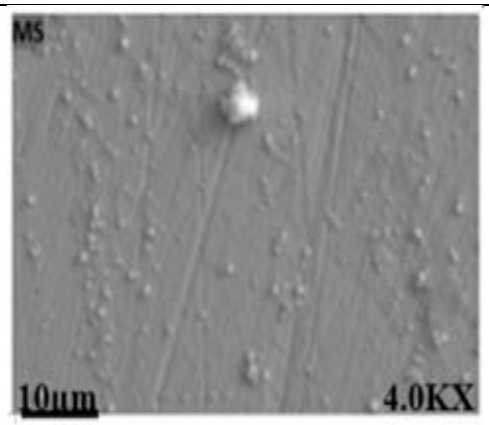
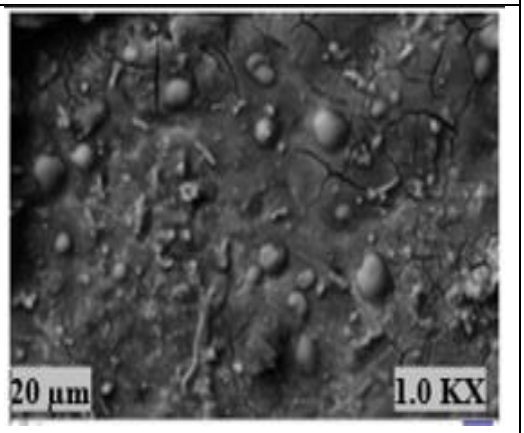
	MS with $Ce(acac)_3$	MS with $La(acac)_3$
20°C		
40°C		
60°C		

Figure 4.10: SEM micrographs of inhibited mild steel sample surfaces with $Ce(acac)_3$ and $La(acac)_3$ obtained after exposure to 3.5 % NaCl solutions at 20°C, 40°C, and 60°C.

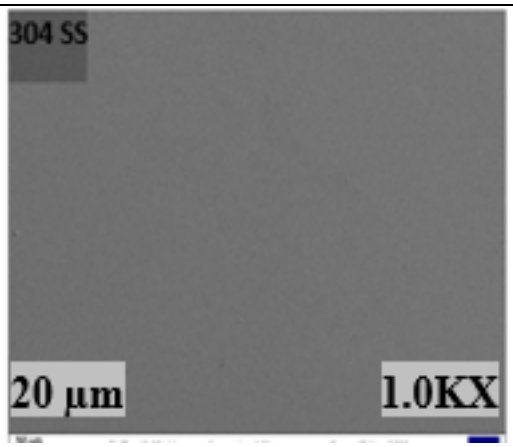
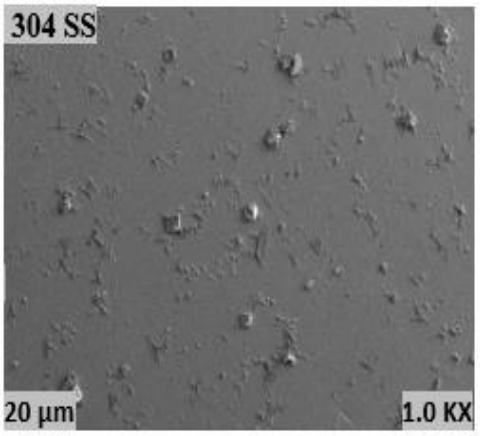
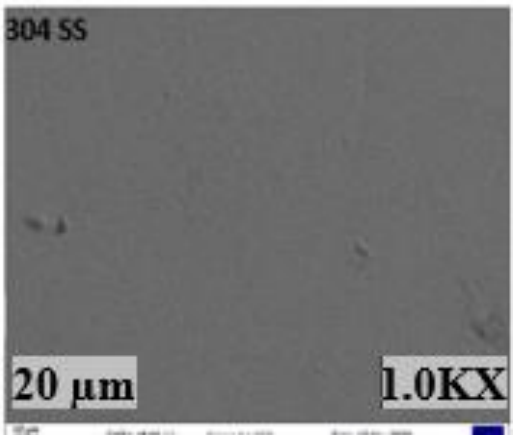
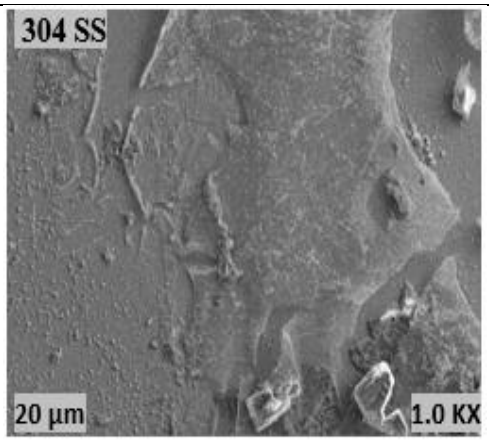
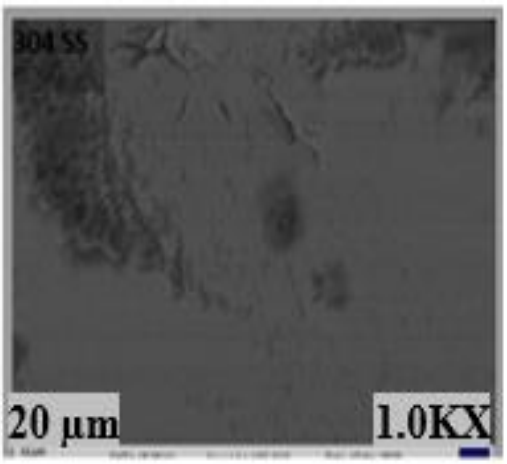
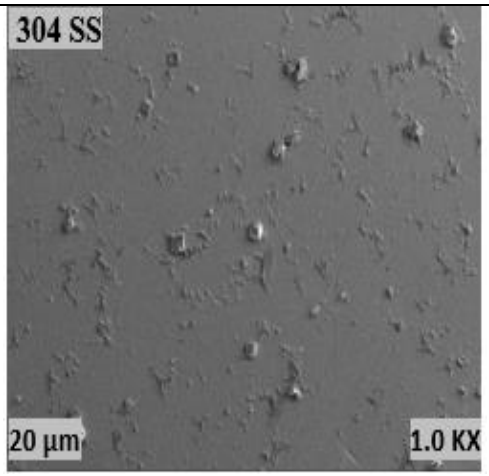
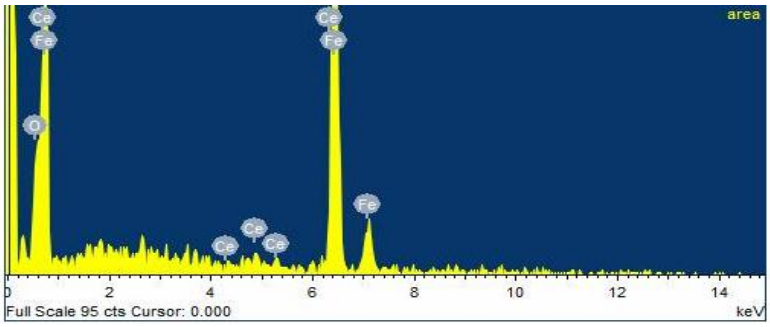
	304 SS with $Ce(hfac)_3$	304 SS with $La(hfac)_3$
20°C		
40°C		
60°C		

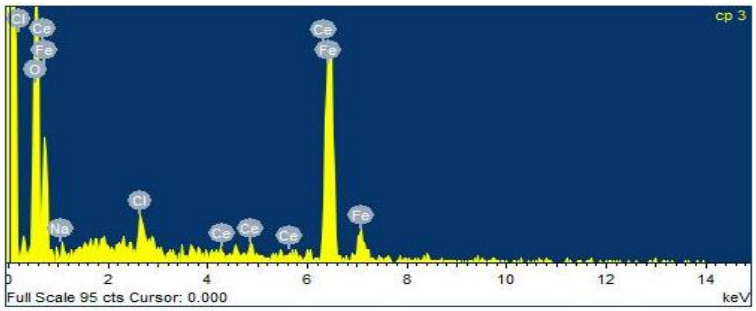
Figure 4.11: SEM micrographs of 304 SS sample surfaces inhibited with $Ce(hfac)_3$ and $La(hfac)_3$ obtained after exposure to 3.5 % NaCl solutions at 20°C, 40°C and 60°C.

(a)



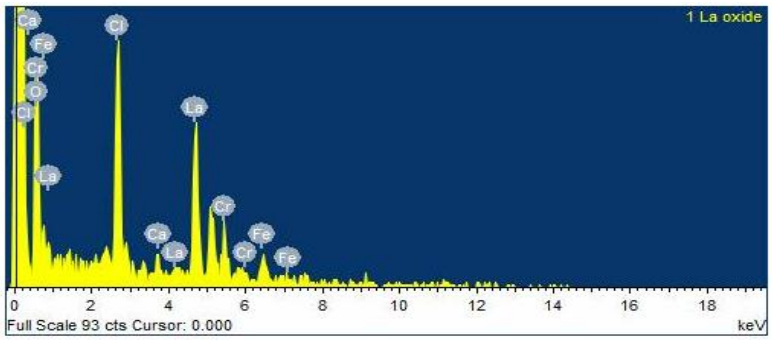
Element	Weight %	Atomic %
O K	5.52	17.13
Cl K	92.35	82.11
Ce L	2.13	0.76
Totals	100.00	

(b)



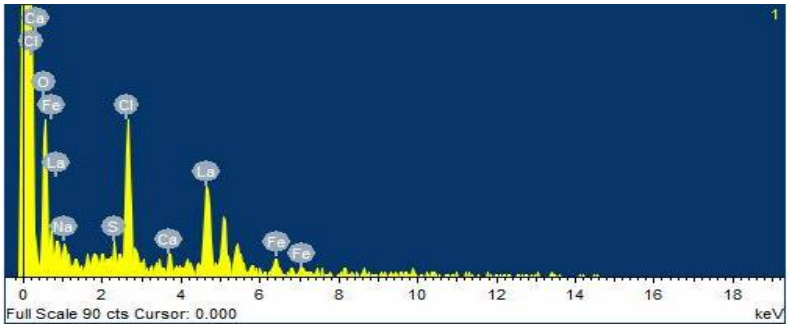
Element	Weight %	Atomic %
O K	29.97	59.88
Na K	0.55	0.75
Cl K	2.02	1.82
Fe K	64.37	36.84
Ce L	3.09	0.71
Totals	100.00	

(c)



Element	Weight %	Atomic %
O K	22.69	58.65
Cl K	14.80	17.27
Ca K	1.26	1.30
Cr K	3.14	2.49
Fe K	6.76	5.00
La L	51.36	15.29
Totals	100.00	

(d)



Element	Weight %	Atomic %
O K	19.86	54.13
Na K	2.64	4.54
S K	1.23	1.48
Cl K	13.60	15.80
Ca K	1.51	1.52
Fe K	7.30	6.05
La L	53.86	16.48
Totals	100.00	

Figure 4.12: EDS of (a) and (b) MS in 3.5 % NaCl solution containing 0.5 % wt. (m/v) of $Ce(acac)_3$ and $Ce(hfac)_3$ and (c) and (d) 304 SS with $La(acac)_3$ and $La(hfac)_3$.

4.9 SURFACE MAPPING OF THE MILD STEEL AND 304 STAINLESS STEEL

4.9.1 FOURIER-TRANSFORM INFRARED SPECTROSCOPY ANALYSIS

To understand the inhibition mechanism, FTIR analysis was carried out to probe the surfaces of the mild steel and 304 SS samples that were immersed in solutions containing $Ce(acac)_3$, $La(acac)_3$, $Ce(hfaca)_3$ or $La(hfac)_3$ after the electrochemical tests. The ν(OH) bands observed above 3000 cm^{-1} for the REE complexes were shifted to the 2967–2874 cm^{-1} range on the surface of the steel. The frequency bands observed at 1408–1632 cm^{-1} on the surface of the examined steel could be assigned to C=O. The disappearance and shift in the frequencies as observed in the spectra suggest that adsorption of the film on the surface of the investigated steel samples has taken place (Verma & Khan, 2016; Nwankwo et al., 2018). While the O–H band shift was significant for all the four corrosion inhibitors between the complex in its pure form and the complex present in the corrosion products, it was not always the case with the shift in the C=O bands. Only the C=O bands of the La type inhibitors displayed a substantial shift in their position in the corrosion film products compared to the pure compounds. This is the first indication from all the collected results that the metal in the β-diketone can indeed play a role in the inhibitor's performance. For comparison, the frequency of the absorption band of the REE complexes and the corrosion products are presented in detail in Table 4.5.

Table 4.5: IR frequency bands of REE $(\beta - \text{diketone})_3$ inhibitors and the corrosion products formed on mild steel and 304 stainless steel.

Inhibitor used	Inhibitor only		Corrosion Product	
	Frequency (cm^{-1})	Assignment	Frequency (cm^{-1})	Assignment
$Ce(acac)_3$	1584	C=O	1576	C=O
	3134	O-H	2967	OH
$La(acac)_3$	1595	C=O	1408	C=O
	3335	O-H	2967	OH
$Ce(hfac)_3$	1644	C=O	1632	C=O
	3041	O-H	2921	OH
$La(hfac)_3$	1648	C=O	1615	C=O
	3041	O-H	2920	OH

4.9.2 RAMAN SPECTROSCOPY

Raman spectroscopy (RS) was used to map the surface of the mild steel 304 stainless steel to analyse the nature and mechanism of the adsorption passive film formed on the surface of both mild steel and 304 stainless steel. The spectrums were measured in the range of 1900–90 cm^{-1}. It appeared that the obtained frequency bands shifted to a lower number. This change in the band could be attributed to the coordination between the inhibitor and the steel surface during the film formation. Details of the obtained frequency band of the corrosion products in comparison with that of the REE β-diketone complexes are presented in Table 4.6.

It is observed that the carbonyl C=O stretching and OH frequency band from the keto-enol group disappeared completely in the steel-REE β-diketone complexes spectrum, indicating the involvement of oxygen present in REE β-diketone complexes in the adsorption process. The shift observed in C-H in-plane, C-H out of place stretching vibration and the C=C vibration could be attributed to the interaction of these frequencies group with the steel surface (Cao et al., 2002; Caldona et al., 2021). The frequency bands observed at 524 cm^{-1} and 377 cm^{-1} are an indication of metal-oxygen bonding formed as a rare earth oxide (REE–O) protective film on the surface of the steels (Markley et al., 2007; Forsyth et al., 2008; Boudellioua et al., 2017; Cotting & Aoki, 2020). The frequencies bands at 248 cm^{-1} and 244 cm^{-1} could be assigned to stretching vibration such as iron oxide/hydroxide, respectively (De Faria et al., 1997; Jubb & Allen, 2010; Babouri et al., 2015; Criado et al., 2015; Lin & Zuo, 2019; Boudellioua et al., 2019).

Table 4.6: Raman frequency shifts of $Ce(acac)_3$, $La(acac)3$, $Ce(hfac)3$ and $La(hfac)3$ inhibitor and the corrosion products on mild steel and 304 stainless steel.

Inhibitor used	Inhibitor only		Corrosion Product	
	Frequency (cm^{-1})	Assignment	Frequency (cm^{-1})	Assignment
$Ce(acac)_3$	1583	C=O	377, 248	Fe–O
	455	REE–O	524	REE–O
$La(acac)_3$	1598	C=O	377, 244	Fe–O
	492	REE–O	524	REE–O
$Ce(hfac)_3$	1654	C=O	377, 250	Fe–O
	445	REE–O	530	REE–O
$La(hfac)_3$	1681	C=O	377, 246	Fe–O
	455	REE–O	526	REE–O

4.10 CONCLUSIONS

- The four tested REE β-diketone inhibitors are reasonably effective corrosion inhibitors against localised corrosion for mild steel and 304 SS in 3.5 % NaCl solution and decrease the overall corrosion rates at the concentration of 0.5 % employed.
- Surface analysis results obtained from Raman spectra confirm the formation of a protective film layer containing a rare earth element oxide and iron oxide/hydroxide on the mild steel and 304 SS.
- As the temperature increased, there was a consistent decrease in the value of cathodic Tafel constants compared to when no inhibitors were used under the same conditions and environment. This decrease in the trend of the cathodic Tafel constant confirms that the tested REE β-diketone complexes act as cathodic corrosion inhibitors. With the stainless steel samples exposed to 3.5 % NaCl, there is a definitive shift in the corrosion potential to more noble values in the presence of all four corrosion inhibitors, hinting that they act as anodic type inhibitors. One can therefore conclude that the inhibitors are probably mixed corrosion inhibitors whose mode of action depends on the environment and material present when they are used.
- The concentration of 0.5% applied is not sufficient to afford a 100% inhibitor efficiency

for either the stainless steel (except at room temperature in the mass loss tests) or the mild steel, especially as the testing temperature increases. It is recommended that a range of higher concentrations be further investigated.

- While one incidence of slight evidence was observed that the type of rare earth element metal present in the corrosion inhibitor could be important, no conclusive evidence could be obtained that either the β-diketone or rare earth element metal played a significant role in the performance of the corrosion inhibitors. Further work with similar inhibitors in which either or both the β-diketone component or rare earth element in the corrosion inhibitor are varied, should be undertaken in the future.

4.11 REFERENCES

Amadeh, A., Allahkaram, S. R., Hosseini, S. R., Moradi, H., & Abdolhosseini, A. (2008). The use of rare-earth cations as corrosion inhibitors for carbon steel in aerated NaCl solution. Anti-corrosion Methods and Materials, 55(3), 135-143.

Ahmed E. F, Mutasem Z. B, Khaled F. F, Taher S, N. S., & A and Hisham S. M. A. (2018). Raman spectra of copper, cobalt, and nickel complexes of nicotinic acid: equilibrium studies. Bulletin of the Chemical Society of Ethiopia, 32(3), 459–467.

Al-Amiery, A. A., Binti Kassim, F. A., Kadhum, A. A. H., & Mohamad, A. B. (2016). Synthesis and characterization of a novel eco-friendly corrosion inhibition for mild steel in 1 M hydrochloric acid. Scientific Reports, 6, 1–13.

ASTM Standard G-31-72, (1999). 'Standard Practice for Laboratory Immersion Corrosion Testing of Metals'. American Society for Testing and Materials International, West Conshohocken, PA, USA.

ASTM Standard G-5-94, (2004). Standard Reference Test for Making Potentiostatic and Potentiodynamic Anodic polarization Measurements. American Society for Testing and Materials International, West Conshohocken, PA, USA.

Avdeev, Y. G., Kuznetsov, Y. I., & Buryak, A. K. (2013). Inhibition of steel corrosion by unsaturated aldehydes in solutions of mineral acids. Corrosion Science, 69, 50–60.

Babouri, L., Belmokre, K., Abdelouas, A., Bardeau, J. F., & El Mendili, Y. (2015). The inhibitive effect of cerium carbonate on the corrosion of brass in 3% NaCl solution. International Journal of Electrochemical Science, 10(9), 7818–7839.

Blin, F., Leary, S.G., Wilson, K., Deacon, G.B., Junk, P.C., & Forsyth, M. (2004). Corrosion mitigation of mild steel by new rare earth cinnamate compounds. Applied Electrochemistry, 34(6), pp. 591-599.

Blin, F., Leary, S. G., Deacon, G. B., Junk, P. C., & Forsyth, M. (2006). The nature of the surface film on steel treated with cerium and lanthanum cinnamate based corrosion inhibitors. Corrosion Science, 48(2), 404–419.

Boudellioua, H., Hamlaoui, Y., Tifouti, L., & Pedraza, F. (2017). Comparison Between the Inhibition Efficiencies of Two Modification Processes with PEG–Ceria Based Layers Against Corrosion of Mild Steel in Chloride and Sulfate Media. Materials Engineering and Performance, 26(9), 4402–4414.

Boudellioua, H., Hamlaoui, Y., Tifouti, L., & Pedraza, F. (2019). Effects of polyethylene glycol (PEG) on the corrosion inhibition of mild steel by cerium nitrate in chloride solution. Applied Surface Science, 473, 449–460.

Boudellioua, H., Hamlaoui, Y., Tifouti, L., & Pedraza, F. (2020). Effect of the temperature of cerium nitrate–NaCl solution on corrosion inhibition of mild steel. Materials and Corrosion, 71(8), 1300–1309.

Caldona, E. B., Zhang, M., Liang, G., Hollis, T. K., Webster, C. E., Smith, D. W., & Wipf, D. O. (2021). Corrosion inhibition of mild steel in acidic medium by simple azole-based aromatic compounds. Journal of Electroanalytical Chemistry, 880, 114858.

Cao, P., Gu, R., & Tian, Z. (2002). Electrochemical and Surface-Enhanced Raman Spectroscopy Studies on Inhibition of Iron Corrosion by Benzotriazole. Langmuir, 18(6), 7609–7615.

Carneiro, J., Tedim, J., Fernandes, S. C. M., Freire, C. S. R., Silvestre, A. J. D., Gandini, A., Ferreira, M. G. S., & Zheludkevich, M. L. (2012). Chitosan-based self-healing protective coatings doped with cerium nitrate for corrosion protection of aluminum alloy 2024. Progress in Organic Coatings, 75, 8–13.

Cotting, F., & Aoki, I. V. (2020). Octylsilanol and Ce(III) ions – Alternative corrosion inhibitors for carbon steel in chloride neutral solutions. Materials Research and Technology, 9(4), 8723–8734.

De Faria, D. L. A., Venâncio Silva, S., & De Oliveira, M. T. (1997). Raman microspectroscopy of some iron oxides and oxyhydroxides. Journal of Raman Spectroscopy, 28(11), 873–878.

Desa, M. N., & Desai, M. B. (1984). Carbonyl compounds as corrosion inhibitors for mild steel in HC1 solutions. Corrosion Science, 24(8), 649–660.

Esmailzadeh, S., Aliofkhazraei, M., & Sarlak, H. (2018). Interpretation of Cyclic Potentiodynamic Polarization Test Results for Study of Corrosion Behavior of Metals: A Review. Protection of Metals and Physical Chemistry of Surfaces, 54(5), 976–989.

Fouda, A. S., Abd El-Wahab, S. M., Attia, M. S., Youssef, A. O., & Elmoher, H. O. (2015). Rare earth metals as eco-friendly corrosion inhibitors for mild steel in produced water. Der Pharma Chemica, 7(8), pp. 74–87.

Forsyth, M., Wilson, K., Behrsing, T., Forsyth, C., Deacon, G. B., & Phanasgoankar, A. (2002). Effectiveness of rare-earth metal compounds as corrosion inhibitors for steel. Corrosion Science, vol 58(11), pp. 953–960.

Forsyth, M., Markley, T., Ho, D., Deacon, G. B., Junk, P., Hinton, B., & Hughes, A. (2008). Inhibition of Corrosion on AA2024-T3 by New Environmentally Friendly Rare Earth Organophosphate Compounds. Corrosion Science, 64(3), 191–197.

Forsyth, M., Seter, M., Hinton, B., Deacon, G., & Junk, P. (2011). New "Green" corrosion inhibitors based on rare earth compounds. Australian Journal of Chemistry, 64(6), pp. 812–819.

Fragoza-Mar, L., Olivares-Xometl, O., Domínguez-Aguilar, M. A., Flores, E. A., Arellanes-Lozada, P., & Jiménez-Cruz, F. (2012). Corrosion inhibitor activity of 1,3-diketone malonates for mild steel in aqueous hydrochloric acid solution. Corrosion Science, 61, 171–184.

Gao, J., Weng, Y., Salitanate, Feng, L., & Yue, H. (2009). Corrosion inhibition of α, β-unsaturated carbonyl compounds on steel in acid medium. Petroleum Science, 6(2), 201–207.

Ghanbari, A., Attar, M. & Mahdavian, M. (2009). Acetylacetonate Complexes as New Corrosion Inhibitors in Phosphoric Acid Medium. Progress in Color, Colorants and Coating, 2(2), 115–122.

Gharbi, O., Thomas, S., Smith, C., & Birbilis, N. (2018). Chromate replacement : what does the future hold ? Npj Materials Degradation, 2, 23–25.

Go, L. C., Depan, D., Holmes, W. E., Gallo, A., Knierim, K., Bertrand, T., & Hernandez, R. (2020). Kinetic and thermodynamic analyses of the corrosion inhibition of synthetic extracellular polymeric substances. PeerJ Materials Science, 2, 1–22.

Gobara, M., Baraka, A., Akid, R., & Zorainy, M. (2020). Corrosion protection mechanism of Ce4+/organic inhibitor for AA2024 in 3.5% NaCl. RSC Advances, 10(4), 2227–2240.

Hinton, B. R. . (1992). Corrosion Inhibition with Rare Earth Metal Salts. Alloys and Compounds, 180, 15–25.

Horiguchi, K., Sawamura, K., Saito., I., & Hayakawa., Y. (1968). β-Diketones as Corrosion Inhibitors for Aluminum in Alkaline Media. Electrochemical Society of Japan, 34(3), 162–164.

Jubb, A. M., & Allen, H. C. (2010). Vibrational spectroscopic characterization of hematite, maghemite, and magnetite thin films produced by vapor deposition. ACS Applied Materials and Interfaces, 2(10), 2804–2812.

Khaled, K. F. (2013). Electrochemical evaluation of environmentally friendly cerium salt as corrosion inhibitor for steel in 3.5 % NaCl. International Journal of Electrochemical Science, 8(3), 3974–3987.

Lin, C. S., & Li, W. J. (2006). Corrosion resistance of cerium-conversion coated AZ31 magnesium alloys in cerium nitrate solutions. Materials Transactions, 47(4), 102–1025.

Markley, T. A., Forsyth, M., & Hughes, A. E. (2007). Corrosion protection of AA2024-T3 using rare earth diphenyl phosphates. Electrochimica Acta, 52(12), 4024–4031.

Mohammadi, I., Shahrabi, T., Mahdavian, M., & Izadi, M. (2020). Cerium/diethyldithiocarbamate complex as a novel corrosion inhibitive pigment for AA2024-T3. Scientific Reports, 1–15.

Matter, E. A., Kozhukharov, S., Machkova, M., & Kozhukharov, V. (2012). Comparison between the inhibition efficiencies of Ce(III) and Ce(IV) ammonium nitrates against corrosion of AA2024 aluminum alloy in solutions of low chloride concentration. Corrosion Science, 62, 22–33.

Nam, N. D., Thang, V. Q., Hoai, N. T., & Hien, P. V. (2016). Yttrium 3-(4-nitrophenyl)-2-propenoate used as inhibitor against copper alloy corrosion in 0.1 M NaCl solution. Corrosion Science, 112, 451–461.

Nam, N. D., Ha, P. T. N., Anh, H. T., Hoai, N. T., & Hien, P. V. (2019). Role of hydroxyl group in cerium hydroxycinnamate on corrosion inhibition of mild steel in 0.6 M NaCl solution. Journal of Saudi Chemical Society, 23(1), 30–42.

Nwankwo, H. U., Olasunkanmi, L. O., & Ebenso, E. E. (2018). Electrochemical and Computational Studies of Some Carbazole Derivatives as Inhibitors of Mild Steel Corrosion in Abiotic and Biotic Environments. Journal of Bio- and Tribo-Corrosion, 4(2), 1–17.

Okawara, T., Ishihama, K., & Takehara, K. (2014). Redetermination of diaquatris(4-oxopent-2-en-2-olato-κ 2O,O0)lanthanum(III). Acta Crystallographica Section E: Structure Reports Online, 70(7).

Peng, Y., Hughes, A. E., Deacon, G. B., Junk, P. C., Hinton, B. R. W., Forsyth, M., Mardel, J. I., & Somers, A. E. (2018). A study of rare-earth 3-(4-methyl benzoyl)-propanoate compounds as corrosion inhibitors for AS1020 mild steel in NaCl solutions. Corrosion Science, 145, 199–211.

Ruiz, M. I., Heredia, A., Botella, J., & Odriozola, J. A. (1995). Study of the reaction of lanthanum nitrate with metal oxides present in the scale formed at high temperatures on stainless steel. Materials Science, 30(20), 5146–5150.

Sastri, V. S., Ghali, E., & Elboujdaini, M. (2007). Corrosion Prevention and Protection: Practical Solutions. John Wiley & Sons, Chichester, England.

Somers, A. E., Hinton, B. R. W., Bruin-Dickason, C. De., Deacon, G. B., Junk, P. C., & Forsyth, M. (2018). New environmentally friendly rare earth carboxylate corrosion inhibitors for mild steel. Corrosion Science, 139, 430–437.

Verma, D. K., & Khan, F. (2016). Corrosion inhibition of mild steel in hydrochloric acid using extract of glycine max leaves. Research on Chemical Intermediates, 42(4), 3489–3506.

Volarič, B., & Milošev, I. (2017). Rare earth chloride and nitrate salts as individual and mixed inhibitors for aluminium alloy 7075-T6 in chloride solution. Corrosion Engineering Science and Technology, 52(3), 201–211.

Yasakau, K. A., Zheludkevich, M. L., Lamaka, S. V., & Ferreira, M. G. S. (2006). Mechanism of corrosion inhibition of AA2024 by rare-earth compounds. Physical Chemistry B, 110(11), pp. 5515–5528.

CHAPTER FIVE

Rare Earth Element (REE) β-diketone Complexes as Novel Corrosion Inhibitors for 304 and 316 Stainless Steel in 0.1 M HCl Solution

O.J. Lawal[1], J.H. Potgieter[1,2*], C. Billing[3]., and D.J. Whitefield[1].

[1]School of Chemical and Metallurgical Engineering, University of the Witwatersrand, Private Bag X3, Wits, 2050, South Africa

[2]Department of Natural Science, Faculty of Science and Engineering, Manchester Metropolitan University, Manchester, M1 5GD, UK

[3]Molecular Sciences Institute, School of Chemistry, University of the Witwatersrand, Private Bag X3, Wits, 2050, South Africa

*Corresponding author: herman.potgieter@wits.ac.za

ABSTRACT

The corrosion inhibition of austenitic stainless steel (304 and 316 SS) in 0.1M HCl solution was investigated in the temperature range of 20–60°C, using cerium and lanthanum acetylacetone and hexafluoroacetylacetone as potential green and novel corrosion inhibitors. Weight loss and potentiodynamic polarisation methods as well as surface analyses were used to investigate the effectiveness of these inhibitors in 0.1 M HCl solution. Experimental results showed that the REE β-diketone complexes are effective inhibitors to reduce the corrosion of 304 and 316 SS. Polarisation measurements indicated that the $Ce(acac)_3$, $La(acac)_3$, $Ce(hfac)_3$ and $La(hfac)_3$ acted as cathodic inhibitors. The nature of the metal surface after exposure to the corrosive solution was analysed by SEM and FTIR spectra, as well as Raman spectroscopy. Scanning electron microscopy (SEM) and Raman spectroscopy confirmed the formation of protective films of the inhibitors on the steel surfaces. The effect of temperature on the corrosion rate and inhibition efficiencies were also determined, and it was found that as the temperature increased, there was an increase in corrosion rate and a decrease in inhibition efficiency.

Keywords: Stainless steels; corrosion inhibitors; REE β-diketone; Polarisation; Raman spectroscopy

5.1 INTRODUCTION

Metallo-organic compounds of β-diketone are widely used due to their diverse application in the field of coordination chemistry research (Nandurkar et al., 2008; Verma et al., 2011; Bhise, et al., 2017). Among these compounds are rare earth element (REE) β-diketone complexes with a general formula of $M(RCOCHCOR')_n$ (where M is a rare earth metal, and R and R' represent alkyl, aryl, chlorinated alkyl, chlorinated aryl or phenyl group) which are produced from a reaction between a rare earth halide and various dicarbonyl compounds (β-diketone). Most investigations reported in the literature on REEs compounds as corrosion inhibitors have been related to the application of REE oxides, chlorides, sulphates and nitrates. They have been reported to be suitable and effective corrosion inhibitors for various steels, aluminium and other alloys in various corrosive environments (Amadeh et al., 2008; Matter et al., 2012; Fouda et al., 2015; Boudellioua et al., 2019; Boudellioua et al., 2020; Dastgheib et al., 2020).

Austenitic stainless steels (304 and 316) are some of the most widely used metals in a range of industries due to their good mechanical strength and excellent resistance to corrosion (Ait Albrimi et al., 2015; Eguchi et al., 2015; Zou et al., 2018; Loto, 2019). However, they are still susceptible to corrosion in an environment that is highly aggressive which contains chloride ions (Woldemedhin et al., 2015; Shakir et al., 2018). To mitigate the effect of the chloride ions, a corrosion inhibitor is frequently added to the environment to prevent localised forms of corrosion on the surface of the steel.

Ghanbari et al. (2009) investigated the inhibitive potential of acetylacetone complexes of transition metals (zinc(II), manganese(II), cobalt(II), and copper(II)) at concentrations of 0.01 M at 25°C in 1M phosphoric acid (H_3PO_4), the same H_3PO_4 solution was added separately with another solution of 0.1 M HCl, and also with 0.1 M NaCl, so that both NaCl and HCl solution would provide chloride ions in the solution. They reported that the addition of acetylacetone complexes to H_3PO_4 and to the two separate acidic chloride solutions shifted the corrosion potential of the mild steel toward more negative potentials. At the same time, there was an increase in the cathodic Tafel slopes, suggesting that the acetylacetone complexes acted as cathodic inhibitors. In solutions of NaCl with H_3PO_4 and HCl with H_3PO_4 the inhibition efficiency of the acetylacetonate complexes increased, gave a corresponding reduction in the corrosion rates.

Somers et al. (2018) studied the effect of rare-earth (La, Ce, Nd, and Y) 3-(4-methyl benzoyl) propanoate compounds ($REE(mbp)_3$) with additions at a concentration of 0.25 mM on the corrosion behaviour of mild steel in 0.01 M NaCl. Detailed surface analysis after immersion revealed that the inhibitors greatly improved the corrosion resistance of mild steel in the NaCl solution. FTIR and EDS showed the presence of a thin film containing inhibitor components on the surface of the tested steel specimens.

Markley et al. (2007) tested the inhibition effectiveness of cerium diphenyl phosphate ($Ce(dpp)_3$) for corrosion inhibition of an aluminium alloy (AA2024-T3) in 0.1 M NaCl solution at 25°C. A concentration 200 ppm $Ce(dpp)_3$ resulted in a high level of corrosion protection with no evidence of corrosion product or pitting.

No previous reports could be found in the literature describing the application of REE β-diketones as potential corrosion inhibitors for the corrosion prevention of stainless steels in acidic media. In this paper, cerium and lanthanum acetylacetone, as well as hexafluoroacetylacetone, will be the focal point as a possible replacement for hexavalent chromium-based corrosion inhibitors for 304 and 316 stainless steels in 0.1 M HCl solution. The investigation will endeavour to establish whether these inhibitors are effective, and also whether they act as anodic, cathodic, or mixed inhibitor.

5.2 EXPERIMENTAL SECTION

5.2.1 Materials and Preparation

The 304 SS had the following composition (wt. %): C, 0.05; Mn, 0.15; Si, 0.320; S, 0.019; Cr, 18.5, Mo, 0.46; Ni, 9.0; Fe, balance and while the 316 SS contained (wt. %): C, 0.05; Mn, 0.10; Si, 0.57; S, 0.007; Cr, 17.0, Mo, 2.0; Ni, 11.0; Fe, balance. The samples were all cut to dimensions of 2 cm × 3 cm × 0.12 cm and a 3.0 mm diameter hole was drilled at the edge for suspending the samples into solution. The samples were ground sequentially with silicon carbide papers, starting with 500 grit followed by 800, 1000, 1200 2400, and 2800 grit until a mirror-like surface was achieved. The prepared samples were rinsed with distilled water, followed by ethanol, and air-dry. For electrochemical measurements, the same materials that were used for the weight loss experiment were mechanically cut to a dimension of 1.0 cm ×

0.7 cm × 0.12 cm. These samples were then mounted using a resin with a conductible cable attached to the samples and successively abraded using the same series of silicon carbide papers as before. The exposed surface area of the samples was 0.7 cm^2, while the rest of the sample was encased by resin. Prior to the experiments, specimens were washed with distilled water, degreased in ethanol, and dried.

Analytical grade 32 % concentrated HCl obtained from Merck (Pty) Ltd was diluted with distilled water to prepare the 0.1 M HCl solutions. The cerium and lanthanum acetylacetone and hexafluoroacetylacetone were synthesised in accordance with the method described in the literature (Krishnankutty et al., 2007; Ukken & Ummathur, 2013; Nath et al., 2017). The chemical reaction is as follows:

$$MX_n.y(H_2O) + nRCOCH_2COR' \xrightarrow{METHANOL} M(RCOCHCOR')_n.yH_2O + nHX\ldots \quad 1$$

where M is the rare earth metal. The structural formulae of the REE β-diketones compounds are shown in Figure 5.1.

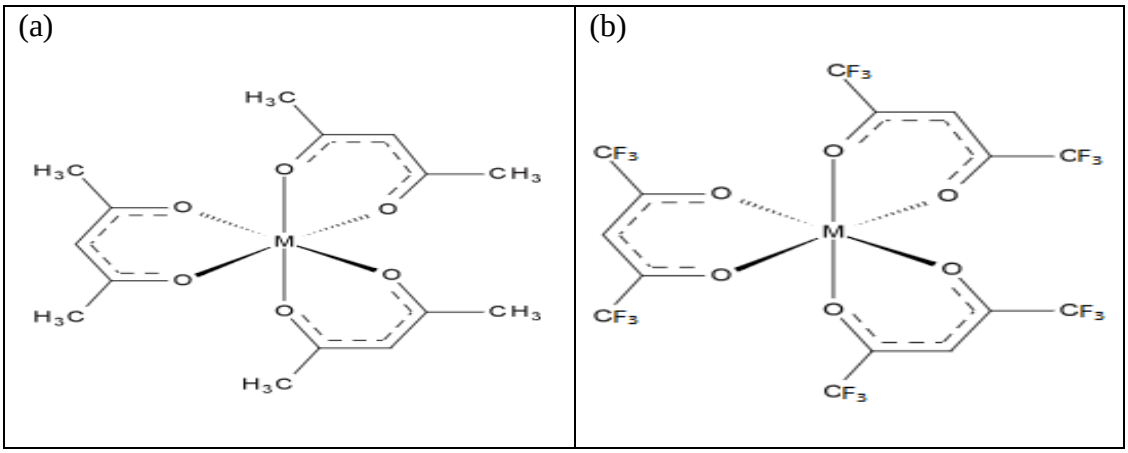


Figure 5.1: Chemical structures of (a) metal acetylacetonate and (b) metal hexafluoroacetylacetone, where M = Ce or La (Modified from Andersen et al., 2020).

5.3 SURFACE ANALYSIS

A Zeiss (51-ADD0048) Scanning Electron Microscope (SEM) instrument operating at 15kV couple with energy-dispersive X-ray spectroscopy (EDS) was used to study the surface morphology of the 304 and 316 SS after immersion in media with and without inhibitor. The characterisation of the REE complexes and the mapping of the surface of the steels were further carried out using Raman Spectroscopy and Fourier Transform Attenuated Total Reflectance Infrared Spectroscopy (FT-ATR-IR). Using a Perkin Elmer Spectrum-2 instrument, the FT-IR spectra were recorded in a frequency range of 420–4000 cm^{-1}. The Raman spectra were acquired using the 514.5 nm line of a Lexel Model 95 SHG argon-ion laser as an excitation source and a Horiba LabRAM HR Raman spectrometer equipped with a high-sensitivity Olympus BX41 microscope. The data were acquired using LabSpec v5 software and the spectra were obtained in the range of 3500-50 cm^{-1}.

5.4 WEIGHT LOSS MEASUREMENTS

The weight loss measurements were performed at room temperature after immersion in 250 mL 0.1 M HCl solution without and with 0.5% wt. (m/v) inhibitor for 7 days. Triplicate experiments were conducted for each and the average weight losses with standard deviation were determined. The average weight losses were then used to calculate the corrosion rates (in μm/y) and inhibition efficiencies according to the following equations:

$$\text{Corrosion rate (CR)} = 3.65\ x\ 10^{6}\ \frac{W_O - W_1}{DAT} \quad \ldots\ldots\ldots\ldots\ldots\ldots\ldots \quad (2)$$

where W_O and W_1 are the mass of the coupon (in grams) before and after immersion, respectively; D is the density of the coupon (in g/cm^3); T is the time of exposure (in days) and A is the exposed area of the coupon in the test solution (in cm^2).

$$\%\ \text{Inhibitor efficiency (IE)} = \frac{100(CR - CR_i)}{CR} \quad \ldots\ldots\ldots\ldots\ldots\ldots\ldots\ldots \quad (3)$$

where CR and CR_i are the average corrosion rates of the uninhibited and inhibited steel samples, respectively.

5.5 POTENTIODYNAMIC POLARISATION EXPERIMENTS

Potentiodynamic polarisation studies were carried out using a Metrohm Autolab-1 Potentiostat/Galvanostat equipped with Nova 2.1 software. A three-electrode setup was employed using a graphite counter electrode and Ag/AgCl (3 M KCl) as a reference electrode (all potentials are quoted with respect to this reference electrode). The stainless steel samples were the working electrodes in the system with an exposed surface of 0.7 cm^2 were immersed in the HCl solutions with and without inhibitor and the open circuit potential was measured after 30 min. Potentiodynamic polarisation studies were performed with a scan rate of 5 mV/s in the potential range from 200 mV below the corrosion potential to 800 mV above the corrosion potential. Measurements were done at 20, 40, and 60˚C. The corrosion parameters, such as corrosion potential (E_{corr}), Tafel slopes (βa and βc), corrosion current density (i_{corr}) and corrosion rate were obtained from the current density-potential graphs using the Nova 2.1 software.

5.6 RESULTS AND DISCUSSION

5.6.1 Weight Loss Measurement

The inhibition of the corrosion of 304 SS and 316 SS after exposure to solutions without and with 0.5% wt. (m/v) concentrations of $Ce(acac)_3$, $La(acac)_3$, $Ce(hfac)_3$ and $La(hfac)_3$ inhibitors were examined at room temperature (approximately 25°C) using weight loss measurements. After 7 days of immersion in each solution, the average corrosion rate was calculated and the results are presented in Table 5.1. At 0.5% wt. (m/v) concentration of $Ce(acac)_3$, $La(acac)_3$, $Ce(hfac)_3$ and $La(hfac)_3$ were 100% effective as no weight loss was observed. The excellent inhibition performance could be as a result of the adsorption of a passive film of REE β-diketone complexes on the steel surface. These results are in line with the report by Desa & Desai (1984), where they used dicarbonyl compounds as a corrosion inhibitor for mild steel at room temperature and in a concentration range of 0.39-0.42 mol/L in 6 N HCl solution for 24 hours.

Table 5.1: Comparison of corrosion rates of 304 SS and 316 SS and the inhibition efficiency in the absence and presence of $Ce(acac)_3$, $La(acac)_3$, $Ce(hfac)_3$ and $La(hfac)_3$ in 0.1 M HCl solution.

	REE β-diketone	CR_i with inhibitor (μm/y)	SD	CR without inhibitor (μm/y)	IE (%)	Standard Deviation
304 SS	$Ce(acac)_3$	0.0	0.0	1.0	100	0.5
	$La(acac)_3$	0.0	0.0	0.8	100	0.3
	$Ce(hfac)_3$	0.0	0.0	0.7	100	0.3
	$La(hfac)_3$	0.0	0.0	0.8	100	0.3
316 SS	$Ce(acac)_3$	0.0	0.0	0.8	100	0.3
	$La(acac)_3$	0.0	0.0	0.8	100	0.3
	$Ce(hfac)_3$	0.0	0.0	0.8	100	0.3
	$La(hfac)_3$	0.0	0.0	0.3	100	0.6

5.6.2 Potentiodynamic Polarisation Measurements

Polarisation curves of 304 and 316 SS at 20, 40, and 60°C measure in in HCl solutions without inhibitor and with $Ce(acac)_3$, $La(acac)_3$, $Ce(hfac)_3$ and $La(hfac)_3$ inhibitors are shown in Figures 5.2 and 5.3. The electrochemical parameters derived from these curves are summarised in Tables 5.2 and 5.3. The E_{corr} in solutions containing each of the inhibitors shifted towards more negative potentials (less noble) compared to E_{corr} when there was no inhibitor present in the solution. The downward decrease in the value of E_{corr} indicated that all of the inhibitors act as cathodic inhibitors (Dastgheib et al., 2020). As expected, the corrosion rates and current densities increased with increasing temperature. It is noteworthy that the inhibition efficiencies of the REE β-diketones obtained were very similar to the inhibition efficiencies obtained by Ghanbari et al. (2009) and when they used acetylacetone complexes of transition metals for corrosion inhibition of mild steel in a 1 M phosphoric acid solution. A similar observation was observed when Desa & Desai (1984) separately used different carbonyl compounds and acetylacetone as a corrosion inhibitor for mild steel at a fixed concentration of inhibitors while

varying the concentration of the HCl solution increases from 1.0, 2.0, 3.0 and 4.0 N. Potentiodynamic polarisation studied of these compounds showed that the inhibition efficiencies of all the tested compounds increase from 22 up to 98% depends on the concentration of the HCl solution that was used. The corrosion rates were found to increase as the concentration of HCl solution increases from 1.0, 2.0, 3.0 and 4.0 N.

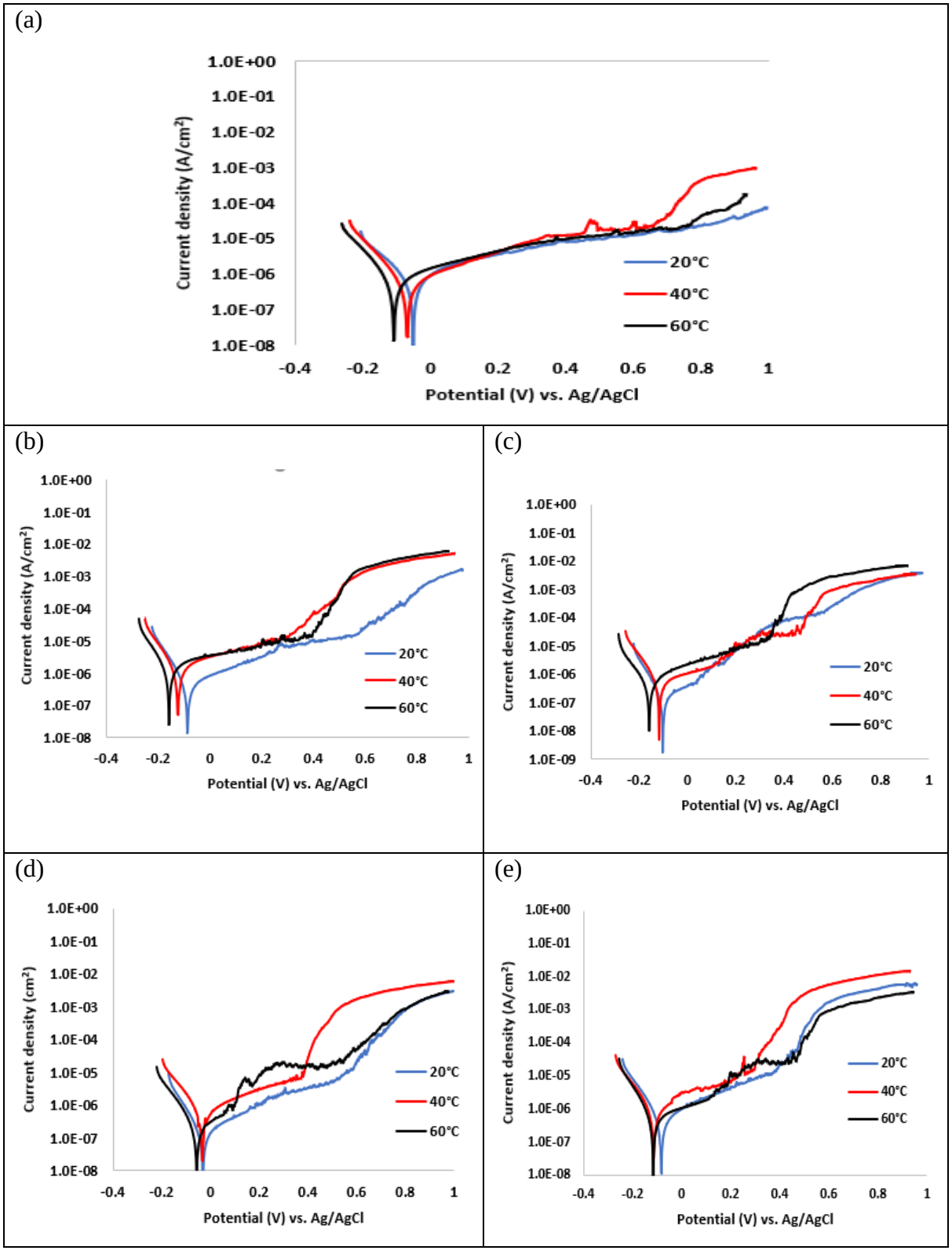


Figure 5.2: Potentiodynamic polarisation curves of 304 SS in 0.1 M HCl solution (a) without inhibitor and with (b) $Ce(acac)_3$, (c) $La(acac)_3$, (d) $Ce(hfac)_3$ and (e) $La(hfac)_3$ inhibitors.

Table 5.2: Electrochemical parameters of 304 SS obtained from potentiodynamic polarisation curves measured in 0.1 M HCl solution and with corrosion inhibitors $Ce(acac)_3$, $La(acac)_3$, $Ce(hfac)_3$ and $La(hfac)_3$ present in the solution. The results presented in Table 5.2 were derived from Figure 5.2.

0.1 M HCl solution without inhibitor						
Temp. (°C)	E_{corr} (V)	i_{corr} (A/cm^2)	βa (mV/dec)	βc (mV/dec)	CR (µm/y)	IE (%)
20	-0.051	4.82×10^{-7}	44	133	4.99	
40	-0.068	4.93×10^{-7}	42	120	5.11	
60	-0.108	5.05×10^{-7}	45	125	5.23	
$Ce(acac)_3$						
Temp. (°C)	E_{corr} (V)	i_{corr} (A/cm^2)	βa (mV/dec)	βc (mV/dec)	CR (µm/y)	IE (%)
20	-0.082	2.74×10^{-7}	26	87	2.84	43
40	-0.136	2.92×10^{-7}	52	87	3.02	41
60	-0.157	3.07×10^{-7}	45	104	3.18	39
$La(acac)_3$						
Temp. (°C)	E_{corr} (V)	i_{corr} (A/cm^2)	βa (mV/dec)	βc (mV/dec)	CR (µm/y)	IE (%)
20	-0.128	2.79×10^{-7}	22	85	2.89	42
40	-0.109	2.95×10^{-7}	25	87	3.06	40
60	-0.160	3.17×10^{-7}	35	96	3.28	37
$Ce(hfac)_3$						
Temp. (°C)	E_{corr} (V)	i_{corr} (A/cm^2)	βa (mV/dec)	βc (mV/dec)	CR (µm/y)	IE (%)
20	-0.030	2.69×10^{-7}	28	92	2.79	44
40	-0.036	2.93×10^{-7}	19	102	3.03	40
60	-0.059	3.16×10^{-7}	42	122	3.27	37
$La(hfac)_3$						
Temp. (°C)	E_{corr} (V)	i_{corr} (A/cm^2)	βa (mV/dec)	βc (mV/dec)	CR (µm/y)	IE (%)
20	-0.083	2.61×10^{-7}	36	90	2.73	45
40	-0.094	2.88×10^{-7}	12	97	3.00	42
60	-0.115	3.13×10^{-7}	43	97	3.26	38

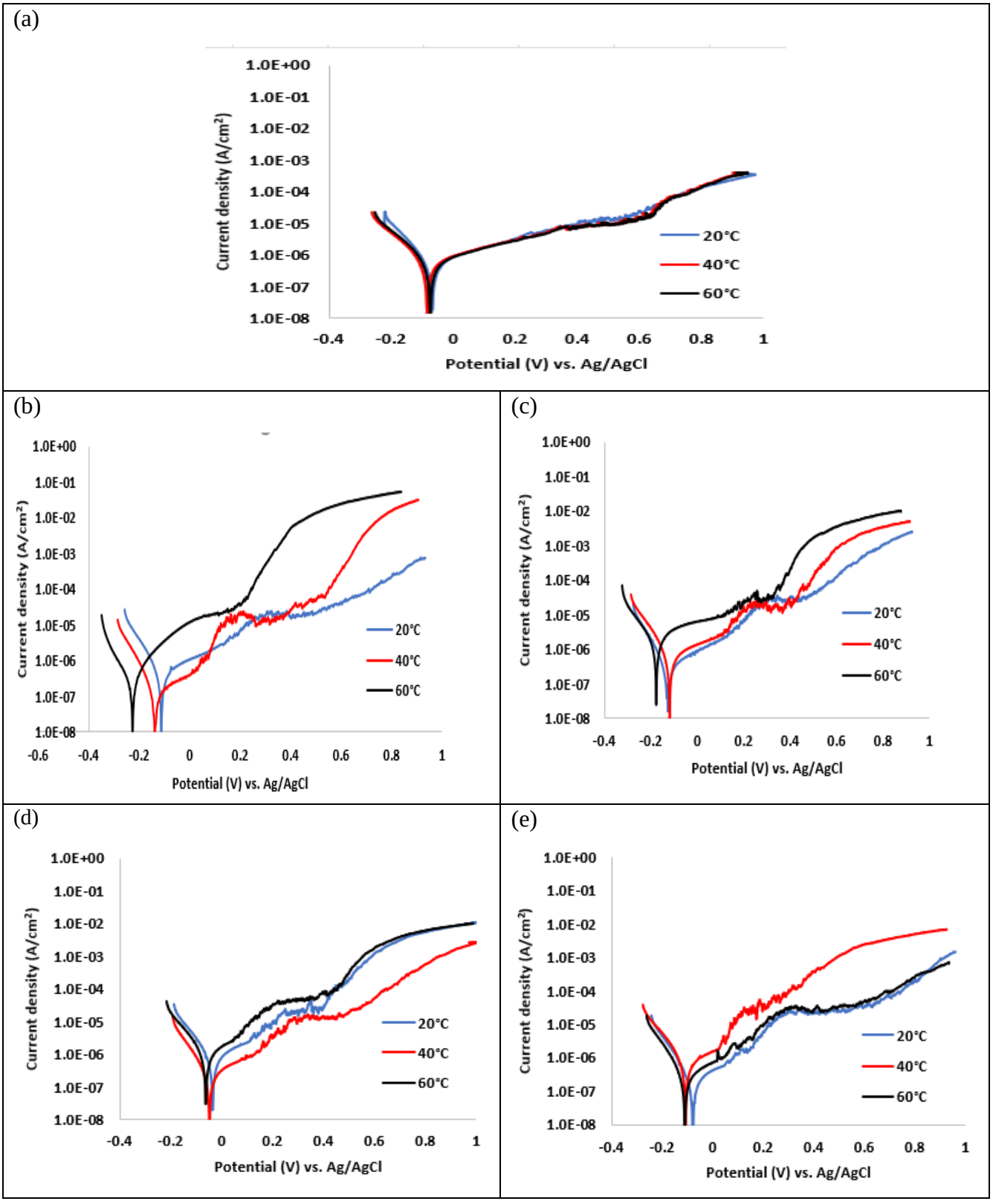


Figure 5.3: Potentiodynamic polarisation curves of 316 SS in 0.1 M HCl solution (a) without inhibitors and with (b) $Ce(acac)_3$, (c) $La(acac)_3$, (d) $Ce(hfac)_3$ and (e) $La(hfac)_3$ inhibitors.

Table 5.3: Electrochemical parameters of 316 SS obtained from potentiodynamic polarisation curves measured in 0.1 M HCl solution and with corrosion inhibitors $Ce(acac)_3$, $La(acac)_3$, $Ce(hfac)_3$ and $La(hfac)_3$ present in the solution. The results presented in Table 5.3 were derived from Figure 5.3.

0.1 M HCl solution without inhibitor						
Temp. (°C)	E_{corr} (V)	i_{corr} (A/cm^2)	βa (mV/dec)	βc (mV/dec)	CR (µm/y)	IE (%)
20	-0.067	3.25×10^{-7}	39	110	3.39	
40	-0.081	3.60×10^{-7}	42	122	3.76	
60	-0.109	4.24×10^{-7}	42	15	4.43	
$Ce(acac)_3$						
Temp. (°C)	E_{corr} (V)	i_{corr} (A/cm^2)	βa (mV/dec)	βc (mV/dec)	CR (µm/y)	IE (%)
20	-0.108	1.70×10^{-7}	38	102	1.78	48
40	-0.126	1.92×10^{-7}	37	106	2.00	47
60	-0.205	2.28×10^{-7}	57	109	2.38	46
$La(acac)_3$						
Temp. (°C)	E_{corr} (V)	i_{corr} (A/cm^2)	βa (mV/dec)	βc (mV/dec)	CR (µm/y)	IE (%)
20	-0.137	1.79×10^{-7}	36	99	1.87	45
40	-0.119	2.00×10^{-7}	39	99	2.09	44
60	-0.177	2.27×10^{-7}	43	105	2.37	42
$Ce(hfac)_3$						
Temp. (°C)	E_{corr} (V)	i_{corr} (A/cm^2)	βa (mV/dec)	βc (mV/dec)	CR (µm/y)	IE (%)
20	-0.108	1.68×10^{-7}	38	102	1.76	48
40	-0.126	1.91×10^{-7}	37	106	2.00	47
60	-0.205	2.35×10^{-7}	57	109	2.46	45
$La(hfac)_3$						
Temp. (°C)	E_{corr} (V)	i_{corr} (A/cm^2)	βa (mV/dec)	βc (mV/dec)	CR (µm/y)	IE (%)
20	-0.076	1.73×10^{-7}	30	92	1.81	47
40	-0.086	1.93×10^{-7}	26	84	2.12	46
60	-0.105	2.32×10^{-7}	31	115	2.33	45

5.7 SURFACE ANALYSES

5.7.1 SCANNING ELECTRON MICROSCOPY (SEM)

The surface morphology of the 304 and 316 SS samples with and without inhibitor after potentiodynamic polarisation tests in 0.1 M HCl solution as determined by SEM are shown in Figures 5.4 and 5.5. The micrographs of both samples in the absence of inhibitor showed damage to the surface, with a deep and wide hole on a 304 SS suggesting an attack by chloride ions. In the presence of the inhibitors EDS results (Figures 5.6 and 5.7) indicate the film formation on the metal surface which could be responsible for corrosion inhibition. It is noteworthy that the tested inhibitors provide a uniform film coverage on the surface of the steel at all temperatures and at a low concentration (0.5% m/v), with no evidence of localised corrosion occurring. EDS analysis was carried out to identify the constituents of the film on the steel surface and the results revealed that the film primarily consists of a rare earth element (Ce or La), oxygen (O), and other elements (Fe, Cr, Ni) that were major constituents of the steel, as indicated in Figures 5.6 and 5.7. These results were consistent with the investigation carried out by Peng et al. (2018) when they studied rare-earth 3-(4-methylbenzoyl)-propanoate compounds ($Ce(dpm)_3$ and $La(dpm)_3$) as corrosion inhibitors for mild steel in 0.1 M NaCl solutions. SEM/EDS analyses showed the steel surface was protected by $Ce(dpm)_3$ and $La(dpm)_3$ despite being used at a low concentration of 0.25 mM. EDS also indicated that a dense layer of deposit on the surface of the steel contained rare earth elements (Ce and La) and iron (Fe). This is presumably due to the deposit consisting of a mixture of a rare-earth rich film (rare earth oxide or hydroxide) as well as iron oxide/ hydroxide.

Nam et al. (2016) investigated corrosion behaviour of copper alloy using 0.15 mM concentration of yttrium 3-(4-nitrophenyl)-2-propenoate ($Y(4NO_2Cin)_3$ inhibitor and 0.1 M NaCl solution as a corrosive medium. SEM analysis was conducted on the copper alloy that was immersed in a chloride solution with and without ($Y(4NO_2Cin)_3$ for a period of 20 hours. Micrographs obtained from SEM revealed that $Y(4NO_2Cin)_3$ actively impede corrosion of copper alloy with no corrosion attack occurred on the copper surface after immersion for 20 hours. When the same experiment was repeated in the absence of $Y(4NO_2Cin)_3$ under the same conditions, deep penetration of chloride ions with a great level of corrosion was observed, suggesting that $Y(4NO_2Cin)_3$ inhibit the corrosion of copper alloy in 0.1 M sodium chloride solution.

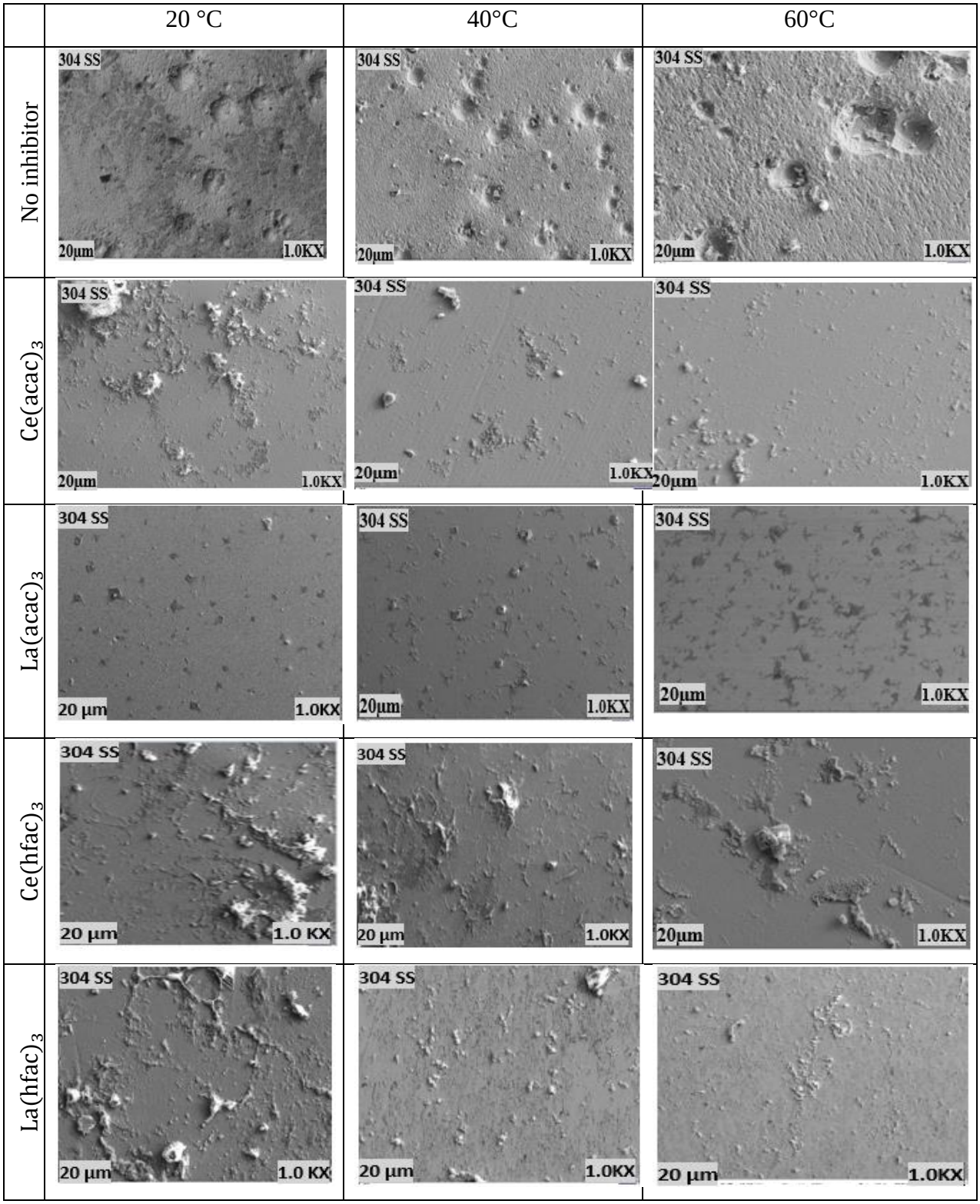


Figure 5.4: SEM micrographs of 304 SS sample surfaces in the absence and presence of $Ce(acac)_3$ and $La(acac)_3$ after exposure to 0.1 M HCl solutions at 20, 40 and 60ºC.

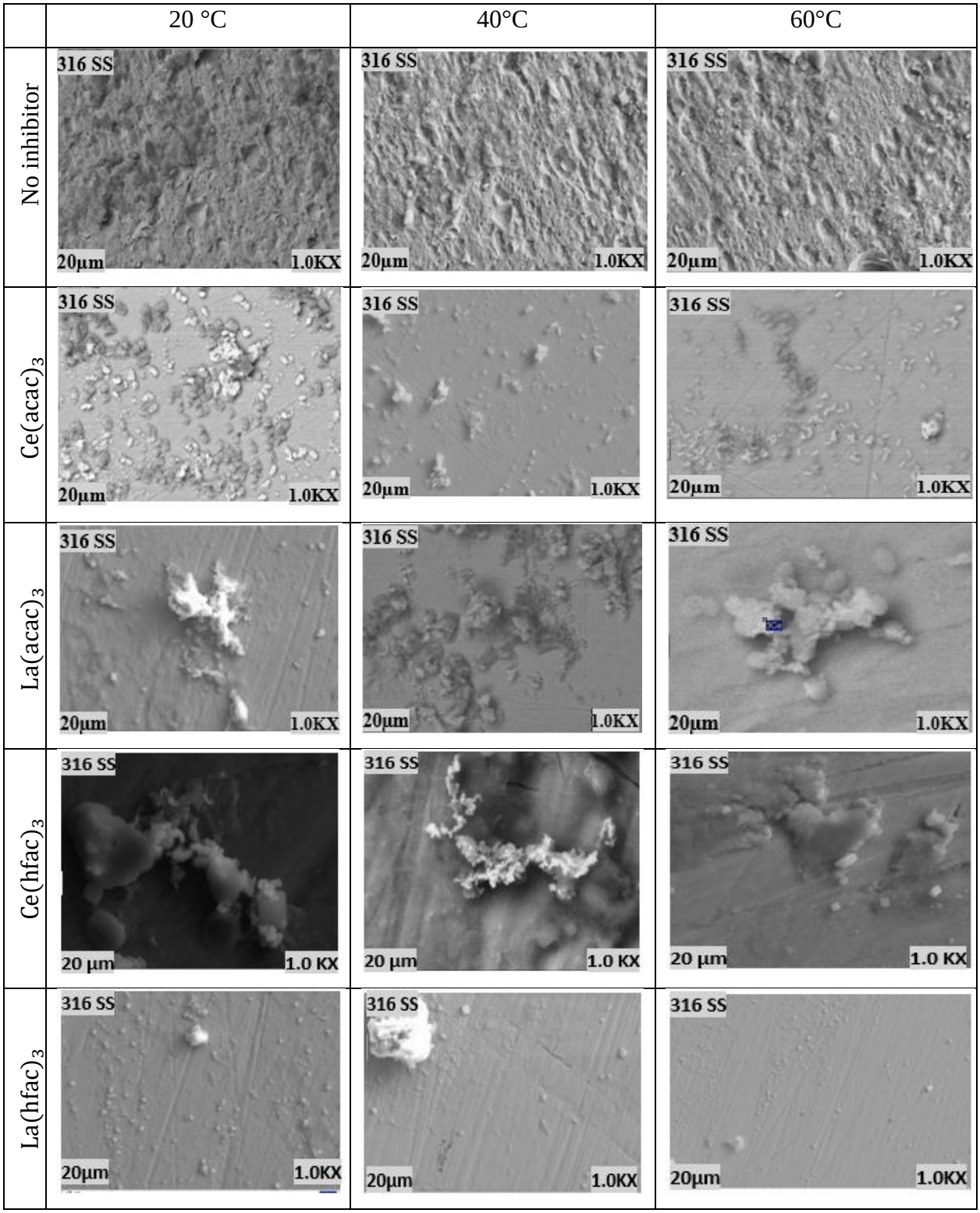
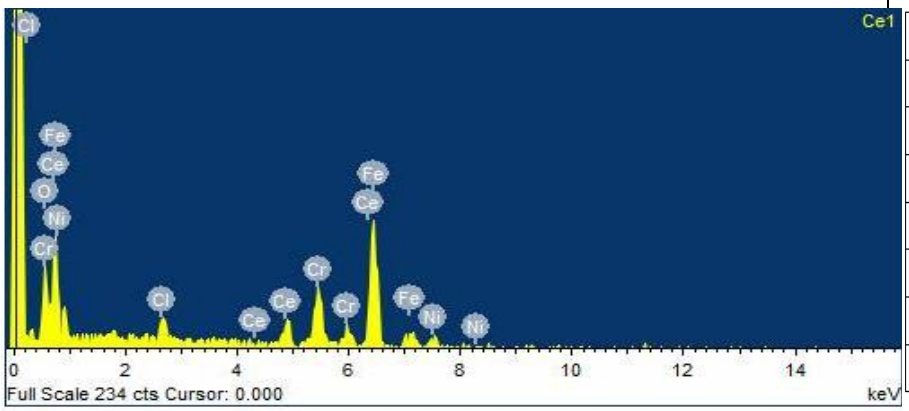


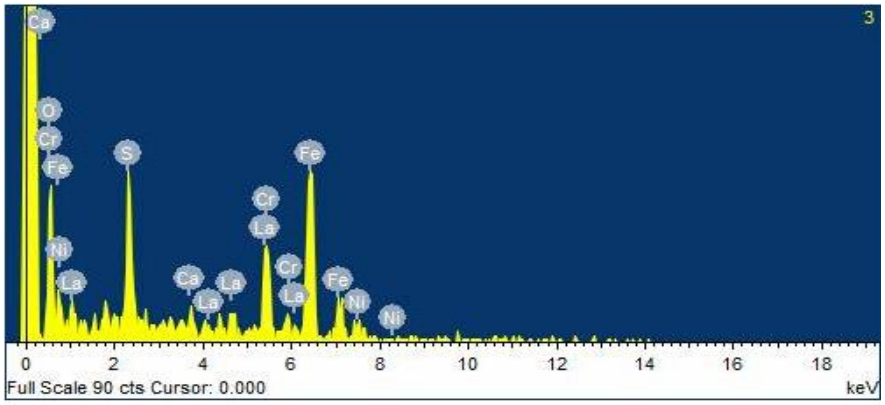
Figure 5.5: SEM micrographs of 316 SS sample surfaces in the absence and presence of $Ce(acac)_3$, $La(acac)_3$, $Ce(hfac)_3$ and $La(hfac)_3$ after exposure to 0.1 M HCl solutions at 20, 40 and 60°C.

(a)



Element	Weight %	Atomic %
O K	9.20	27.20
Cl K	2.41	3.22
Cr K	15.99	14.55
Fe K	54.43	46.12
Ni K	6.07	4.89
Ce L	11.90	4.02
Totals	100.00	

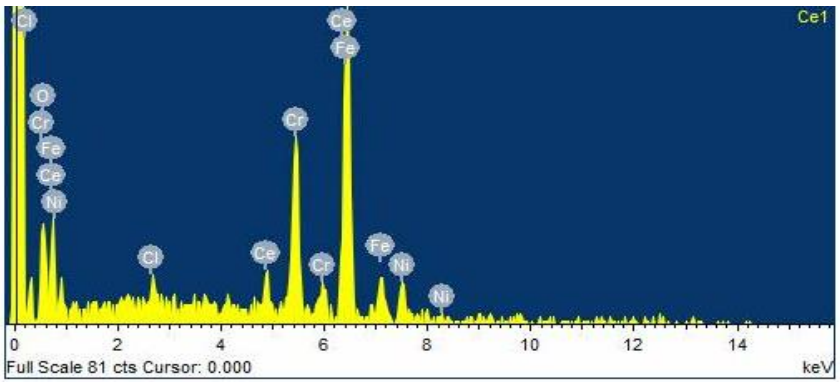
(b)



Element	Weight %	Atomic %
O K	14.32	36.20
Cr K	15.03	11.69
Fe K	48.56	35.15
Ni K	5.90	4.07
La L	7.38	2.25
Totals	100.00	

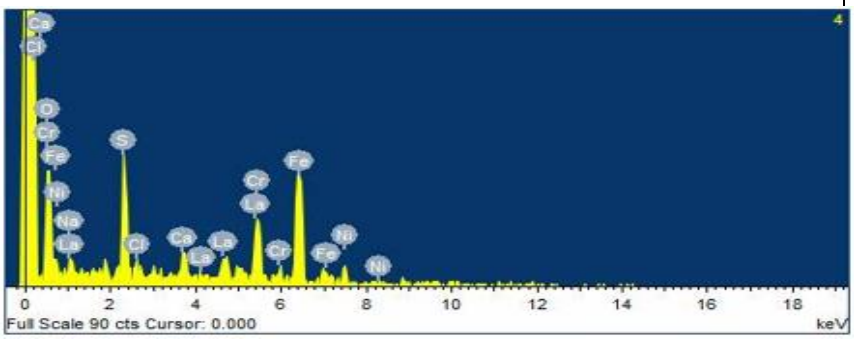
Figure 5.6: EDS of 304 SS after exposure to a HCl solution containing (a) $Ce(acac)_3$ at 20ºC and (b) $La(acac)_3$ at 60ºC with inhibitors at 0.5 % wt. (m/v) concentration.

(c)



Element	Weight %	Atomic %
O K	3.83	12.56
Cl K	0.62	0.91
Cr K	18.64	18.83
Fe K	59.00	55.48
Ni K	10.59	9.48
Ce L	7.32	2.74
Totals	100.00	

(d)



Element	Weight %	Atomic %
O K	11.41	29.46
Cr K	12.98	10.31
Fe K	44.63	33.00
Ni K	6.61	4.65
La L	9.50	2.82
Totals	100.00	

Figure 5.7: EDS of 316 SS after exposure to a HCl solution containing (c) $Ce(hfac)_3$ 20°C and (d) $La(hfac)_3$ at 60°C with inhibitors at 0.5 % wt. (m/v) concentration.

5.8 RAMAN SPECTROSCOPY

Raman Spectroscopy was employed to map the surface of the steel samples after performing electrochemical tests in a corrosive medium that contained the REE β-diketones in order to further investigate the nature of the corrosion inhibitors' action. The Raman spectra for the synthesised REE β-diketone powders and the film layer deposited on the steel surface after the electrochemical tests are shown in Figure 5.8. The frequency shifts identified in the Raman spectra were compared with published results and they confirmed the formation of the REE β-diketone complexes (Tsaryuk et al. 2020) and complex film formation on the surface of the steel (Boudellioua et al., 2017). For the steel surface exposed to REE β-diketone complex inhibited solution, the bands associated with carbonyl functional group (C=O) and enolic group (OH) disappear. The disappearance of these bands may be attributed to the coordination

between the steel, the enolic structure and carbonyl function group resulting in the formation of a protective layer of rare earth oxide or hydroxide $REE(OH)_3$ (Markley et al., 2007). The Raman shift with frequency bands at ~248 and ~1311 cm^{-1}, and at 377 cm^{-1} could be assigned to stretching vibrations which correspond to hematite (α-Fe_2O_3) and lepidocrocite (γ-FeOOH), respectively (De Faria et al., 1997; Jubb & Allen, 2010; Święch et al., 2018; Boudellioua et al., 2019). Details of the frequency bands with the associated functional groups for the spectra peaks are shown in Table 5.4. Raman analysis for the corrosion product tests were done on samples 304 SS doped in solutions containing $Ce(acac)_3$ or $La(acac)_3$ and 316 SS doped in solutions containing $Ce(hfac)_3$ or $La(hfac)_3$ as shown in Figure 5.8.

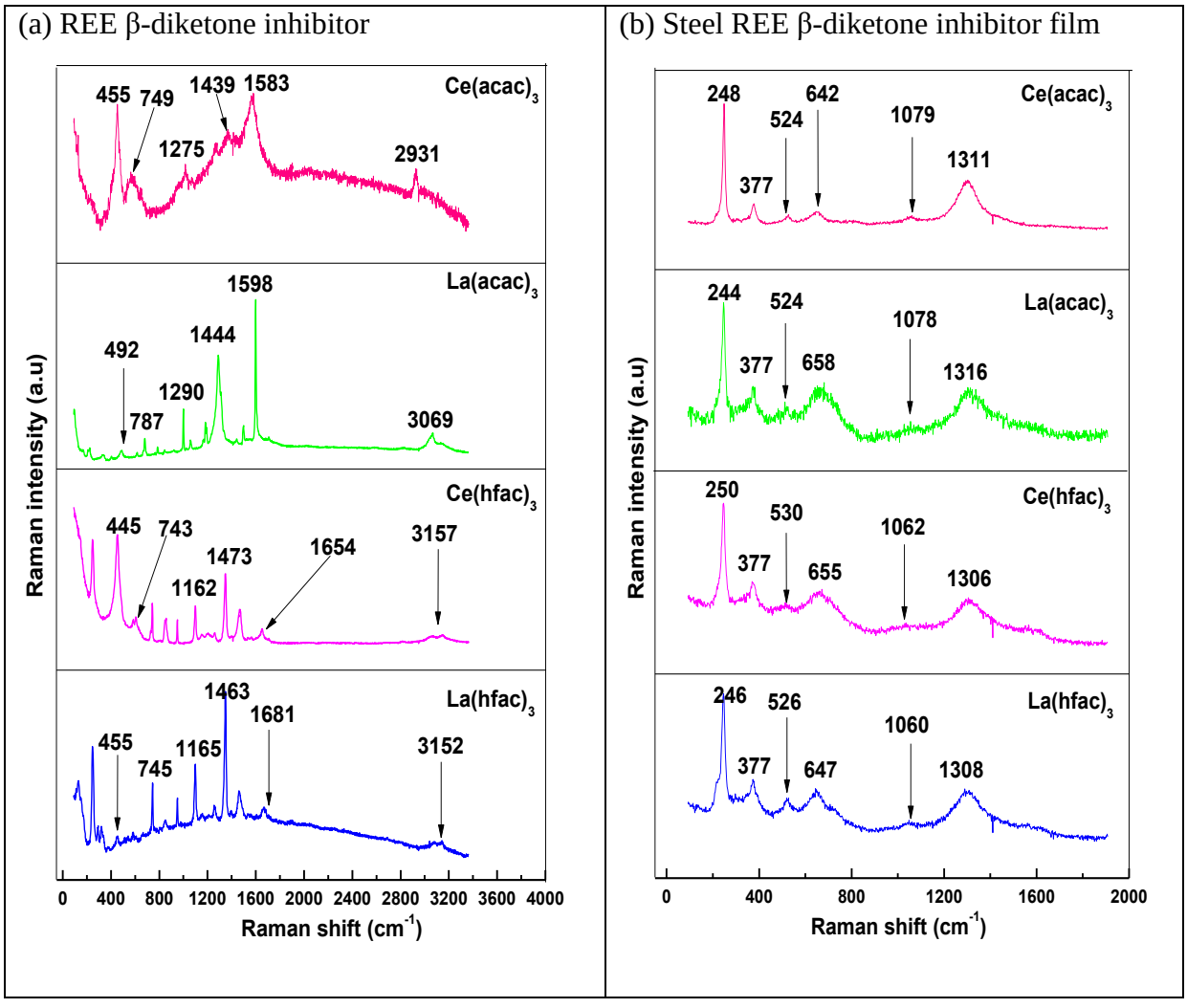


Figure 5.8: Raman spectra of $Ce(acac)_3$, $La(acac)_3$, $Ce(hfac)_3$and $La(hfac)_3$ inhibitors and the corrosion products formed on 304 and 316 SS.

Table 5.4: Raman frequency$Ce(acac)_3$, $La(acac)_3$, $Ce(hfac)_3$and $La(hfac)_3$ inhibitors and the corrosion products formed on 304 and 316 SS.

Inhibitor $\mathbf{Ce(acac)_3}$		Corrosion Product on 304 SS	
Frequency (cm^{-1})	Assignment	Frequency (cm^{-1})	Assignment
1583	C=O	248, 1311	α-Fe_2O_3
455	M-O	524	REE-O
2931	O-H	377	γ-FeOOH
Inhibitor $\mathbf{La(acac)_3}$		Corrosion Product on 304 SS	
Frequency (cm^{-1})	Assignment	Frequency (cm^{-1})	Assignment
1598	C=O	244, 1306	α-Fe_2O_3
492	M-O	524	REE-O
3069	O-H	377	γ-FeOOH
Inhibitor $\mathbf{Ce(hfac)_3}$		Corrosion Product on 316 SS	
Frequency (cm^{-1})	Assignment	Frequency (cm^{-1})	Assignment
1654	C=O	250, 1306	α-Fe_2O_3
445	M-O	530	REE-O
3157	O-H	377	γ-FeOOH
Inhibitor $\mathbf{La(hfac)_3}$		Corrosion Product on 316 SS	
Frequency (cm^{-1})	Assignment	Frequency (cm^{-1})	Assignment
1681	C=O	246, 1308	α-Fe_2O_3
455	M-O	526	REE-O
3152	O-H	377	γ-FeOOH

5.9 FOURIER TRANSFORM INFRARED SPECTROSCOPY (FTIR)

Fourier Transform Infrared spectroscopy (FTIR) was used to further characterise the REE β-diketone inhibitors and the films that were formed on the surface of the two stainless steel samples (304 & 316) after electrochemical corrosion tests in the solutions containing a 0.5% concentration of the REE β-diketone inhibitor (Figure 5.9). The bands associated with the functional groups of the synthesised REE β-diketone complexes were all assigned according

to that in the literature (Song et al., 2003; Nath et al., 2017). The appearance of a band in the region 583 and 518 cm^{-1} indicate bonding of the metal ion with the β-diketone molecules and can be ascribed to the M-O vibration (Al-Wassil et al., 1998; Kumar & Sharma, 2012; Ferenc et al., 2013; Ukken & Ummathur, 2013; Nath et al., 2017). The main functional groups present in REE β-diketone that are responsible for film formation on the steel, are the carbonyl functional group and enolic structure. It was observed that the frequency band of the enolic structure and the carbonyl functional group that appear on the metal surface shifted to a lower frequency compared to the frequencies noted for the synthesised REE β-diketone complexes.

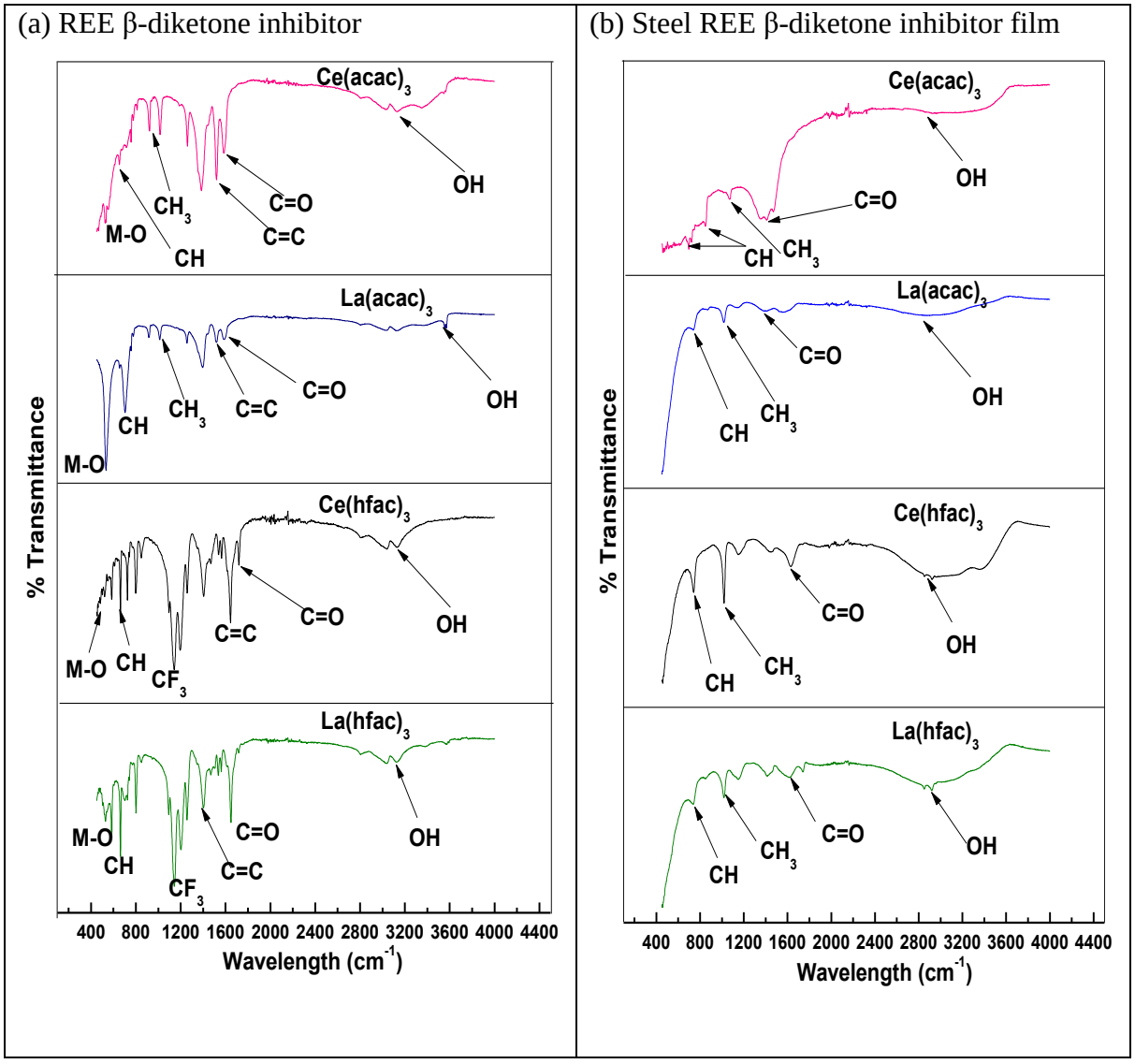


Figure 5.9: IR spectra of $Ce(acac)_3$, $La(acac)_3$, $Ce(hfac)_3$and $La(hfac)_3$ inhibitors and the corrosion products formed on 304 and 316 SS.

5.10 CONCLUSIONS

The SEM results proved that $Ce(acac)_3$, $La(acac)_3$, $Ce(hfac)_3$ and $La(hfac)_3$ efficiently inhibit the corrosion of 304 and 316 SS even at low concentration (0.5 % m/v) in 0.1 M HCl solution in the temperature range of 20-60°C. Raman spectroscopy confirmed that the complexes form a rare earth oxide/hydroxide containing film on the surface of the samples. Iron oxide/hydroxide on the surface of the steels were also observed. According to the potentiodynamic polarisation results, $Ce(acac)_3$, $La(acac)_3$, $Ce(hfac)_3$ and $La(hfac)_3$ act as cathodic inhibitors in HCl solution which led to a shift in the corrosion potential in a negative direction. The slight decreases in the Tafel slope values when the two inhibitors were added compared to the cases when no inhibitors are present, is further confirmation that all the tested REE β-diketone compounds act as cathodic inhibitors. It is apparent that all the inhibitors had a nearly similar inhibition efficiency as calculated from the potentiodynamic polarisation data. This corresponds to the observations made with the mass loss test results.

5.11 REFERENCES

Ait Albrimi, Y., Ait Addi, A., Douch, J., Souto, R. M., & Hamdani, M. (2015). Inhibition of the pitting corrosion of 304 stainless steel in 0.5M hydrochloric acid solution by heptamolybdate ions. Corrosion Science, 90, 522–528.

Al-Wassil, A. I., Al-Farhan, K. A., Mukhalalati, M., & Mahfouz, R. M. (1998). Coordination Chemistry of Thenoyltrifluoroacetone 1- Synthesis and characterization of In^{3+} thenoyltrifluoroacetone Complex. Spectroscopy Letters, 31(2), 299–305.

Amadeh, A., Allahkaram, S. R., Hosseini, S. R., Moradi, H., & Abdolhosseini, A. (2008). The use of rare earth cations as corrosion inhibitors for carbon steel in aerated NaCl solution. Anti-Corrosion Methods and Materials, 55(3), 135–143.

Andersen, A. B. A., Pyykkönen, A., Jensen, H. J. A., McKee, V., Vaara, J., & Nielsen, U. G. (2020). Remarkable reversal of 13C-NMR assignment in d1, d2 compared to d8, d9 acetylacetonate complexes: Analysis and explanation based on solid-state MAS NMR and computations. Physical Chemistry Chemical Physics, 22(15), 8048–8059.

Bhise, N. A., Agale, A. A., Gaikwad, S. T., & Rajbhoj A. S. (2017). Synthesis and Characterization of Mn(II), Fe(III), Co(II), Ni(II) and Cu(II) Complexes of β-Diketone. Asian Journal of Chemistry, 29(11), 2372–2378.

Boudellioua, H., Hamlaoui, Y., Tifouti, L., & Pedraza, F. (2019). Effects of polyethylene glycol (PEG) on the corrosion inhibition of mild steel by cerium nitrate in chloride solution. Applied Surface Science, 473, 449–460.

Boudellioua, H., Hamlaoui, Y., Tifouti, L., & Pedraza, F. (2020). Effect of the temperature of cerium nitrate–NaCl solution on corrosion inhibition of mild steel. Materials and Corrosion, 71(8), 1300–1309.

Dastgheib, A., Mohammadzadeh Attar, M., & Zarebidaki, A. (2020). Evaluation of Corrosion Inhibition of Mild Steel in 3.5 wt% NaCl Solution by Cerium Nitrate. Metals and Materials International, 26(11), 1634–1642.

De Faria, D. L. A., Venâncio Silva, S., & De Oliveira, M. T. (1997). Raman microspectroscopy

of some iron oxides and oxyhydroxides. Raman Spectroscopy, 28(11), 873–878.

Desa, M. N., & Desai, M. B. (1984). Carbonyl compounds as corrosion inhibitors for mild steel in HC1 solutions. Corrosion Science, 24(8), 649–660.

Eguchi, K., Ishiguro, Y., & Ota, H. (2015). Corrosion behavior of multi-phase stainless steel in 15% hydrochloric acid at a temperature of 80C. Corrosion, 71(11), 1398–1405.

Ferenc, W., Cristóvão, B., & Sarzynski, J. (2013). Magnetic, thermal and spectroscopic properties of lanthanide (III) 2-(4-chlorophenoxy)acetates, $Ln(C_8H_6ClO_3).nH_2O$. Serbian Chemical Society, 78(9), 1335–1349.

Fouda, A. S., Abd El-Wahab, S. M., Attia, M. S., Youssef, A. O., & Elmoher, H. O. (2015). Rare earth metals as eco-friendly corrosion inhibitors for mild steel in produced water. Der Pharma Chemica, 7(8), 74–87.

Jubb, A. M., & Allen, H. C. (2010). Vibrational spectroscopic characterization of hematite, maghemite, and magnetite thin films produced by vapor deposition. ACS Applied Materials and Interfaces, 2(10), 2804–2812.

Krishnankutty, K., Ummathur, M. B., & Ukken M. P. (2007). Some unsaturated β-diketones and their metal chelates. Analytical Chemistry, 6(2), 4–8.

Kumar, M., & Sharma, T. R. (2012). Synthesis, characterization and properties of metal complexes of beta-diketonate complexes. Oriental Journal of Chemistry, 28(4), 1827–1831.

Loto, R. T. (2019). Effect of elevated temperature variations on the corrosion resistance of S31603 and SS2562 austenitic stainless steels in chloride-sulphate environments. Materials Research and Technology, 8(6), 5415–5421.

Markley, T. A., Forsyth, M., & Hughes, A. E. (2007). Corrosion protection of AA2024-T3 using rare earth diphenyl phosphates. Electrochimica Acta, 52(12), 4024–4031.

Matter, E. A., Kozhukharov, S., Machkova, M., & Kozhukharov, V. (2012). Comparison between the inhibition efficiencies of Ce(III) and Ce(IV) ammonium nitrates against corrosion of AA2024 aluminum alloy in solutions of low chloride concentration.

Corrosion Science, 62, 22–33.

Nam, N. D., Thang, V. Q., Hoai, N. T., & Hien, P. V. (2016). Yttrium 3-(4-nitrophenyl)-2-propenoate used as inhibitor against copper alloy corrosion in 0.1 M NaCl solution. Corrosion Science, 112, 451–461.

Nandurkar, N. S., Patil, D. S., & Bhanage, B. M. (2008). Ultrasound assisted synthesis of metal-1,3-diketonates. Inorganic Chemistry Communications, 11(7), 733–736.

Nath, P., Bharty, M. K., Dani, R. K., Tomar, M. S., & Acharya, A. (2017). Mn(II), Co(III), Ni(II), Cd(II) and Cu(II) Complexes of 2-Thenoyltrifluoroacetone: Syntheses, Structures, Photoluminescence, Thermal, Electrochemical and Antitumor Studies on Dalton's Lymphoma Cells. Chemistry Select, 2(32), 10449–10458.

Peng, Y., Hughes, A. E., Deacon, G. B., Junk, P. C., Hinton, B. R. W., Forsyth, M., Mardel, J. I., & Somers, A. E. (2018). A study of rare-earth 3-(4-methyl benzoyl)-propanoate compounds as corrosion inhibitors for AS1020 mild steel in NaCl solutions. Corrosion Science, 145, 199–211.

Shakir, I. K., Mohammed, A.-K., Alsamurraee, A., Mahdi, S., & Phd, S. (2018). Pitting Corrosion Behavior of 304 SS and 316 SS Alloys in Aqueous Chloride and Bromide Solutions. Engineering, 24(1), 53–69.

Song, H., Jiang, Y., Xia, C., Meng, G., & Peng, D. (2003). Synthesis and characterization of volatile metal b -diketonate chelates of M (DPM) n (M = Ce , Gd , Y , Zr , n = 3 , 4) used as precursors for MOCVD. 250, 423–430.

Święch, D., Paluszkiewicz, C., Piergies, N., Pieta, E., Lelek-Borkowska, U., & Kwiatek, W. (2018). Identification of corrosion products on Fe and Cu metals using spectroscopic methods. Acta Physica Polonica A, 133(2), 286–288.

Tsaryuk, V. I., Zhuravlev, K. P., Szostak, R., & Vologzhanina, A. V. (2020). Structure, Luminescence, and Raman Spectroscopy of Europium and Terbium Dipivaloylmethanates and other β-diketones with 2,2′-Bipyridine. Structural Chemistry, 61(7), 1026–1037.

Ukken, M. P., & Ummathur, M. B. (2013). Synthesis and characterization of two conjugated β -diketones and their metal complexes. Inorganic Chemistry, 4(2), 247–250.

Verma, P. N., Sheikh, J. I., & Juneja, H. D. (2011). Synthesis of β-diketone and its Metal Complexes. 14(8), 1154–1157.

Volarič, B., & Milošev, I. (2017). Rare earth chloride and nitrate salts as individual and mixed inhibitors for aluminium alloy 7075-T6 in chloride solution. Corrosion Engineering Science and Technology, 52(3), 201–211.

Woldemedhin, M. T., Srinivasan, J., & Kelly, R. G. (2015). Effects of environmental factors on key kinetic parameters relevant to pitting corrosion. Solid State Electrochemistry, 19(12), 3449–3461.

Zou, G., Shi, W., Xiang, S., Ji, X., Ma, G., & Ballinger, R. G. (2018). Corrosion behavior of 904L austenitic stainless steel in hydrofluoric acid. RSC Advances, 8(5), 2811–2817.

CHAPTER SIX

6.1 CONCLUSIONS AND RECOMMENDATIONS

A novel type of corrosion inhibitor has been synthesised from REE halides and various β-diketone ligands as starting materials. The synthesised inhibitors were characterised and confirmed by different techniques such as melting point analysis, fourier transform infrared spectroscopy, Raman spectroscopy, mass spectroscopy and X-ray diffraction analysis in conjunction with results reported in the literature. The synthesised complexes have a general formula $M(RCOCHCOR')_n$ where M is the rare earth element, R and R′could be a methyl group, fluorinated methyl, or alkyl group, thiophene or benzene ring depending on the type of β-diketone ligand that is used as a base component for the synthesis of the REE β-diketone complex. The performance of the synthesised inhibitors were examined in 3.5% NaCl and 0.1 M HCl solution at different temperature (20, 40 and 60^{o}C) against localised corrosion of mild steel and austenitic stainless steel (304 and 316 SS) respectively. Detailed surface analyses using optical microscopy (OP) and scanning electron microscopy (SEM) revealed that four of the synthesised inhibitors ($Ce(acac)_3$, $La(acac)_3$, $Ce(hfac)_3$ and $La(hfac)_3$) that were tested against localised corrosion are effective, even at low concentrations. However, the calculated inhibition efficiencies from potentiodynamic polarisation curves are below (50%) average at a 0.5 % (m/v) concentration of the inhibitors in a wide range of temperatures. This shows that even though the four REE β-diketones are effective against localised corrosion, the calculated inhibition efficiencies are not good enough to mitigate corrosion in the tested corrosive environment.

With the mild steel sample in 3.5% NaCl solution, the potentiodynamic polarisation curve showed that there was a consistent decrease in the value of cathodic Tafel constants compared to when no inhibitors were used under the same range of temperature and environment. This decrease in the trend of the cathodic Tafel constant shows that the tested REE β-diketone complexes act as cathodic corrosion inhibitors. With the 304 SS samples exposed to the same 3.5 % NaCl solution, the behaviour of the tested REE β-diketone complexes were quite different compared to when mild steel was used in the same environment. Potentiodynamic polarisation curve of 304 SS shows that there was a shift in the corrosion potential to more noble values in the presence of all four REE β-diketone complexes confirming that the

inhibitors act as anodic type inhibitors in NaCl solution. Therefore, one can conclude that the inhibitors are probably mixed corrosion inhibitors whose mode of action depends on the tested material and the environment where they are used. This assertion was further confirmed when 304 and 316 SS was used in HCl solution. It was noted that the four inhibitors in this environment when used for both 304 and 316 SS show that the corrosion potentials shift in the negative direction, hinting that the four inhibitors act as a cathodic inhibitor in HCl solution.

6.2 RECOMMENDATIONS

It is highly recommended that a range of concentrations of the four tested REE β-diketone complexes ($Ce(acac)_3$, $La(acac)_3$, $Ce(hfac)_3$ and $La(hfac)_3$) should be explore in addition to the 0.5% that was used in this work to further investigate the efficacy of the inhibitors, and their mechanism and mode of operation. Furthermore, other forms of electrochemical analyses such as electrochemical impedance spectroscopy (EIS), linear polarisation resistance (LPR) and cyclic voltammetry (CV) should be use to further investigate the effects of the synthesised inhibitors on the steel samples.

It is also highly recommended to test the efficacy and potency of other inhibitors that have not been tested. However, trifluoroacetylacetone series could be left out as some of the characterisation results of this series (Raman spectroscopy and melting point analysis) did not yield an appreciable positive result in comparison to the results obtained in the literature.

APPENDIX

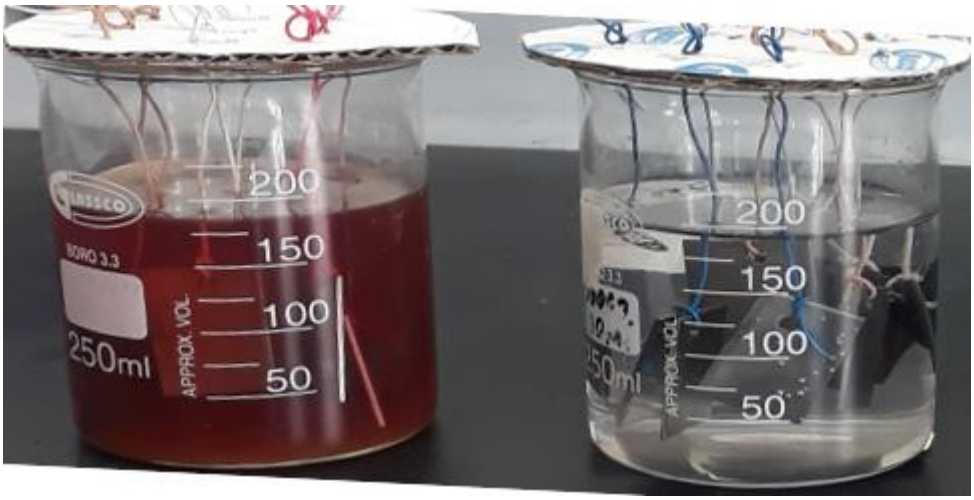


Figure A1: Suspended coupons in a corrosive media containing REE β-diketone complex shown weight loss test.

Table A1: Corrosion rate expression with different units.

Corrosion rate $\left(\mathbf{CR} = \mathbf{K}\frac{\mathbf{W_0 - W_1}}{\mathbf{DAT}}\right)$	Units used	K-value
mpy	W (mg), D (g/cc), A (cm^2), T (h)	3,450
mpy	W (mg), D (g/cc), A (in^2), T (h)	534
mpy	W (g), D (g/cc), A (in^2), T (days)	22,300
mpy	W(g), D (g/cc), A(cm^2), T (days)	14,370
mm/year	W(g), D (g/cc), A(in^2), T (days)	566
μm/year	W(g), D (g/cc), A(in^2), T (days)	566000
mm/year	W(g), D (g/cc), A(cm^2), T (days)	3,650
μm/year	W(g), D (g/cc), A(cm^2), T (days)	3,650000
μm/year	W(g), D (g/cc), A(cm^2), T (year)	10,000
mm/year	W (mg), D (g/cc), A (in^2), T (h)	1.36
μm/year	W (mg), D (g/cc), A (in^2), T (h)	1,360
mm/year	W (mg), D (g/cc), A (cm^2), T (h)	87.6
mm/year	W (g), D (g/cc), A (cm^2), T (h)	87,600
μm/year	W (mg), D (g/cc), A (cm^2), T (h)	87,600

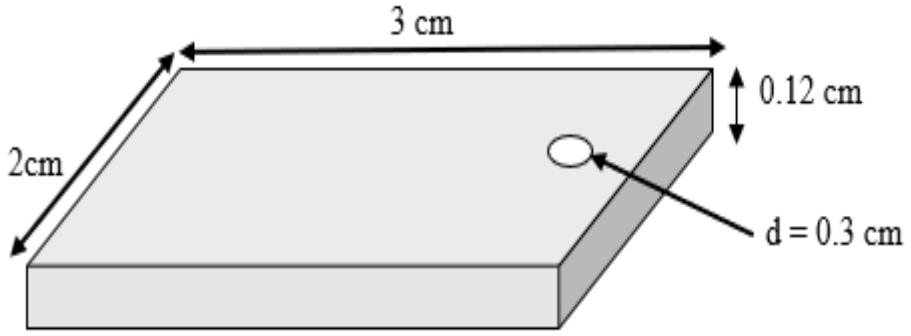


Figure A2: Specification for mild steel, 304 and 316 stainless steel coupons used for weight loss test.

DERIVATION OF FORMULAE FOR THE EXPOSED TOTAL SURFACE AREA OF COUPON

The total surface area of a cuboid is the sum of the areas of its faces, which is given by:

Total surface area = $2(LB + LT + BT)$……. (1)

where T = thickness of the coupon, L = length of the coupon, and B = breath of the coupon.

In drilling a hole, a cylindrical portion of the sample was removed.

Therefore, the total area extruded out of the specimen is equal to the total area of a cylinder.

The total surface area of the cylinder $= 2\pi RT + 2\pi R^2$……. (2)

where R= radius of the hole bore on the coupon

In terms of diameter (d), the above formula can be written as

The total surface area of the cylinder $= \pi dT + \frac{\pi d^2}{2}$……. (3)

Recall that the hollow surface area of the cylinder (i.e., inner cylindrical part) is wholly exposed to a solution during immersion.

Therefore, the total area of the coupon exposed to a solution
$=$ area of a cuboid $+$ hollow area
$-$ an area of the two circular surfaces of the extruded cylinder

Since the circular surface area of the extruded hollow cylinder (i.e., $2 \times \pi R^2$) is not part of the area immersed in a solution, it will carry a negative sign as shown in Equation (4)

The total surface area of the coupon = $2(LB + LT + BT) + \pi dT - \frac{\pi d^2}{2}$ ……... (4)

For the coupon used, L= 3 cm, B = 2 cm, d = 0.3 cm.

Thickness of the coupon (MS = 0.095 cm, 304 SS = 0.12 cm. 316 SS =0.12 cm)

Taking the thickness of the mild steels and stainless steel (304 and 316) into consideration, the total area of the specimens were calculated using Equation 4 and recorded below.

Table A2: Calculated area of the exposed to the surface area of the mild steel and stainless steels and their densities.

Specimen	Area (cm^2)	Density (g/cm^3) (ASTM G1-90, 1999).
MS	12.90	7.85
304 SS	13.17	7.94
316 SS	13.17	7.98

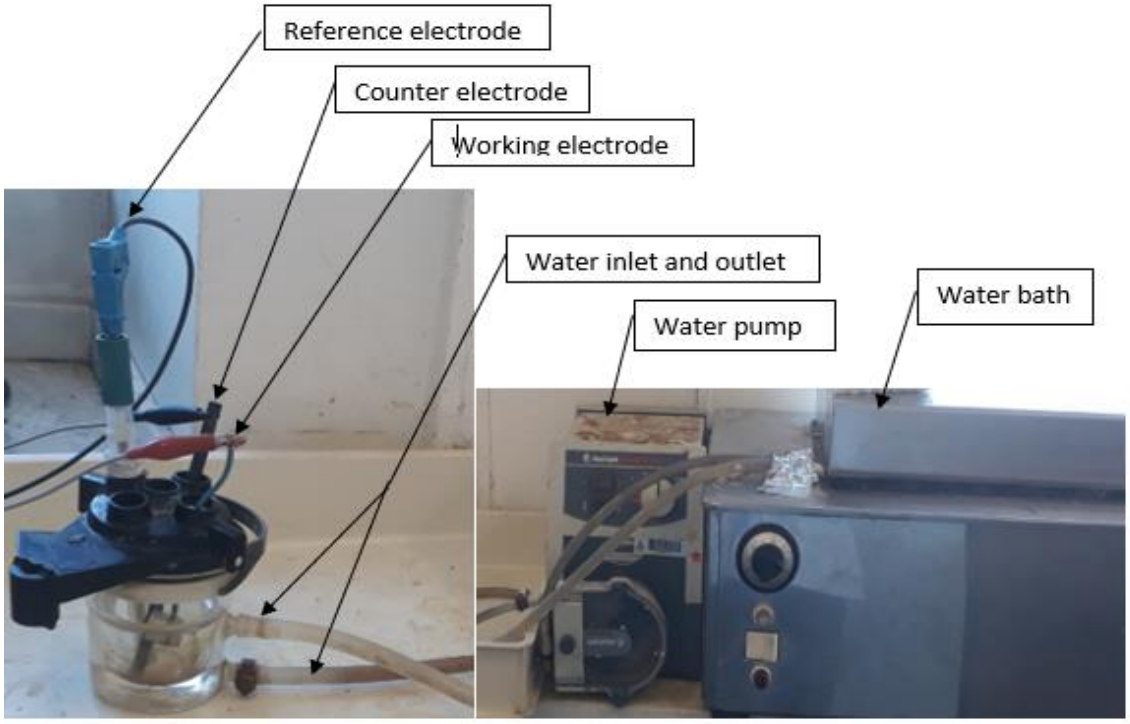


Figure A3: A schematic diagram showing the corrosion cell setup including all three electrodes as labeled (working, reference and counter), water pump and water bath.

CALCULATED YIELDS OF THE SYNTHESISED REE β-DIKETONE COMPLEXES

The yield of each complex was calculated based on the limiting reactant (i.e., β-diketone) according to balanced equations for the synthesis of the REE β-diketone complexes (see Equations 8 -22).

For lanthanum complexes, the yield was calculated based on the data given below.

The actual mass of lanthanum chloride used = 3.5 g

Molar mass of lanthanum acetylacetone = 436.05 g/mol

Volume of acetylacetone used = 2.5 ml

Density of acetylacetone = 0.975 g/ml

Molar mass of acetylacetone = 100.13 g/mol

Thus, the mass of acetylacetone was = 2.4 g

From the mass, density, and volume relationship,

$$\text{Mass} = \text{Density} \times \text{Volume} \ldots\ldots \quad (5)$$

$$\text{Number of moles (n)} = \frac{\text{mass of acac (m)}}{\text{Molecular mass of acac (M.M)}} \ldots\ldots \quad (6)$$

$$\text{Number of moles of acetylacetone (n)} = n = \frac{2.4}{100.13} = 0.0240 \text{ mole}$$

The theoretical yield of lanthanum complex, $La(acac)_3$ according to the balanced equation for the synthesis of $La(acac)_3$ is:

$$\text{is } 0.0240 \text{ mole of acac} \times \frac{1 \text{ mole } La(acac)_3}{3 \text{ mole of acac}} \times \frac{436.05 \text{ g of } La(acac)_3}{1 \text{ mole of } La(acac)_3} = 3.4884 \text{ g}$$

$$\%\text{ yield of } La(acac)_3 = \frac{\text{Actual mass of } La(acac)_3}{\text{Theoretical mass of } La(acac)_3} \times 100 \ldots\ldots \quad (7)$$

$$\%\text{ yield of } La(acac)_3 = \frac{3.3670}{3.4884} \times 100 = 96\%$$

Table A3: Actual masses and the yields obtained for the synthesised REE β-diketone complexes.

β-diketone complex	Mass (g)	Yield (%)
Lanthanum acetylacetone complex	3.367	95
Cerium acetylacetone complex	3.316	94
Scandium acetylacetone complex	0.533	82
Lanthanum dibenzyolmethane complex	3.794	94
Cerium dibenzyolmethane complex	3.826	95
Scandium dibenzyolmethane complex	1.230	91
Lanthanum trifluoroacetylacetone complex	3.604	87
Cerium trifluoroacetylacetone complex	3.671	89
Scandium trifluoro acetylacetone complex	1.213	89
Lanthanum hexafluoroacetylacetone complex	3.942	81
Cerium hexafluoroacetylacetone complex	2.856	64
Scandium hexafluoroacetylacetone complex	1.232	91
Cerium thenoyltrifluoroacetone complex	3.757	94
Lanthanum thenoyltrifluoroacetone complex	3.437	87
Scandium thenoyltrifluoroacetone complex	1.211	90

REACTION EQUATION FOR THE SYNTHESISES REE β-DIKETONE COMPLEXES

Case 1: Reacting a rare earth chloride of scandium, lanthanum, and cerium with acetylacetone (acac)

$$ScCl_3.6H_2O + 3CH_3COCH_2COCH_3 \rightarrow Sc(CH_3COCHCOCH_3)_3.6H_2O + 3HCl \quad (8)$$

$$LaCl_3.7H_2O + 3CH_3COCH_2COCH_3 \rightarrow La(CH_3COCHCOCH_3)_3.7H_2O + 3HCl \quad (9)$$

$$CeCl_3.7H_2O + 3CH_3COCH_2COCH_3 \rightarrow Ce(CH_3COCHCOCH_3)_3.7H_2O + 3HCl \quad (10)$$

Case 2: Reacting a rare earth chloride of scandium, lanthanum, and cerium with trifluoroacetylacetone (tfac) or 1,1,1-trifluoro-2,4-pentanedione.

$$ScCl_3.6H_2O + 3CH_3COCH_2COCF_3 \rightarrow Sc(CH_3COCHCOCF_3)_3.6H_2O + 3HCl\ldots \quad (11)$$

$$LaCl_3.7H_2O + 3CH_3COCH_2COCF_3 \rightarrow La(CH_3COCHCOCF_3)_3.7H_2O + 3HCl\ldots \quad (12)$$

$$CeCl_3.7H_2O + 3CH_3COCH_2COCF_3 \rightarrow Ce(CH_3COCHCOCF_3)_3.7H_2O + 3HCl \quad (13)$$

Case 3: Reacting a rare earth chloride of scandium, lanthanum and cerium with hexafluoroacetylacetone (hfac) or 1,1,1,5,5,5-hexafluoro-2,4-pentanedione.

$$ScCl_3.6H_2O + 3CF_3COCH_2COCF_3 \rightarrow Sc(CF_3COCHCOCF_3)_3.6H_2O + 3HCl \quad (14)$$

$$LaCl_3.7H_2O + 3CF_3COCH_2COCF_3 \rightarrow La(CF_3COCHCOCF_3)_3.7H_2O + 3HCl \quad (15)$$

$$CeCl_3.7H_2O + 3CF_3COCH_2COCF_3 \rightarrow Ce(CF_3COCHCOCF_3)_3.7H_2O + 3HCl \quad (16)$$

Case 4: Reacting a rare earth chloride of scandium, lanthanum, and cerium with dibenzoylacetylacetone (dbm) or 1,3-diphenylpropane-1,3-dione.

$$ScCl_3.6H_2O + 3C_6H_5COCH_2COC_6H_5 \rightarrow Sc(C_6H_5COCHCOC_6H_5)_3.6H_2O + 3HCl \quad (17)$$

$$LaCl_3.7H_2O + 3C_6H_5COCH_2COC_6H_5 \rightarrow La(C_6H_5COCHCOC_6H_5)_3.7H_2O + 3HCl \quad (18)$$

$$CeCl_3.7H_2O + 3C_6H_5COCH_2COC_6H_5 \rightarrow Ce(C_6H_5COCHCOC_6H_5)_3.7H_2O + 3HCl \quad (19)$$

Case 5: Reacting a rare earth chloride of scandium, lanthanum, and cerium with thenoyltrifluoroacetone (tta) or 2-thenoyltrifluoroacetone.

$$ScCl_3.6H_2O + 3C_4H_3SCOCH_2COCF_3 \rightarrow Sc(C_4H_3SCOCHCOCF_3)_3.6H_2O + 3HCl \quad (20)$$

$$LaCl_3.7H_2O + 3C_4H_3SCOCH_2COCF_3 \rightarrow La(C_4H_3SCOCHCOCF_3)_3.7H_2O + 3HCl \quad (21)$$

$$CeCl_3.7H_2O + 3C_4H_3SCOCH_2COCF_3 \rightarrow Ce(C_4H_3SCOCHCOCF_3)_3.7H_2O + 3HCl \quad (22)$$

CALCULATION FOR THE PREPARATION OF 0.1 M HYDROCHORIC SOLUTION

A diluted hydrochloric acid solution was prepared in the laboratory from a commercial grade 32% v/v concentrated HCl. The preparation of the acid was done based on the required volume to be used (1000 ml) and the concentration of the acid to be used for the corrosion test (i.e., 0.1 M). This was achieved by converting the 32% v/v to molar concentration with a given density of 1.16 g/ml or 1160 g/L. The conversion of concentration of 32% HCl concentrated acid in terms of percentage to molar concentration is calculated mathematically below:

$$\text{Mass} = \text{Density} \times \text{Volume} \quad (23)$$

Mass of HCl $= 1.16\ \text{g/ml} \times 0.32\ \text{ml} = 0.3712\ \text{g} = 371.2\ \text{g}$

Molecular weight of HCl is 36.5 g/mol.

$$\text{Number of moles of HCl (n)} = \frac{\text{weight of HCl (W)}}{\text{Molecular mass of substance of HCl (M.M)}} \quad (24)$$

$$\text{Number of moles of HCl} = \frac{371.2\ \text{g}}{36.5\ \text{g/mol}} = 10\ \text{moles}$$

$$\text{Molarity} = \frac{\text{moles}}{\text{Litres of solution}} \quad (25)$$

$$\text{Molarity} = \frac{10}{1} = 10\ \text{M}$$

The converted molarity in Equation (3.27) will be the value of C_1. This value will be substituted into the dilution formula below:

$$C_1V_1 = C_2V_2 \quad (26)$$

$$\text{Or } V_1 = \frac{C_2V_2}{C_1} \quad (27)$$

where C_1 is the initial commercial-grade HCl concentration (i.e., 32% v/v which has been converted to molar concentration.

C_2 is the required acid concentration for the corrosion test (final concentration).

V_1 is the required volume of the 32% HCl solution which needs to be diluted.

V_2 is the final volume subsequently to be diluted to (prepared).

$$V_1 = \frac{0.1 \times 1000}{10} = 10 \text{ ml}$$

Therefore, 10 ml of 32 % conc. HCl will be added to 1 L of deionized water to create 0.1 M acid concentration that will be needed for the corrosion test.